SPO 2026

Book of Abstracts

27th Symposium on Photonics and Optics

Kyiv · 2–6 November 2026 · online

MONDAY 2	Workshop on Ultrafast Phenomena
TUESDAY 3	Workshop on Advanced Laser Science and Applications
WEDNESDAY 4	3rd Workshop of the Ukrainian Synchrotron and Neutron Community (USyNC)
THURSDAY 5	Workshop on Laser Processing of Materials for Advanced Optoelectronic Applications
THURSDAY 5	Workshop on Sustainable Materials and Technologies for Optoelectronics and Sensors
FRIDAY 6	Conference on Optics and High Technology Material Science

ORGANISED BY

Taras Shevchenko National University of Kyiv — Department of Optics

Kyiv Academic University

ISP NAS Ukraine

PSI

IPR Institut de Physique de Rennes

USyNC Ukrainian Synchrotron and Neutron Community

27th Symposium on Photonics and Optics (SPO 2026)

Book of Abstracts

Kyiv, Ukraine (online) · 2–6 November 2026

ORGANISER	Department of Optics, Faculty of Physics, Taras Shevchenko National University of Kyiv, Ukraine
PUBLISHER	Taras Shevchenko National University of Kyiv, 60 Volodymyrska Street, Kyiv 01033, Ukraine
EDITORS	*to be confirmed*
FULL TEXT	eKNUTSHIR, the KNU institutional repository — *URL after deposit*
PUBLISHED	*November 2026*
LICENCE	*CC BY 4.0 (to be confirmed)*

PROGRAMME COMMITTEE

Prof. Serhiy Kondratenko (Chair)
Dean of the Faculty of Physics, Taras Shevchenko National University of Kyiv, Ukraine

Prof. Alexander Kordyuk
Kyiv Academic University and Institute of Metal Physics, NAS of Ukraine

Prof. Toru Aoki
Shizuoka University, Japan

Prof. Volodymyr Dzhagan
V. Lashkaryov Institute of Semiconductor Physics, NAS of Ukraine

Dr. Maciej Lorenc
Institut de Physique de Rennes (IPR), CNRS, Université de Rennes, France

Dr. Oksana Chukova
Taras Shevchenko National University of Kyiv, Ukraine

Dr. Rostyslav Danylo
Max Born Institute, Berlin, Germany

Dr. Artem Levchuk
Laboratoire des Solides Irradiés, École Polytechnique, CNRS, France

Dr. Oleksandr Tomchuk
ISIS Neutron and Muon Source, Rutherford Appleton Laboratory, UK

Dr. Kateryna Yablochkova
Head of the Department of Optics, Faculty of Physics, Taras Shevchenko National University of Kyiv, Ukraine

LOCAL COMMITTEE

Dr. Kateryna Yablochkova
Head of the Department of Optics, Faculty of Physics, Taras Shevchenko National University of Kyiv, Ukraine

Dr. Danylo Babich
Paul Scherrer Institute, Switzerland

HOW TO CITE

Book of Abstracts of the 27th Symposium on Photonics and Optics (SPO 2026), Kyiv, Ukraine, 2–6 November 2026. Kyiv: Taras Shevchenko National University of Kyiv, 2026.

The abstracts are published as submitted by the authors, after formatting; the authors are responsible for their content. Times are given in CET and Kyiv time. Programme and updates: www.spo.optics.org.ua · indico.psi.ch/event/19016

Contents

Monday 2 November	Workshop on Ultrafast Phenomena	Mo1.1–Mo4.3
Tuesday 3 November	Workshop on Advanced Laser Science and Applications	no abstracts
Wednesday 4 November	3rd Workshop of the Ukrainian Synchrotron and Neutron Community (USyNC)	We1.1–We4.10
Thursday 5 November	Workshop on Laser Processing of Materials for Advanced Optoelectronic Applications	Th1.1–Th2.4
Thursday 5 November	Workshop on Sustainable Materials and Technologies for Optoelectronics and Sensors	Th3.1–Th4.5
Friday 6 November	Conference on Optics and High Technology Material Science	Fr1.1–Fr6.14
Index	Author index	

How to read an abstract

Mo1.2 PLENARY · MONDAY 09:00 CET · 10:00 KYIV #223

1. **Code** Mo1.2 = Monday, session 1, talk 2. The same code is printed in the programme; abstracts follow code order, so the code is all you need to find a talk.
2. **Type and time.** Plenary 35+5 min, invited 25+5, oral 12+3, poster "rapid" talk 4 min. Times are given in CET (UTC+1) and in Kyiv time (UTC+2), one hour later.
3. **#223** is the Indico abstract number (indico.psi.ch/event/19016).
4. The underlined name is the presenter. All authors are listed, in the order submitted; the author index gives the codes of every author's abstracts.
5. Up to 500 words; at most one figure, printed across the text width (11.7 cm), with a caption.

Monday

2 November 2026

Workshop on Ultrafast Phenomena

Mo1 Session 1 · 08:30–10:10 CET · 09:30–11:10 Kyiv

Mo1.1	Ultrafast Time-Resolved X-ray Scattering at XFELs to Study Nonequilibrium Phenomena in Quantum Materials	Nelson N. Hua
Mo1.2	Laser excitation of giant acoustic waves	Thomas Pezeril
Mo1.3	Steering ultrafast phase transitions through photoexcited strain waves in quantum materials	Ritwika Mandal

Mo2 Session 2 · 10:25–12:20 CET · 11:25–13:20 Kyiv

Mo2.1	Is Landau Potential Picture Useful for Photoinduced Phase Transitions?	Hervé Cailleau
Mo2.2	Ultrafast electron diffraction study of Ti_3O_5 insulator-to-metal photoinduced phase transition	Damien Léa
Mo2.3	Heat-diffusion simulations of photoinduced phase transitions in Ti_3O_5 probed by ultrafast electron microscopy	Denisa Colțuneac
Mo2.4	THz-induced phonon mode mixing and collective dynamics in a polar nanolattice	Elizabeth M. Skoropata

Mo3 Session 3 · 13:10–14:50 CET · 14:10–15:50 Kyiv

Mo3.1	Coherent Sub-Picosecond Magnon Pulses for Ultrafast Spin Transport	Lukáš Nádvorník
Mo3.2	Tabletop terahertz: generating, shaping and detecting THz pulses with 1 kHz and 80 MHz Ti:Sapphire lasers	Artem Levchuk
Mo3.3	Role of electronic and magnonic spin-dissipation channels in terahertz spin-Hall magnetoresistance	Peter Kubaščík

Mo4 Session 4 · 15:10–16:50 CET · 16:10–17:50 Kyiv

Mo4.1	Driving atoms to study the spin-lattice interaction	Urs Staub
Mo4.2	Before the Pulse: Equilibrium Benchmarks for Ultrafast Magnetophononics	Leonie C. Spitz
Mo4.3	Coupled atomistic spin-lattice dynamics simulations of ultrafast magnetisation dynamics	Maryna Pankratova

Mo1.1 INVITED · MONDAY 08:30 CET · 09:30 KYIV #203

Ultrafast Time-Resolved X-ray Scattering at XFELs to Study Nonequilibrium Phenomena in Quantum Materials

Adrian Rutschmann[1], Aidan McConnell[1], Boyan Stoychev[2], Corinna Burri[1], Diling Zhu[3], Dragan Mihailović[4], Eric Fullerton[2], Erik Lamb[2], Faris Dizdarević[1], Hasan Yavaş[3], Henrik T. Lemke[1], Henry G. Bell[1], Ian Robinson[5], Jan Ravnik[1], Mathias Hoffmann[3], Mathias Sander[1], Maël Clémence[1], Meera Madhavi[6], Nanna Zhou Hagström[6], Nelson N. Hua[1], Oleg Shpyrko[2], Patrick Kramer[3], Pooja Rao[6], Roman Mankowsky[1], Roopali Kukreja[6], Sanghoon Song[3], Serhane Zerdane[1], Shih-Wen Huang[1], Simon Gerber[1], Spencer Jeppson[6], Surya Botu[6], Swan Htun[7], Takahiro Sato[3], Travis Frazer[7], Vincent Esposito[3], Wenxiang Hu[1], Xun Jia[7], Yanwen Sun[3]

[1]Paul Scherrer Institute PSI, Villigen, Switzerland [2]University of California San Diego, La Jolla, CA, USA [3]SLAC National Accelerator Laboratory, Menlo Park, CA, USA [4]Jožef Stefan Institute, Ljubljana, Slovenia [5]Brookhaven National Laboratory, Upton, NY, USA [6]University of California, Davis, Davis, CA, USA [7]Argonne National Laboratory, Lemont, IL, USA

X-ray free-electron lasers (XFELs) offer two key advantages over synchrotron sources for studying ultrafast phenomena: superior temporal resolution and significantly higher coherent photon flux. Here, I will highlight how these two capabilities can be exploited to investigate nonequilibrium phase transitions in quantum materials using time-resolved X-ray scattering. First, I will demonstrate how time-resolved X-ray diffraction with three-dimensional reciprocal-space resolution allows us to identify the coherent phonon modes and interlayer dynamics underlying the nonthermal transition to the hidden charge-density-wave (CDW) phase in 1T-TaS_2. I will then turn to coherent X-ray diffraction, showing how speckle patterns can be used to probe the fluctuation timescales of nanoscale heterogeneities, focusing on trimeron domains associated with charge order in magnetite (Fe_3O_4).

Cite as: Adrian Rutschmann et al., "Ultrafast Time-Resolved X-ray Scattering at XFELs to Study Nonequilibrium Phenomena in Quantum Materials", in *Book of Abstracts of the 27th Symposium on Photonics and Optics (SPO 2026)*, Kyiv, 2–6 November 2026, p. 5.

Mo1.2 PLENARY · MONDAY 09:00 CET · 10:00 KYIV #223

Laser excitation of giant acoustic waves

Thomas Pezeril

Institut de Physique de Rennes (IPR), CNRS – University of Rennes, Rennes, France

Pulsed lasers are routinely used to excite and detect acoustic waves over a broad frequency range, from MHz to THz. Laser ultrasonics enables non-contact, non-invasive, and non-destructive mechanical probing of samples with dimensions ranging from millimetres to nanometres. Although established for decades, the technique is constrained by optical damage thresholds, which typically limit the achievable acoustic pressures to values well below the gigapascal range. Higher pressures, sufficient to generate shock waves, can be reached at the expense of irreversible sample damage. Such experiments therefore require single-shot measurements, often with limited reproducibility and low signal-to-noise ratios. These limitations motivate the development of alternative optical approaches capable of generating large-amplitude strain pulses without damaging the sample, opening new perspectives for strain engineering of materials.

In this talk, I will present a novel methodology for generating non-destructive shock waves at high repetition rates, with amplitudes limited only by the mechanical strength of the sample [1]. Through selected case studies, I will show how this approach can be combined with time-domain Brillouin scattering, a time-resolved optical technique based on the generation and detection of GHz acoustic waves, to probe the mechanical response induced by the passage of these shock waves. This methodology opens new opportunities for systematic investigations of subtle strain-induced phenomena in strain-sensitive correlated materials.

[1] J. Deschamps, Y. Kai, J. Lem, I. Chaban, A. Lomonosov, A. Anane, S. Kooi, K. Nelson, T. Pezeril, Additive laser excitation of giant nonlinear surface acoustic wave pulses, Phys. Rev. Appl. 20, 044044 (2023).

Cite as: Thomas Pezeril, "Laser excitation of giant acoustic waves", in *Book of Abstracts of the 27th Symposium on Photonics and Optics (SPO 2026)*, Kyiv, 2–6 November 2026, p. 6.

Mo1.3 INVITED · MONDAY 09:40 CET · 10:40 KYIV #257

Steering ultrafast phase transitions through photoexcited strain waves in quantum materials

Ritwika Mandal[1], Céline Mariette[2], Etienne Janod[1], Maciej Lorenc[3]

[1]Institut des Matériaux de Nantes Jean Rouxel (IMN), CNRS – Nantes University, Nantes, France [2]European Synchrotron Radiation Facility (ESRF), Grenoble, France [3]Institut de Physique de Rennes (IPR), CNRS – University of Rennes, Rennes, France

Control of light-matter interaction in quantum materials offers a pathway to access non-equilibrium states with emergent functionalities beyond thermal equilibrium [1, 2]. In strongly correlated systems, particularly those involving large volume changes associated or not to a symmetry breaking, ultrafast laser excitation can drive phase transitions [3, 4]. Recent work [5] further highlights the effect of nanoscopic morphology on the mechanism of macroscopic transformation as well as relaxation dynamics.

In this work, we investigate a geometry controlled strain wave dynamics during photoinduced phase transition in morphologically tailored single crystals of V2O3, a prototypical strongly correlated system. Using time-resolved X-ray diffraction and ultrafast optical reflectivity, we track the coupled structural and electronic dynamics during such a transition.

We identify a multistep process after laser excitation, starting with an initial monoclinic-to-hexagonal inverse ferroelastic transition, within ~ 10 ps. At several tens of ps, the propagation of a unidirectional and coherent strain wave perpendicular to the large surface hit by the ultrafast laser induces a symmetry-lowered state with intermediate volume, stabilising a transient monoclinic metallic phase - a long sought missing link in the V2O3 phase diagram. At longer delays, additional strain waves propagating in-plane drive the system towards the hexagonal phase, with dynamics governed by the speed of acoustic propagation and the crystal lateral size. These results demonstrate that the strain wave mechanism can act as a dynamical symmetry-breaking field enabling control of photoinduced transition pathways and access to emergent phases.

[1] Koshihara, S. et al. Physics Reports 942, 1 (2022)

[2] Zhang, J. & Averitt, R. D. Annual Review of Materials Research 44, 19 (2014)

[3] Amano, T. et al. Nature Physics 20, 1778 (2024)

[4] Mariette, C. et al. Nature communications 12, 1239 (2021)

[5] Mandal, R. et al. Communications Materials 6, 209 (2025)

Cite as: Ritwika Mandal et al., "Steering ultrafast phase transitions through photoexcited strain waves in quantum materials", in *Book of Abstracts of the 27th Symposium on Photonics and Optics (SPO 2026)*, Kyiv, 2–6 November 2026, p. 7.

Mo2.1 PLENARY · MONDAY 10:25 CET · 11:25 KYIV #264

Is Landau Potential Picture Useful for Photoinduced Phase Transitions?

Hervé Cailleau

Institut de Physique de Rennes (IPR), CNRS – University of Rennes, Rennes, France

Thanks to remarkable developments of ultrafast techniques operating on a few fs, i.e. faster than atomic motions, many functionalities of materials can be manipulated on demand in unprecedented ways [1]. Thus, ultrafast laser systems allow to photoexcite a macroscopic number of carriers (typically few percent of valence band electrons) and hence to strongly perturb the electronic state of materials to drive the system toward another phase. The resulting electronic, magnetic and/or structural reorganization can be probed in real-time by ultrafast spectroscopies and X-ray/electron scattering.

Thermodynamics and symmetry considerations offer an universal approach of phase transition at thermal equilibrium through the Landau potential picture. A fundamental question arises whether it is applicable to ultrafast photoinduced phase transitions.

Different essential points will be discussed in views of recent ultrafast experiments:

- symmetry breaking (instability) vs. isosymmetric (switching) phase transitions;
- from short-range interactions in fluid to infinite-range ones in elastic solid;
- laser pulse vs. thermostat energy deposit;
- displacive dynamics for structural symmetry breaking [2];
- volume strain dynamics driving isosymmetric transformations in solids [3,4];
- influence of material morphology on transformation dynamics;
- comparison with nonlinear bistable systems like neuromorphic ones.

[1] D.N. Basov et al., Towards properties on demand in quantum materials, Nature Materials 16, 1077 (2017).

[2] T. Huber et al., Coherent structural dynamics of a prototypical charge-density-wave-to-metal transition, Physical Review Letters 113, 026401 (2014).

[3] C. Mariette et al., Strain wave pathway to semiconductor-to-metal transition revealed by time-resolved X-ray powder diffraction, Nature Communications 12, 1239 (2021).

[4] T. Amano et al., Propagation of insulator-to-metal transition driven by photoinduced strain waves in a Mott Material, Nature Physics 20, 1778 (2024).

Cite as: Hervé Cailleau, "Is Landau Potential Picture Useful for Photoinduced Phase Transitions?", in *Book of Abstracts of the 27th Symposium on Photonics and Optics (SPO 2026)*, Kyiv, 2–6 November 2026, p. 8.

Mo2.2 INVITED · MONDAY 11:05 CET · 12:05 KYIV #212

Ultrafast electron diffraction study of Ti_3O_5 insulator-to-metal photoinduced phase transition

Damien Léa[1], Arnaud Arbouet[2], Denisa Colţuneac[1], Florian Banhart[3], Gael Privault[4], Hilaire Mba[3], Hiroko Tokoro[4], Maciej Lorenc[1], Masaki Hada[4], Matthieu Picher[3], Philippe Rabiller[1], Riku Seiki[4]

[1]Institut de Physique de Rennes (IPR), CNRS – University of Rennes, Rennes, France [2]DYNACOM International Research Laboratory (IRL 2015), CNRS – University of Rennes – The University of Tokyo, Tokyo, Japan [3]Institut de Physique et Chimie des Matériaux de Strasbourg (IPCMS), CNRS – University of Strasbourg, Strasbourg, France [4]University of Tsukuba, Tsukuba, Japan

Ti_3O_5 exhibits a photoinduced insulator-to-metal transition (IMT) at room temperature, offering promising technological applications such as optical data storage based on the bistability of its insulating and metallic phases at the nanoscale, and thermal energy storage enabled by the transition's large latent heat [1,2]. Understanding the mechanisms governing the transition dynamics remains a major challenge in photoinduced phase transitions.

The IMT in Ti3O5 is particularly interesting as this isosymmetric (both phases retain the same space group C2/m) transition involves a substantial unit-cell volume expansion of approximately 6%, dominated by a ~5% expansion along the c-axis, while the a- and b-axes change by only ~1% [2,3]. Previous studies of Ti3O5 have shown that photoinduced strain waves drive the phase transition in polycrystalline samples at picosecond timescales, followed by crystallite-size-dependent dynamics during heat diffusion [3,4]. These observations, together with the pronounced anisotropy of the structural changes, raise important questions regarding the dependence of the phase-transition dynamics on crystal morphology and crystallographic orientation relative to the excitation geometry. Addressing these questions requires single-crystal specimens with controlled morphologies and orientations.

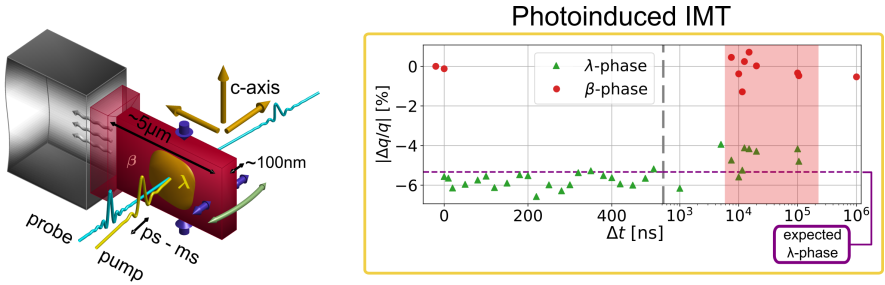


Figure. Sample layout for UED/UTEM experiment on Ti3O5 (Orange) Relative change of the (0,0,-6) lattice vector length, with the expected change expected for the β→λ transition. Red-shaded region corresponds to the coexistence of the β and λ phases respectively.

In this work, we present the first study of the photoinduced IMT in single-crystal nanoscale samples using nanosecond time-resolved electron diffraction. We observe the complete transformation to the metallic phase within 10 ns at the largest fluence used. We also provide evidence of phase coexistence both during the relaxation dynamics (~10–100 µs) and at the excitation plateau, with the extent of the transformation depending on the excitation

fluence. These results establish a first step towards investigating the photoinduced IMT in dedicated nanoscale specimens and demonstrate their suitability for future studies at picosecond timescales.

Before observing the photoinduced phase transition, we identified several photoinduced macroscopic sample motions, ranging from random displacements of freestanding Ti_3O_5 nanocrystals to coherent cantilever-like oscillations [5] in focused ion beam (FIB)-prepared samples. To disentangle these motions from the structural signatures of the phase transition, we implemented a pattern-matching approach analogous to those used in 4D-STEM phase and orientation mapping [6]. This method quantitatively determines the photoinduced changes in sample orientation, enabling reliable separation of macroscopic sample motion from the phase transition dynamics.

[1] S. Ohkoshi et al., Nat. Chem., vol. 2, no. 7, pp. 539–545, Jul. 2010, doi: 10.1038/nchem.670.

[2] H. Tokoro et al., Nat. Commun., vol. 6, no. 1, p. 7037, May 2015, doi: 10.1038/ncomms8037.

[3] C. Mariette et al., Nat. Commun., vol. 12, no. 1, p. 1239, Feb. 2021, doi: 10.1038/s41467-021-21316-y.

[4] R. Mandal et al., Commun. Mater., vol. 6, no. 1, p. 209, Sep. 2025, doi: 10.1038/s43246-025-00896-y.

[5] J. S. Baskin, H. S. Park, and A. H. Zewail, Nano Lett., vol. 11, no. 5, pp. 2183–2191, May 2011, doi: 10.1021/nl200930a.

[6] E. F. Rauch and M. Véron, Mater. Charact., vol. 98, pp. 1–9, Dec. 2014, doi: 10.1016/j.matchar.2014.08.010.

Cite as: Damien Léa et al., "Ultrafast electron diffraction study of Ti_3O_5 insulator-to-metal photoinduced phase transition", in *Book of Abstracts of the 27th Symposium on Photonics and Optics (SPO 2026)*, Kyiv, 2–6 November 2026, p. 9.

Mo2.3 ORAL · MONDAY 11:35 CET · 12:35 KYIV #211

Heat-diffusion simulations of photoinduced phase transitions in Ti_3O_5 probed by ultrafast electron microscopy

Denisa Colțuneac[1,2], Damien Léa[1], Laurentiu Stoleriu[2], Maciej Lorenc[1]

[1] *Institut de Physique de Rennes (IPR), CNRS – University of Rennes, Rennes, France* [2] *Alexandru Ioan Cuza University of Iași, Iași, Romania*

Titanium oxide Ti_3O_5 is a remarkable transition-metal oxide that exists in a few crystal phases and can be switched reversibly between them by temperature, pressure or light excitation[1]. The transition between its β and λ phases is first-order and is accompanied by a change in its electronic and optical properties, which makes the material a good candidate for optical switching and storage, heat-storage ceramics and solar steam generation[2]. Understanding how fast such a transition can be driven, and what limits its reversal, is therefore essential for any use of this material. [3,4]

Ultrafast transmission electron microscopy (UTEM) makes it possible to follow these processes directly. A laser pump excites a nanometre-thin Ti_3O_5 lamella, and a time-delayed electron pulse records the diffraction pattern, from which the structural response is followed from nanoseconds up to milliseconds. In such experiments the sample is thermally connected to its surroundings only through its mount, so heat transport plays a central role in how the system returns to its initial phase.

This presentation covers the numerical modelling developed to support the UTEM experiments performed on Ti_3O_5 lamellae. We describe a three-dimensional heat-diffusion model that includes the first-order character of the transition and the thermal coupling between the lamella and its mount. The simulations are presented as time-dependent relaxation curves of the transformed phase fraction and as spatial maps of temperature and phase, for different excitation conditions and thermal contacts, in a form that can be compared directly with the measured diffraction data.

[1] S. Ohkoshi et al., Nature Chemistry 2, 539–545 (2010).

[2] H. Tokoro et al., Nature Communications 6, 7037 (2015).

[3] C. Mariette et al., Nature Communications 12, 1239 (2021).

[4] R. Mandal et al., Communications Materials 6, 209 (2025).

Cite as: Denisa Colțuneac et al., "Heat-diffusion simulations of photoinduced phase transitions in Ti_3O_5 probed by ultrafast electron microscopy", in *Book of Abstracts of the 27th Symposium on Photonics and Optics (SPO 2026)*, Kyiv, 2–6 November 2026, p. 11.

Mo2.4 INVITED · MONDAY 11:50 CET · 12:50 KYIV #273

THz-induced phonon mode mixing and collective dynamics in a polar nanolattice

Elizabeth M. Skoropata

Paul Scherrer Institute PSI, Villigen, Switzerland

I will describe the THz induced dynamics of an SrTiO3 thin film with a nanoscale ordered interfacial dislocation network probed with 2- and 3-dimensional time-resolved X-ray diffraction and classical molecular dynamics simulations. I will share our findings that reveal that symmetry breaking at all length scales is an effective means to create dynamical electric polarization and to control phonon mixing that generates previously unreported collective modes in the THz regime.

Cite as: Elizabeth M. Skoropata, "THz-induced phonon mode mixing and collective dynamics in a polar nanolattice", in *Book of Abstracts of the 27th Symposium on Photonics and Optics (SPO 2026)*, Kyiv, 2–6 November 2026, p. 12.

Mo3.1 PLENARY · MONDAY 13:10 CET · 14:10 KYIV #275

Coherent Sub-Picosecond Magnon Pulses for Ultrafast Spin Transport

Lukáš Nádvorník[1], P. Kubaščík[1], M. Leiviskä[2], M. Bušina[1], Z. Kašpar[1], K. Müller[3], J. Mak[4], M. Scheufele[3], G. Lemut[4], J. Solano[2], O. Franke[4], R. Matuška[2], J. Jechumtál[1], E. Schmoranzerová[1], P. Němec[1], P. Kužel[2], T. Kampfrath[4], P. W. Brouwer[4], M. Opel[3], M. Althammer[3], T. Jungwirth[2], H. Reichlova[2]

[1]Charles University, Prague, Czech Republic [2]Institute of Physics of the Czech Academy of Sciences, Prague, Czech Republic [3]Walther-Meißner-Institute for Low Temperature Research, Bavarian Academy of Sciences and Humanities, Garching, Germany [4]Freie Universität Berlin, Berlin, Germany

Magnons, the elementary excitations of magnetic order, offer a promising route towards ultrafast information processing without charge transport. However, generating sub-picosecond magnon pulses that propagate over technologically relevant distances without losing coherence or broadening has remained a major challenge. Achieving this combination requires broadband excitation, coherent phase control, weak dispersion and predominantly ballistic transport.

In this talk, we demonstrate the generation and propagation of coherent, ultrashort magnon pulses in the altermagnetic insulator α-Fe_2O_3 (hematite) using terahertz spin-orbit torques in an adjacent platinum layer. By employing phase-resolved terahertz transmission spectroscopy, we investigate the dynamics and transport properties of these pulses, showing their coherent, ballistic and non-dispersive propagation. The talk will present the experimental approach and the key characteristics of the observed magnon dynamics, highlighting the potential of this method for ultrafast magnonic information processing and for exploring high-frequency spin dynamics in altermagnets and other magnetic materials.

Cite as: Lukáš Nádvorník et al., "Coherent Sub-Picosecond Magnon Pulses for Ultrafast Spin Transport", in *Book of Abstracts of the 27th Symposium on Photonics and Optics (SPO 2026)*, Kyiv, 2–6 November 2026, p. 13.

Mo3.2 INVITED · MONDAY 13:50 CET · 14:50 KYIV #259

Tabletop terahertz: generating, shaping and detecting THz pulses with 1 kHz and 80 MHz Ti:Sapphire lasers

Artem Levchuk

Laboratoire des Solides Irradiés (LSI), École Polytechnique, Institut Polytechnique de Paris, Palaiseau, France

Between microwaves and the infrared, terahertz (THz) radiation was long hard to produce and to measure. Yet it is the natural frequency range of many low-energy excitations in condensed matter: lattice vibrations, spin waves and the motion of free carriers all leave their signatures there. A THz pulse can both probe these excitations and drive them, on a subpicosecond timescale [1]. Thanks to femtosecond lasers, such experiments no longer require large-scale facilities: they fit on an optical table, around a Ti:Sapphire laser that many ultrafast laboratories already own.

This talk surveys what two complementary machines of this kind make possible. A 1 kHz amplifier delivers energetic pulses and therefore intense THz fields; an 80 MHz oscillator delivers far weaker pulses, but many more of them, which favours sensitivity. The laser largely dictates the source. With the amplifier, optical rectification in lithium niobate reaches field strengths of several hundred kV/cm, enough to drive matter into the nonlinear regime [2]. Organic crystals pumped by an optical parametric amplifier (OPA) push such fields to higher frequencies [3], and difference-frequency mixing at the OPA output yields multicycle THz pulses [4]. Spintronic emitters, metal films a few nanometres thick, radiate over an exceptionally broad band with a polarization set by a magnet, and work with either laser [5]. With the oscillator, photoconductive antennas remain the reference for compact, stable spectroscopy [6], while on-chip devices guide the wave through micrometre-scale structures and open up samples too small for a free-space beam [7].

Detection involves the same trade-offs. Electro-optic sampling, available with both lasers, records the amplitude and phase of the field directly [8]; with the amplifier, air-biased coherent detection extends the usable bandwidth considerably [9]. In between, passive components - spectral filters, polarizers, waveplates - select a frequency window and control the polarization state, which matters above all for magnetic studies.

Most of these approaches will be illustrated with results obtained on such systems, in particular pump-probe experiments on ultrafast magnetization dynamics, on the coupling between nonlinear optical modes, and on subcycle modulation in plasmonic systems. The aim is to give non-specialists practical guidance in matching laser, source and detector to their physical question, and to show that this spectral range is now within reach of most ultrafast optics laboratories.

[1] T. Kampfrath, K. Tanaka, K. A. Nelson, Nat. Photonics 7, 680 (2013).

[2] H. Hirori, A. Doi, F. Blanchard, K. Tanaka, Appl. Phys. Lett. 98, 091106 (2011).

[3] C. P. Hauri, C. Ruchert, C. Vicario, F. Ardana, Appl. Phys. Lett. 99, 161116 (2011).

[4] A. Sell, A. Leitenstorfer, R. Huber, Opt. Lett. 33, 2767 (2008).

[5] T. Seifert et al., Nat. Photonics 10, 483 (2016).

[6] D. H. Auston, K. P. Cheung, P. R. Smith, Appl. Phys. Lett. 45, 284 (1984).

[7] A. M. Potts et al., Nano Lett. 23, 3835 (2023).

[8] Q. Wu, X.-C. Zhang, Appl. Phys. Lett. 67, 3523 (1995).

[9] J. Dai, X. Xie, X.-C. Zhang, Phys. Rev. Lett. 97, 103903 (2006).

Cite as: Artem Levchuk, "Tabletop terahertz: generating, shaping and detecting THz pulses with 1 kHz and 80 MHz Ti:Sapphire lasers", in *Book of Abstracts of the 27th Symposium on Photonics and Optics (SPO 2026)*, Kyiv, 2–6 November 2026, p. 14.

Mo3.3 INVITED · MONDAY 14:20 CET · 15:20 KYIV #284

Role of electronic and magnonic spin-dissipation channels in terahertz spin-Hall magnetoresistance

Peter Kubaščík[1], R. Schlitz[2], O. Gueckstock[3], O. Franke[3], M. Borchert[4], M. Bušina[1], G. Jakob[5], K. Olejník[6], A. Farkaš[1,6], Z. Kašpar[1,6], J. Jechumtál[1], E. Schmoranzerová[1], P. Němec[1], Y. Z. Wu[7,8], G. Woltersdorf[9], M. Kläui[5], P. W. Brouwer[3], S. T. B. Goennenwein[2], T. Kampfrath[3], L. Nádvorník[1]

[1]Charles University, Prague, Czech Republic [2]University of Konstanz, Konstanz, Germany [3]Freie Universität Berlin, Berlin, Germany [4]Max Born Institute for Nonlinear Optics and Short Pulse Spectroscopy, Berlin, Germany [5]Johannes Gutenberg University Mainz, Mainz, Germany [6]Institute of Physics of the Czech Academy of Sciences, Prague, Czech Republic [7]Fudan University, Shanghai, China [8]Shanghai Research Center for Quantum Sciences, Shanghai, China [9]Martin Luther University Halle-Wittenberg, Halle (Saale), Germany

Spin-Hall magnetoresistance (SMR) is a magnetoresistive effect observed in bilayers comprising a heavy metal (HM) and a magnetically ordered layer (M). It arises from the interaction between spin-Hall-effect-induced spin accumulation in the HM and the magnetic order in M, mediated by interfacial spin torque and spin transport through magnons or electrons. While SMR has been extensively studied at DC and GHz frequencies, its ultrafast dynamics and the underlying spin-sink channels remain poorly understood.

Here, we investigate SMR in YIG|Pt and CoFeB|Pt bilayers over a frequency range of 0.2–25 THz. Combining sensitive THz detection with high-frequency magnetic-field modulation, we observe a pronounced magnonic low-pass response in YIG|Pt, whereas SMR in CoFeB|Pt remains frequency independent up to 25 THz. Our modelling attributes this spectral filtering to the finite response time of the magnon chemical potential generated by the time-dependent interfacial spin accumulation. In contrast, the broadband response of CoFeB|Pt is enabled by fast and efficient electronic spin-sink channels.

These findings establish thermal magnon transport as a key factor governing the ultrafast SMR response. They further show that electronic spin relaxation can weaken the magnonic low-pass filtering by providing an additional, faster channel for spin dissipation. Metallic magnetic structures are therefore promising for broadband, high-frequency applications, while THz SMR spectroscopy in magnetic insulators offers a sensitive probe of magnon transport and relaxation.

Cite as: Peter Kubaščík et al., "Role of electronic and magnonic spin-dissipation channels in terahertz spin-Hall magnetoresistance", in *Book of Abstracts of the 27th Symposium on Photonics and Optics (SPO 2026)*, Kyiv, 2–6 November 2026, p. 16.

Mo4.1 PLENARY · MONDAY 15:10 CET · 16:10 KYIV #263

Driving atoms to study the spin-lattice interaction

Urs Staub

Paul Scherrer Institute PSI, Villigen, Switzerland

The spin-lattice interaction is of central importance in magnetic solids. Being able to coherently move atoms and by that, directly affecting magnetism is not only interesting for manipulating magnetic properties, but studying it in real time allows to address a completely new view on the interactions itself. Here we use THz pulses to drive ions and fs X-ray pulses from X-Ray Free-Electron-Lasers (XFELS) to probe its motion and the underlying magnetism. The first case addresses electromagnons, hybrid magnon-phonon excitations, where we determine the spin and ion motions in real time [1,2]. This allows us not only a direct view on the magnetoelectric coupling, but also open the door for defining a time dependent magnetic Hamiltonian that could describe the magnetic interactions during the coherent motion in a lattice vibration. The second example addresses the circular drive of ions, its angular momentum [3] and its time reversal symmetry breaking in connection to the possible induced magnetization [4].

[1] T. Kubacka et al., Large Amplitude Spin Dynamics Driven by a THz Pulse in Resonance with an Electromagnon, Science 343, 1333 (2014).

[2] H. Ueda et al., Non-Equilibrium Dynamics of Spin-Lattice Coupling, Nature Commun. 14, 7778 (2023).

[3] R. Mankowsky et al., Quantifying Angular Momentum of Coherently Driven Circular Phonons, arXiv:2607.01841 (2026).

[4] C. J. Allington et al., Disentangling Spin Polarization from Driven Circular Ionic Motion in EuTiO3, arXiv:2609.282241 (2026).

Cite as: Urs Staub, "Driving atoms to study the spin-lattice interaction", in *Book of Abstracts of the 27th Symposium on Photonics and Optics (SPO 2026)*, Kyiv, 2–6 November 2026, p. 17.

Mo4.2 INVITED · MONDAY 15:50 CET · 16:50 KYIV #242

Before the Pulse: Equilibrium Benchmarks for Ultrafast Magnetophononics

Leonie C. Spitz

Paul Scherrer Institute PSI, Villigen, Switzerland

In strongly correlated systems, the coupling between different degrees of freedom opens the prospect to manipulate one by selectively driving another — a strategy made accessible on ultrafast timescales by the advent of intense laser technologies. In quantum magnets, intense THz pulses have been used to drive the lattice far from equilibrium to study magnetoelastic phenomena. However, the prediction of the out-of-equilibrium magnetoelastic phenomena and the interpretation of the experimental data require thorough understanding and reliable models of the magnetic interactions and the phonon spectra — usually obtained from density functional theory (DFT), which has well-known shortcomings when it comes to getting quantum magnetism right and requires rigorous experimental validation. I will present how we combine inelastic neutron scattering (INS) with state-of-the-art DFT calculations to meet these requirements.

[1] L. Spitz et al., Phys. Rev. B 112, 184302 (2025)

[2] F. Pisani, L. Spitz, L. Vojacek et al., arxiv:2604.13751 (2026)

Cite as: Leonie C. Spitz, "Before the Pulse: Equilibrium Benchmarks for Ultrafast Magnetophononics", in *Book of Abstracts of the 27th Symposium on Photonics and Optics (SPO 2026)*, Kyiv, 2–6 November 2026, p. 18.

Mo4.3 INVITED · MONDAY 16:20 CET · 17:20 KYIV #243

Coupled atomistic spin-lattice dynamics simulations of ultrafast magnetisation dynamics

Maryna Pankratova[1,2], Ivan Miranda[3], Anna Delin[4], Olle Eriksson[1], Anders Bergman[1]

[1] *Uppsala University, Uppsala, Sweden* [2] *University of Skövde, Skövde, Sweden* [3] *Linnaeus University, Kalmar, Sweden* [4] *KTH Royal Institute of Technology, Stockholm, Sweden*

Ultrafast demagnetisation was discovered in a pioneering experiment of Beaurepaire and co-authors [1] while studying the magnetisation of a thin nickel film following the absorption of a femtosecond laser pulse. Their work established a new and rapidly growing research field with numerous promising applications in all-optical magnetization switching, magnetic data storage, and spintronics. First experiments were quickly followed by other studies of ultrafast demagnetisation of ferromagnets (FM) [2-3], and later ferrimagnets (FI) and antiferromagnets (AFM) [4]. In addition, the initial studies of ultrafast demagnetisation were followed by element-resolved measurements, enabling the investigation of the magnetisation dynamics of different magnetic elements in materials containing multiple magnetic species [5].

To study ultrafast demagnetisation, we use the combination of density functional theory (DFT) and atomistic spin-lattice dynamics together with a heat-conserving three-temperature model (HC3TM) developed in our group. In the HC3TM, similarly to Beaurepaire's 3TM, we assume three temperatures: spin, lattice, and electronic. In contrast to 3TM, we compute spin and lattice temperatures during the coupled atomistic spin-lattice dynamics simulations, which are based on ab initio material-specific parameters, and then calculate the electronic temperature from energy conservation. In addition, our studies allow us to quantify the impact of spin-lattice coupling, which we model as the dependence of exchange interactions on atomic displacements [2-4, 6]. Our results show that even for materials with weak spin-lattice coupling, the impact of the lattice on the magnetisation dynamics can still be significant [3, 4]. Moreover, we demonstrate that the approach can reproduce the demagnetization rate of 3d FMs [2,3], lanthanide-based 4f AFM $LnRh_2Si_2$ (Ln = Tb, Gd, Dy, Sm, Ho) [4], and FI, such as FeGd. Following these results, we perform coupled atomistic spin-lattice dynamics simulations of FeNi to investigate the surprising delay in Ni demagnetisation observed in recent experiments [4]. We investigate whether the observed delay can be described using a combination of HC3TM and atomistic spin-lattice dynamics simulations.

[1] E. Beaurepaire, et al, Phys. Rev. Lett., 76, (1996), 4250.

[2] M. Pankratova, et al., Physical Review B, 106, 174407 (2022).

[3] M. Pankratova, et al. Scientific Reports 14, 8138 (2024).

[4] M. Pankratova et al., Physical Review Materials, 09, 094408 (2025).

[5] S. Jana, Physical Review B, 112, 214412 (2025).

[6] I. Miranda, et al. Physical Review Materials, 09, 024409 (2025).

Cite as: Maryna Pankratova et al., "Coupled atomistic spin-lattice dynamics simulations of ultrafast magnetisation dynamics", in *Book of Abstracts of the 27th Symposium on Photonics and Optics (SPO 2026)*, Kyiv, 2–6 November 2026, p. 19.

Wednesday

4 November 2026

3rd Workshop of the Ukrainian Synchrotron and Neutron Community (USyNC)

WED

We1 Session 1 · 08:10–09:30 CET · 09:10–10:30 Kyiv

We1.1	SOLARIS and CERIC-ERIC - research offer and access modes	Marcin Sikora
We1.2	The URANOS Beamline: An Advanced Tool for Electronic Band Structure Research	Natalia Olszowska
We1.3	MAVKA at SOLARIS: progress of the “Light for Ukraine” beamline towards first light	Danylo Babich
We1.4	IR imaging capabilities at the CIRI Beamline in Solaris	Tomasz Wróbel

We2 Session 2 · 10:00–12:10 CET · 11:00–13:10 Kyiv

We2.1	SwissFELplus: Enabling the Next Generation of Ultrafast X-ray Science	Luc Patthey
We2.2	Spin-orbit excitons and magnetic excitations in iridates across the Mott boundary	Eugenio Paris
We2.3	Bringing Light to Chemical Processes at the Balder Beamline, MAX IV	Myron Huzan
We2.4	NEPHEWS and beyond: Sustainable user access to external Photon and Neutron Infrastructures	Cormac McGuinness
We2.5	High-Resolution Soft X-ray Microscopy at MAX IV: New Capabilities and Opportunities	Igor Beinik

We3 Session 3 · 13:00–14:00 CET · 14:00–15:00 Kyiv

We3.1	ARPES-Based Search for Topological Quantum Materials	Volodymyr Bezguba
We3.2	Exploring ferroelectricity and topology in IV–VI semiconductors: an ARPES perspective	Tetiana Zakusylo
We3.3	Synchrotron VUV and structural characterization of zirconia-based nanopowders and ceramics	Larysa Khomenkova

We4 Session 4 · 14:00–16:35 CET · 15:00–17:35 Kyiv

We4.1	ENSA – European Neutron Science Association	Astrid Schneidewind
We4.2	Generation and properties of free neutrons	Anatoliy Senyshyn
We4.3	Neutron Diffraction	Oleksandr Prokhnenko
We4.4	Small-Angle Neutron Scattering: Principles and Applications	Oleksandr Tomchuk
We4.5	Neutron Reflectometry: the interfaces study technique overview and use-cases	Yehor Kosiachkin
We4.6	Introduction to Neutron Spectroscopy	Oleg Petrenko
We4.7	Imaging and tomography using monochromatic beams of thermal neutrons	Vasyl Ryukhtin
We4.8	Advancing Fast-Neutron Imaging with Metal-Halide Detectors	Anastasiia Sakhatska
We4.9	Neutron source at the MAC NSC “KIPT”	Ivan Guk
We4.10	Subcritical Assembly “Neutron Source” at NSC KIPT: Start-Up Results and Current Status	Andrii Zelinsky

We1.1 INVITED · WEDNESDAY 08:10 CET · 09:10 KYIV #215

SOLARIS and CERIC-ERIC - research offer and access modes

Marcin Sikora

SOLARIS National Synchrotron Radiation Centre, Jagiellonian University, Kraków, Poland

The SOLARIS synchrotron in Krakow, Poland, is a third-generation light source operating at 1.5 GeV electron energy. At present, SOLARIS Centre offer access to research instruments at seven beamlines and cryo-electron microscopy laboratory. These instruments provide a state-of-the-art portfolio of spectroscopic and microscopic probes with 200kV accelerated electrons and photons wavelength spanning from infra-red, through vacuum ultraviolet to soft, tender and hard X-rays. SOLARIS is a member of CERIC-ERIC consortium that gathers partner facilities in 8 countries of Central Europe and associated facilities in Italy, France and the Netherlands. The consortium offers access to NMR, mass spectroscopy, neutrons, two synchrotrons and FEL, ions beams, electron microscopes, nanolabs, battery testing, pathogen testing facilities, etc. Use of research infrastructure at SOLARIS and CERIC-ERIC facilities is free of charge for non-proprietary users. CERIC-ERIC is welcoming single and multitechnique proposals and offering to cover travel and accommodation costs for its users.

Cite as: Marcin Sikora, "SOLARIS and CERIC-ERIC - research offer and access modes", in *Book of Abstracts of the 27th Symposium on Photonics and Optics (SPO 2026)*, Kyiv, 2–6 November 2026, p. 22.

We1.2 INVITED · WEDNESDAY 08:30 CET · 09:30 KYIV #294

The URANOS Beamline: An Advanced Tool for Electronic Band Structure Research

Natalia Olszowska[1], Dawid Wutke[1], Rafał Kurleto[1], Jacek J. Kołodziej[1,2]

[1]SOLARIS National Synchrotron Radiation Centre, Jagiellonian University, Kraków, Poland [2]Marian Smoluchowski Institute of Physics, Jagiellonian University, Kraków, Poland

High-Resolution, Low-Temperature and Spin-Resolved ARPES

The URANOS (Ultra Resolved ANgular phOtoelectron Spectroscopy) beamline at the SOLARIS National Synchrotron Radiation Centre is dedicated to investigating the electronic and spin properties of solid-state materials using angle and spin-resolved photoemission techniques (Spin-ARPES) at low-temperature capabilities.

The beamline provides a highly monochromatic photon beam with continuously tuneable energy (8–160 eV) and selectable polarization, including linear, circular, and elliptical modes. Its experimental endstation features a hemispherical DA30L electron energy analyser equipped with deflection optics, a six-axis cryogenic manipulator operating over a temperature range of 4–500 K, and two orthogonally arranged VLEED spin detectors enabling three-dimensional spin-polarization measurements. Extensive in situ sample preparation facilities, together with complementary techniques such as LEED and XPS, support comprehensive surface characterization.

This presentation will introduce the main experimental configurations and capabilities of the URANOS beamline, with particular emphasis on high-resolution, low-temperature, photon-polarization-dependent, and spin-resolved ARPES. Selected research examples will demonstrate how these complementary approaches can be used to investigate electronic band dispersions, surface states, and spin-dependent phenomena.

Acknowledgement. Research at the National Synchrotron Radiation Centre SOLARIS is supported by the Ministry of Science and Higher Education, Poland, under contract no. MNiSW/2026/DWM/928.

[1] N. Olszowska, D. Wutke, M. Rosmus, R. Kurleto, J.J. Kołodziej; URANOS — Low-Energy Photon Beamline for ARPES Measurements; DOI: https://doi.org/10.12693/APhysPolA.149.S235

Cite as: Natalia Olszowska et al., "The URANOS Beamline: An Advanced Tool for Electronic Band Structure Research", in *Book of Abstracts of the 27th Symposium on Photonics and Optics (SPO 2026)*, Kyiv, 2–6 November 2026, p. 23.

We1.3 ORAL · WEDNESDAY 09:00 CET · 10:00 KYIV #288

MAVKA at SOLARIS: progress of the "Light for Ukraine" beamline towards first light

Artem Yakovliev[2], Danylo Babich[1], Anna Wach[2], Rolf Follath[1], Marco Calvi[1], David M. Just[1], Marcel Brüstle[1], Daniel Grolimund[1], Ilaria Besana[1], Jochem Snuverink[1], Jakub Szlachetko[2], Marcin Zając[2], Michał Młynarczyk[2], Marcin Sikora[2], Adriana Wawrzyniak[2], Jarosław Wiechecki[2], Andrzej Marendziak[2], Paweł Bulira[2], Paweł Nowak[2], Volodymyr Bezguba[3], Volodymyr Karbivskyy[4], Ihor Sukhenko[4], Andrei Gloskovskii[5], Oksana Chukova[5], Leonid Rivkin[1], Martin Sandhop[5], Wolfgang Drube[5], Alexander Kordyuk[3], Luc Patthey[1]

[1]Paul Scherrer Institute PSI, Villigen, Switzerland [2]SOLARIS National Synchrotron Radiation Centre, Jagiellonian University, Kraków, Poland [3]Kyiv Academic University, Kyiv, Ukraine [4]G. V. Kurdyumov Institute for Metal Physics of the National Academy of Sciences of Ukraine, Kyiv, Ukraine [5]Deutsches Elektronen-Synchrotron DESY, Hamburg, Germany

WED

MAVKA is an X-ray micro-probe beamline for the Ukrainian research community, built within the LEAPS initiative "Light for Ukraine" by PSI, SOLARIS, the National Academy of Sciences of Ukraine and partner institutions on straight section 2 of the 1.5 GeV SOLARIS ring in Kraków. It is designed for 0.5–12 keV and will serve three planned stations that follow the 2023 survey of the Ukrainian user community: UHV micro-XPS/XAS/XRF, ambient-pressure HAXPES and micro-probe XAS/XRD.

This talk reviews the progress since the last USyNC workshop. The front end, designed at PSI on the SLS 2.0 model, is in production at PSI, and the source will be a refurbished U19 in-vacuum undulator from the Swiss Light Source. The beamline layout and ray tracing are complete. The first stage uses the first mirror and the cryo-cooled Si(111) double-crystal monochromator (2.5–12 keV) from the SLS microXAS beamline; a plane-grating monochromator for 0.5–2.5 keV is planned in the same beam path. Ray tracing predicts 10^{12}–10^{13} photons/s in micrometre-sized spots focused by Kirkpatrick–Baez mirrors. Further components no longer used after the SLS 2.0 upgrade are being integrated into a new lead-shielded optical hutch, designed together with SOLARIS, whose shielding is being optimised with FLUKA Monte Carlo calculations. Stations 1 and 2 are being prepared with partners in Germany (DESY with Helmholtz partners) and Poland (SOLARIS). Station 3 starts with pilot experiments in the optical hutch, with a goniometer and a PILATUS 2M detector from PSI. First light is planned for the end of 2027 and pilot experiments for 2028.

Acknowledgement. The project team gratefully acknowledges the CHF 1.5 million grant from the Swiss State Secretariat for Education, Research and Innovation (SERI) and the Swiss National Science Foundation (SNSF). The project is partially supported by the Ministry of Science and Higher Education, Poland (contract 1/SOL/2021/2).

Cite as: Artem Yakovliev et al., "MAVKA at SOLARIS: progress of the 'Light for Ukraine' beamline towards first light", in *Book of Abstracts of the 27th Symposium on Photonics and Optics (SPO 2026)*, Kyiv, 2–6 November 2026, p. 24.

We1.4 ORAL · WEDNESDAY 09:15 CET · 10:15 KYIV #295

IR imaging capabilities at the CIRI Beamline in Solaris

Tomasz Wróbel

SOLARIS National Synchrotron Radiation Centre, Jagiellonian University, Kraków, Poland

Abstract not yet received

Cite as: Tomasz Wróbel, "IR imaging capabilities at the CIRI Beamline in Solaris", in *Book of Abstracts of the 27th Symposium on Photonics and Optics (SPO 2026)*, Kyiv, 2–6 November 2026, p. 25.

We2.1 PLENARY · WEDNESDAY 10:00 CET · 11:00 KYIV #296

SwissFELplus: Enabling the Next Generation of Ultrafast X-ray Science

Luc Patthey, on behalf of the SwissFEL team
Paul Scherrer Institute PSI, Villigen, Switzerland

SwissFELplus is a major upgrade project aimed at enhancing the capabilities of the Swiss Free Electron Laser (SwissFEL) and maintaining Switzerland's leading position in ultrafast science, medicine, and engineering. The project will enable highly coherent X-ray pulses with sub-femtosecond durations, two-color and polarization-controlled operation at both beamlines, and an extended photon-energy range up to 18 keV. These advances will be achieved through innovations in the injector, accelerator, undulator systems, photon diagnostics, experimental endstations, detectors, and computing infrastructure. The presentation will begin with a brief introduction to X-ray free-electron laser (XFEL) technology and the scientific opportunities enabled by XFELs, followed by an overview of the SwissFELplus project, its key objectives, and the technologies being developed to enable the next generation of ultrafast X-ray experiments.

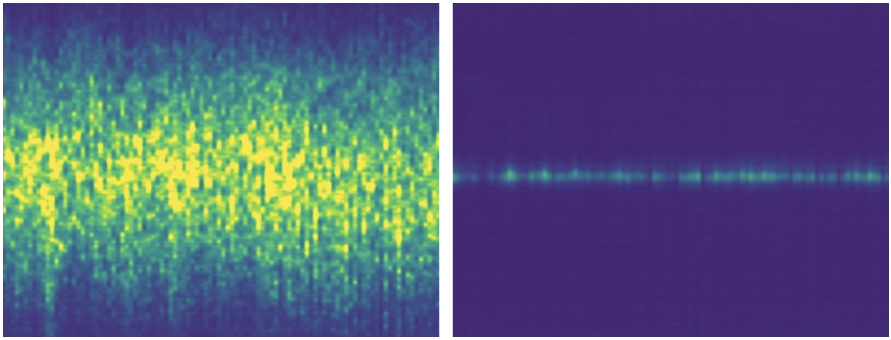


Figure. Towards highly coherent X-ray pulses: a series of single shots with stochastic, spiky SASE (self-amplified spontaneous emission) output (left) and narrow-band emission (right).

Cite as: Luc Patthey, "SwissFELplus: Enabling the Next Generation of Ultrafast X-ray Science", in *Book of Abstracts of the 27th Symposium on Photonics and Optics (SPO 2026)*, Kyiv, 2–6 November 2026, p. 26.

We2.2 INVITED · WEDNESDAY 10:40 CET · 11:40 KYIV #283

Spin-orbit excitons and magnetic excitations in iridates across the Mott boundary

Eugenio Paris

Paul Scherrer Institute PSI, Villigen, Switzerland

The spin-orbit exciton (SOE) in iridates is a propagating quasiparticle whose dispersion in a Mott insulator directly reflects the underlying antiferromagnetic (AF) order. The Ruddlesden-Popper iridates $Sr_{n+1}Ir_nO_{3n+1}$ evolve from the Jeff = ½ AF insulators Sr_2IrO_4 and $Sr_3Ir_2O_7$ to the semimetallic perovskite $SrIrO_3$, with an insulator-metal transition (IMT) governed by strong spin-orbit coupling, dimensionality, and electronic correlations. Despite extensive RIXS studies of the insulating members, the fate of the magnetic and spin-orbital excitations on the metallic side of the phase diagram has remained unresolved.

Here I present a study of $SrIrO_3$, a "strange (semi-)metal" with high-mobility carriers and no magnetic order, but on the verge of a Mott insulating state. Using Ir L_3-edge RIXS on a series of heterostructures spanning the metallic side of the IMT, we find a magnetic mode with an AF-like dispersion, but with a large gap and large linewidth, revealing remnants of AF Mott physics. In contrast, the SOE shows an inverted dispersion and doubled periodicity, reflecting its decoupling from the magnetic sector and the dominant role of charge fluctuations. Localized and itinerant physics therefore coexist in this material, and the SOE dispersion emerges as a sensitive fingerprint of the balance between spin correlations and charge fluctuations.

[1] E. Paris et al., Phys. Rev. Lett. 135, 186506 (2025).

Cite as: Eugenio Paris, "Spin-orbit excitons and magnetic excitations in iridates across the Mott boundary", in *Book of Abstracts of the 27th Symposium on Photonics and Optics (SPO 2026)*, Kyiv, 2–6 November 2026, p. 27.

We2.3 INVITED · WEDNESDAY 11:10 CET · 12:10 KYIV #235

Bringing Light to Chemical Processes at the Balder Beamline, MAX IV

Myron Huzan

MAX IV Laboratory, Lund University, Lund, Sweden

Balder, named after the Norse god of light, is a dedicated hard X-ray spectroscopy beamline at the MAX IV laboratory in Sweden, designed for real-time observation of chemical processes. Through the application of X-ray absorption spectroscopy (XAS) and X-ray emission spectroscopy (XES), the beamline enables detailed analysis of material structures and electronic states under realistic conditions. Its broad energy range covers the K- and L-edges of much of the periodic table, supporting research across diverse scientific disciplines.

Many essential processes, such as catalytic conversion, battery cycling, and metal behaviour in soils, occur under challenging operando conditions, including high temperatures, reactive gases, liquid phases, and rapidly changing states. X-ray spectroscopy overcomes these challenges by offering elemental and orbital specificity. Tuning the X-ray energy to a particular absorption edge enables the isolation of individual elements, even at low concentrations in disordered or liquid samples. X-ray absorption near-edge structure (XANES) reveals oxidation states and chemical speciation, extended X-ray absorption fine structure (EXAFS) determines bond distances and coordination numbers, and XES examines occupied electronic states, spin, and ligand environments, providing complementary insights beyond those available from absorption measurements alone.

This presentation introduces X-ray absorption and emission spectroscopy, outlines the capabilities of the Balder beamline, and demonstrates how complementary multimodal techniques elucidate the electronic structure of diverse functional materials. The objective is to contextualise these methods, highlighting the types of scientific questions they address in studies focused on local structure and chemical properties.

Cite as: Myron Huzan, "Bringing Light to Chemical Processes at the Balder Beamline, MAX IV", in *Book of Abstracts of the 27th Symposium on Photonics and Optics (SPO 2026)*, Kyiv, 2–6 November 2026, p. 28.

We2.4 ORAL · WEDNESDAY 11:40 CET · 12:40 KYIV #277

NEPHEWS and beyond: Sustainable user access to external Photon and Neutron Infrastructures

Cormac McGuinness[1,2], Astrid Schneidewind[3], Rosen Georgiev[2], Piotr Piwowarczyk[4]

[1]European Synchrotron and Free Electron Laser User Organisation (ESUO) [2]Trinity College Dublin, Dublin, Ireland [3]Forschungszentrum Jülich GmbH, Jülich, Germany [4]SOLARIS National Synchrotron Radiation Centre, Jagiellonian University, Kraków, Poland

The NEPHEWS project currently provides Trans-National Access (TNA) funding for users from across all of Europe to perform experiments at the majority of synchrotron, FEL and neutron research infrastructures (RI) of the LEAPS and LENS consortia. This access has been particularly aimed at Widening countries, countries without these facilities and eight targeted countries for priority access which includes Ukraine. Scientists from Ukraine, in addition to TNA support for experiments, have also been able to benefit as Twinning guests participating in experiments with expert host groups, as well as benefitting from internship opportunities for Early-Stage Researchers at these research infrastructures. Future NEPHEWS style Access projects are clearly desirable.

Ongoing changes in European Commission funding leading to FP10 are intended to lead to more sustainable continuous baseline access to RI across Europe, and are being implemented through a sequence of Horizon Europe calls leading to a cross-domain Infrastructure Service pilot access project that could begin in 2028. The most sustainable access funding for national user communities lie within the policies of each nations science funding agencies and science and research ministries. We present an optimal model for scientific user communities, through the combination of i) membership of international research organisations aligned with national objectives; ii) investment in external research infrastructures; and iii) in structural access supports for national users to all the Open external research infrastructure. The best example is the long extant Danish model of membership, investment, and of user support, the latter occurring through the DanScatt project. Ukraine is well positioned to implement new policy and a similar future scheme to take best advantage of access to the European research infrastructure networks. A sustained scheme to access the state-of-the-art cutting edge instruments located at the European world class research facilities will continue to underpin European research and technological sovereignty and place Ukrainian researchers at the heart of this initiative within Europe.

Cite as: Cormac McGuinness et al., "NEPHEWS and beyond: Sustainable user access to external Photon and Neutron Infrastructures", in *Book of Abstracts of the 27th Symposium on Photonics and Optics (SPO 2026)*, Kyiv, 2–6 November 2026, p. 29.

We2.5 ORAL · WEDNESDAY 11:55 CET · 12:55 KYIV #268

High-Resolution Soft X-ray Microscopy at MAX IV: New Capabilities and Opportunities

Igor Beinik, Jörg Schwenke, Linus Roslund, Karina Thånell
MAX IV Laboratory, Lund University, Lund, Sweden

Soft X-ray microscopy combines high spatial resolution with sensitivity to the chemical composition, electronic structure, and magnetic properties of materials. By tuning the photon energy across characteristic absorption edges, it becomes possible to visualize the spatial distribution of different elements and their chemical states, providing valuable insights into the structure and functionality of complex materials.

The SoftiMAX beamline at MAX IV Laboratory offers these capabilities through scanning transmission X-ray microscopy (STXM) and ptychography, a coherent imaging technique that uses recorded diffraction patterns to reconstruct high-resolution images of a sample. The recently developed CHIARA end-station brings together these complementary methods, enabling chemical and magnetic imaging with spatial resolution down to the nanometre scale.

This contribution will introduce the principles and applications of soft X-ray spectromicroscopy, present the current capabilities of CHIARA, and highlight recent developments aimed at improving imaging performance and efficiency. Particular attention will be given to the integration of fast pixelated detectors and emerging multi-beam imaging approaches, which offer promising opportunities for faster measurements and larger fields of view.

These developments expand the possibilities of synchrotron-based microscopy for investigating nanoscale phenomena in functional materials and other complex systems.

Cite as: Igor Beinik et al., "High-Resolution Soft X-ray Microscopy at MAX IV: New Capabilities and Opportunities", in *Book of Abstracts of the 27th Symposium on Photonics and Optics (SPO 2026)*, Kyiv, 2–6 November 2026, p. 30.

We3.1 INVITED · WEDNESDAY 13:00 CET · 14:00 KYIV #267

ARPES-Based Search for Topological Quantum Materials

Volodymyr Bezguba, Alexander Kordyuk
Kyiv Academic University, Kyiv, Ukraine

Quantum materials are a broad class of solids whose properties emerge from quantum-mechanical and collective electronic effects that have no classical counterpart, superconductivity being one of the best-known examples. Non-trivial band topology gives rise to further exotic phenomena, such as robust spin-polarized surface states, making these materials highly attractive for spintronics and quantum computing. Angle-resolved photoemission spectroscopy (ARPES) is ideally suited to studying these systems, as it directly maps their electronic band structure. Synchrotron radiation adds key advantages. Tuneable photon energy gives access to the three-dimensional band structure (especially relevant for Co-based shandites covered in this talk) and helps separate surface states from bulk bands, while variable light polarization reveals the orbital character of individual bands. Resolving this complex, multiband electronic structure is key both to understanding quantum materials and to designing new ones with tailored properties. This talk will present ARPES studies of several different topological materials, including recent beamtime results at the SOLARIS synchrotron.

Cite as: Volodymyr Bezguba et al., "ARPES-Based Search for Topological Quantum Materials", in *Book of Abstracts of the 27th Symposium on Photonics and Optics (SPO 2026)*, Kyiv, 2–6 November 2026, p. 31.

We3.2 ORAL · WEDNESDAY 13:30 CET · 14:30 KYIV #280

Exploring ferroelectricity and topology in IV–VI semiconductors: an ARPES perspective

Tetiana Zakusylo[1], Auguste Majou[2], Dawid Wutke[3], Elies Ben Achour[2], Gauthier Krizman[2], Gunther Springholz[1], Günter Bauer[1], Joaquin Bermejo-Ortiz[2], Lakshmi Sajeev[4], Liang Fu[5], Louis-Anne de Vaulchier[2], Mahdi Hajlaoui[1], Marcin Rosmus[3], Martin Heinrich[1], Natalia Olszowska[3], Ondřej Caha[4], Rafal Kurleto[3], Takuya Takashiro[1], Yugo Onishi[5], Yves Guldner[2]

[1]Johannes Kepler University Linz, Linz, Austria [2]École Normale Supérieure, PSL University, Paris, France [3]SOLARIS National Synchrotron Radiation Centre, Jagiellonian University, Kraków, Poland [4]Masaryk University, Brno, Czech Republic [5]Massachusetts Institute of Technology, Cambridge, MA, USA

WED

Ferroelectric topological materials combining ferroelectricity and non-trivial band topology open promising frontiers in topological matter by introducing ferroelectric-driven inversion symmetry breaking in the system [1-3]. In particular, ferroelectricity in topological crystalline insulator has been predicted to support the emergence of inversion breaking Weyl semimetal phase, which so far has been experimentally realized only in time-reversal breaking systems, such as TaAs material family [4-6]. Furthermore, controlling novel topological phases via ferroelectric polarization switching induced by electric fields is a core idea in topological spintronics [7].

Here, we report the experimental realization of a new ferroelectric topological crystalline insulator (FETCI) based on IV–VI compounds that hosts non-trivial topological surface states in co-existence with emergent ferroelectric phase. Using molecular beam epitaxy, high-quality quantum well heterostructures (QWs) as well as thin film geometries were grown on (111)-oriented BaF2 substrates using PbSe, SnSe, and GeSe sources. We demonstrate the dual functionality in FETCI QWs by means of temperature-dependent angle resolved photoemission spectroscopy (ARPES), spanning over the whole temperature range of the ferroelectric and topological phase transitions from room temperature down to 20 K. In particular, ARPES measurements at the high symmetry M-point reveal simultaneously ferroelectric Rashba-split states and topological surface states emerging as the system undergoes a topological phase transition below the ferroelectric Curie temperature. The character of the observed topological and ferroelectric phase transitions is further proven by temperature-dependent x-ray diffraction, transport, and magneto-optical measurements.

Our results evidence that ferroelectric phase and topological crystalline insulator phase coexist simultaneously in a single material based on the group of IV-VI compounds. This opens a new platform for electrically tunable topological phases, promising for demonstrating and manipulating novel band topologies.

[1] Ando, Y. & Fu, L. Topological crystalline insulators and topological superconductors: From concepts to materials. *Annu. Rev. Condens. Matter Phys.* **6**, 361, (2015).

[2] Lau, A. & Ortix, C. Topological semimetals in the SnTe material class: Nodal lines and Weyl points. *Phys. Rev. Lett.* **122**, 186801, (2019).

[3] Stefanato, E. D. et al. Metallicity-driven polar transitions in topological epilayers, *Commun. Phys.* **8**, 419, (2025).

[4] Armitage, N. P., Mele, E. J., Vishwanath, A. Weyl and Dirac semimetals in three-dimensional solids, *Rev. Mod. Phys.* **90**, 15001, (2018).

[5] Yan, B. & Felser, C. Topological materials: Weyl semimetals, *Ann. Rev. Cond. Mat. Phys.* **8**, 337, (2017).

[6] Jia, S., Xu, S.Y., Hasan, M.Z. Weyl semimetals: Fermi arcs and chiral anomalies, *Nat. Mater.* **15**, 1140, (2016).

[7] Liu, J. et al. Spin-filtered edge states with an electrically tunable gap in a two-dimensional topological crystalline insulator. *Nat. Mater.* **13**, 178, (2014).

Cite as: Tetiana Zakusylo et al., "Exploring ferroelectricity and topology in IV–VI semiconductors: an ARPES perspective", in *Book of Abstracts of the 27th Symposium on Photonics and Optics (SPO 2026)*, Kyiv, 2–6 November 2026, p. 32.

We3.3 ORAL · WEDNESDAY 13:45 CET · 14:45 KYIV #300

Synchrotron VUV and structural characterization of zirconia-based nanopowders and ceramics

Larysa Khomenkova[1], Kostyantyn Kozoriz[1], Igor Vorona[1], Nadiia Korsunska[1], Lyudmyla Borkovska[1], Dmytro Khomenkov[1,2], Liudmyla Melnichuk[2], Oleksandr Melnichuk[2], Yevheniia Smortsova[3], Aleksei Kotlov[3], Oksana Chukova[3], Arno Jeromin[4], Volodymyr Khomenkov[5]

[1]V. Lashkaryov Institute of Semiconductor Physics of the National Academy of Sciences of Ukraine, Kyiv, Ukraine [2]Nizhyn Mykola Gogol State University, Nizhyn, Ukraine [3]Deutsches Elektronen-Synchrotron DESY, Hamburg, Germany [4]Centre for X-ray and Nano Science (CXNS), Deutsches Elektronen-Synchrotron DESY, Hamburg, Germany [5]Institute for Nuclear Research of the National Academy of Sciences of Ukraine, Kyiv, Ukraine

Zirconia-based materials are widely used in optical, energy-related, and functional ceramic applications owing to their excellent mechanical, thermal, dielectric, and chemical stability. Their properties can be tailored through stabilization with aliovalent dopants, including luminescent rare-earth (Eu, Yb, Gd) and transition-metal (Mn, Cu) ions. Such modifications affect phase composition, defect concentration, and local crystal structure, which in turn determine the optical response of the material. Due to their sensitivity to the host lattice, luminescent centers can serve as probes of structural transformations, defect formation, and energy-transfer processes in zirconia-based systems.

In this work, synchrotron vacuum ultraviolet (VUV) spectroscopy combined with structural characterization was applied to investigate two groups of zirconia-based materials. The first group consisted of Y-stabilized and rare-earth-doped ZrO2 ceramics, where the yttrium content was varied to control phase composition, while rare-earth ions served as luminescent probes of the local crystal environment. The second group included cubic zirconia stabilized with approximately 10 mol.% rare-earth oxides, in which dopant ions simultaneously acted as structural stabilizers and emitting centers.

Undoped and doped zirconia nanopowders and ceramics containing Y, Eu, Yb, Gd, Mn and Cu were synthesized by coprecipitation and impregnation methods and calcined at 400 °C. The obtained powders were compacted and sintered in the temperature range 600-1600 °C. Structural and microstructural characterization was performed using Raman spectroscopy, Fourier-transform infrared spectroscopy, UV-Vis diffuse reflectance spectroscopy, scanning electron microscopy, and energy-dispersive X-ray spectroscopy.

Luminescence excitation and emission spectra were measured at the P66 beamline of PETRA III (DESY, Hamburg) in the 120-330 nm and 290-1100 nm spectral ranges, respectively. The analysis of recorded emission-excitation maps allowed separating intrinsic host-related emission from dopant-related luminescence and provided insight into the excitation pathways in zirconia-based materials.

The optical response was found to depend strongly on both phase composition and dopant incorporation. In Y- and rare-earth-codoped zirconia ceramics, changes in the relative fractions of monoclinic, tetragonal, and cubic phases significantly modified the intrinsic and dopant-related luminescence. Excitation-dependent measurements revealed rare-earth excitation through both host band-to-band absorption and charge-transfer states and enabled separation of intrinsic defect emission from impurity-related luminescence. Similar competition

between defect- and impurity-related recombination channels was observed in Mn- and Cu-doped materials. These findings indicate the coexistence of multiple luminescence pathways involving intrinsic defects, oxygen vacancies, and impurity centers, with their relative contributions governed by crystal structure and dopant type.

The results demonstrate the potential of synchrotron VUV spectroscopy as a powerful tool for elucidating the relationships between crystal structure, defects, excitation mechanisms, and luminescent properties in zirconia-based materials.

Acknowledgement. The authors are thankful to DESY User Office for financial support from the NEPHEWS project funded by the HORIZON-Europe program (project IC-20251517-EC).

Cite as: Larysa Khomenkova et al., "Synchrotron VUV and structural characterization of zirconia-based nanopowders and ceramics", in *Book of Abstracts of the 27th Symposium on Photonics and Optics (SPO 2026)*, Kyiv, 2–6 November 2026, p. 34.

We4.1 INVITED · WEDNESDAY 14:00 CET · 15:00 KYIV #285

ENSA – European Neutron Science Association

Astrid Schneidewind

Forschungszentrum Jülich GmbH, Jülich, Germany

Abstract not yet received

Cite as: Astrid Schneidewind, "ENSA – European Neutron Science Association", in *Book of Abstracts of the 27th Symposium on Photonics and Optics (SPO 2026)*, Kyiv, 2–6 November 2026, p. 36.

We4.2 INVITED · WEDNESDAY 14:10 CET · 15:10 KYIV #221

Generation and properties of free neutrons

Anatoliy Senyshyn

Heinz Maier-Leibnitz Zentrum (MLZ), Technical University of Munich, Garching, Germany

In the current contribution the principles of free neutron generations will be introduced along with the basic properties of free neutrons relevant for scattering experiments. Different types of neutron interaction with matter, its parametrisation and features will be discussed in brief as a base for various neutron related experimental techniques.

Cite as: Anatoliy Senyshyn, "Generation and properties of free neutrons", in *Book of Abstracts of the 27th Symposium on Photonics and Optics (SPO 2026)*, Kyiv, 2–6 November 2026, p. 37.

We4.3 INVITED · WEDNESDAY 14:35 CET · 15:35 KYIV #250

Neutron Diffraction

Oleksandr Prokhnenko

Helmholtz-Zentrum Berlin für Materialien und Energie, Berlin, Germany

This talk will introduce the basic principles of neutron diffraction and how it can be used to investigate structure and properties of modern materials. It will provide an overview of the experimental setups, type of information that can be obtained, and make a comparison with x-ray scattering techniques. The talk is aimed at beginners with no prior experience in neutron diffraction and will offer an accessible starting point for understanding its applications in materials research.

Cite as: Oleksandr Prokhnenko, "Neutron Diffraction", in *Book of Abstracts of the 27th Symposium on Photonics and Optics (SPO 2026)*, Kyiv, 2–6 November 2026, p. 38.

We4.4 INVITED · WEDNESDAY 14:50 CET · 15:50 KYIV #286

Small-Angle Neutron Scattering: Principles and Applications

Oleksandr Tomchuk

ISIS Neutron and Muon Source, STFC Rutherford Appleton Laboratory, Didcot, United Kingdom

Small-angle neutron scattering (SANS) is a versatile technique for investigating structural features and spatial correlations in materials over length scales typically ranging from approximately 1 to 100 nm, with the accessible range depending on the instrument configuration. By probing variations in neutron scattering length density, SANS provides insight into nanoscale structures in a wide variety of systems, including nanoparticles, porous materials, polymers, colloidal dispersions and supramolecular assemblies.

This introductory lecture will outline the fundamental principles of SANS, from the origin of neutron scattering contrast to the interpretation of scattering curves in reciprocal space. Particular attention will be given to the structural information that can be extracted from experimental data, including particle size and shape distributions, internal morphology, pore dimensions, characteristic distances and the organisation of multicomponent systems. The sensitivity of SANS to different length scales and volume fractions will also be discussed, together with the advantages of isotopic contrast variation, particularly through hydrogen/deuterium substitution.

Beyond characterising individual structural units, SANS offers a powerful means of investigating interactions and collective behaviour in complex systems. The separation of the scattering intensity into form-factor and structure-factor contributions provides access to interparticle correlations, enabling the analysis of attractive and repulsive interactions, aggregation, and concentration-dependent structural organisation.

The lecture will demonstrate how SANS connects nanoscale structure with the physical properties and behaviour of soft and complex materials, highlighting both the possibilities and limitations of the technique.

Cite as: Oleksandr Tomchuk, "Small-Angle Neutron Scattering: Principles and Applications", in *Book of Abstracts of the 27th Symposium on Photonics and Optics (SPO 2026)*, Kyiv, 2–6 November 2026, p. 39.

We4.5 INVITED · WEDNESDAY 15:05 CET · 16:05 KYIV #216

Neutron Reflectometry: the interfaces study technique overview and use-cases

Yehor Kosiachkin

Data Management and Software Centre (DMSC), European Spallation Source ERIC, Copenhagen, Denmark

Neutron Reflectometry (NR) is a technique to study interfaces and surfaces along normal direction to the sample surface. This talk covers technique overview followed by use-case examples from different scientific fields.

Cite as: Yehor Kosiachkin, "Neutron Reflectometry: the interfaces study technique overview and use-cases", in *Book of Abstracts of the 27th Symposium on Photonics and Optics (SPO 2026)*, Kyiv, 2–6 November 2026, p. 40.

We4.6 INVITED · WEDNESDAY 15:20 CET · 16:20 KYIV #225

Introduction to Neutron Spectroscopy

Oleg Petrenko

Institut Laue-Langevin, Grenoble, France

Presentation aims to give a very brief introduction into neutron spectroscopy. Inelastic neutron scattering probes the dynamics of materials by measuring the energy exchanged between neutrons and a sample during scattering. This allows access to a wide range of phenomena, including atomic diffusion, molecular rotations and vibrations, phonons, magnons, crystal-field excitations, and other magnetic or electronic processes. Atomic and magnetic excitations govern key properties including heat capacity, thermal transport, electrical behaviour, and the interactions between atoms. Neutron scattering provides direct access to excitations and yields data that can be compared with theoretical models. It is one of the most powerful techniques for measuring phonon and magnon dispersions, investigating phase transitions, and studying hydrogen dynamics in condensed matter systems.

Cite as: Oleg Petrenko, "Introduction to Neutron Spectroscopy", in *Book of Abstracts of the 27th Symposium on Photonics and Optics (SPO 2026)*, Kyiv, 2–6 November 2026, p. 41.

We4.7 INVITED · WEDNESDAY 15:35 CET · 16:35 KYIV #226

Imaging and tomography using monochromatic beams of thermal neutrons

Anatoliy Senyshyn[2], Mykhailo Drozdenko[1], Vasyl Ryukhtin[1], Gergely Farkas[1]

[1]Nuclear Physics Institute of the Czech Academy of Sciences, Řež, Czech Republic [2]Heinz Maier-Leibnitz Zentrum (MLZ), Technical University of Munich, Garching, Germany

Neutron imaging using thermal neutrons is well suited for the investigation of, for example, damaged concrete, lithium batteries, fuel elements for fusion reactors, munition, cultural heritage objects, and fossils. A particularly powerful application of neutron beams lies in biological research, such as monitoring water transport in plants or performing in-vivo observations of bee larva development.

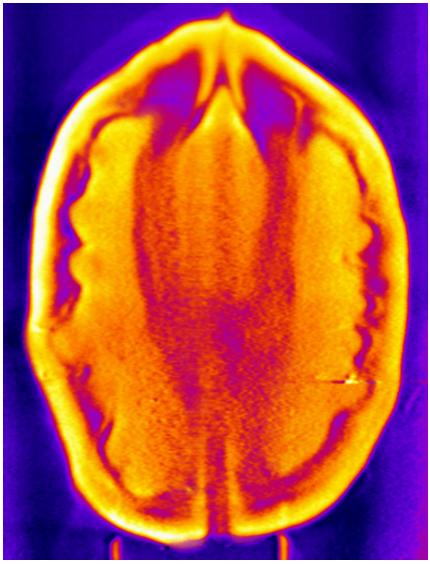


Figure. 3D model of walnut reconstructed using neutron tomography

Recently, neutron imaging and tomography techniques have become available in the Laboratory of Neutron Physics at the light-water reactor LVR-15 in Řež near Prague. In this contribution, we briefly introduce the basic instrumentation and present the first results.

Cite as: Anatoliy Senyshyn et al., "Imaging and tomography using monochromatic beams of thermal neutrons", in *Book of Abstracts of the 27th Symposium on Photonics and Optics (SPO 2026)*, Kyiv, 2–6 November 2026, p. 42.

We4.8 INVITED · WEDNESDAY 15:50 CET · 16:50 KYIV #258

Advancing Fast-Neutron Imaging with Metal-Halide Detectors

Aditya Bhardwaj[1], Kostiantyn Sakhatskyi[1], Anastasiia Sakhatska[1], Andrey L. Rogach[2], Han Kai[3], Maksym V. Kovalenko[1], Markus Strobl[4], Pavel Trtik[4], Sergii Yakunin[1], Vladyslav Orlov[1], Wu Ye[2], Yevhenii Padniuk[1], Yuliia Kominko[1], Zhiguo Xia[3]

[1]ETH Zurich, Zurich, Switzerland [2]City University of Hong Kong, Hong Kong SAR, China [3]South China University of Technology, Guangzhou, China [4]Paul Scherrer Institute PSI, Villigen, Switzerland

Fast-neutron imaging offers unique capabilities for the nondestructive investigation of dense and compositionally heterogeneous objects, particularly those containing both light and heavy elements. However, its wider application is limited by the efficiency of existing detection technologies. Conventional scintillator screens typically combine hydrogen-rich polypropylene (PP) with luminescent ZnS microparticles. Their heterogeneous structure limits the conversion of recoil-proton energy into scintillation light and introduces optical scattering that compromises spatial resolution.

Here, we demonstrate fast-neutron imaging using a monocompound organic-inorganic metal halide scintillator, tetraphenylphosphonium manganese bromide (TPP_2MnBr_4). Its structure combines hydrogen-rich organic cations and luminescent inorganic units within a single compound, enabling more efficient conversion of recoil-proton energy into visible light. Fast-neutron experiments performed at the NEUTRA beamline of the Paul Scherrer Institute demonstrate approximately 1.5 times higher light output from a 1.8 mm-thick TPP_2MnBr_4 screen compared to a commercial 2.5 mm-thick PP/ZnS reference. Moreover, the light yield normalized to neutron absorption is nearly four times higher. Radiographic experiments with polymer and mixed-material objects demonstrate a spatial resolution of approximately 1 line pair per millimeter, comparable to commercial screens.

These results highlight the potential of monocompound metal halide scintillators for improving the efficiency of fast-neutron imaging while maintaining high spatial resolution.

Cite as: Aditya Bhardwaj et al., "Advancing Fast-Neutron Imaging with Metal-Halide Detectors", in *Book of Abstracts of the 27th Symposium on Photonics and Optics (SPO 2026)*, Kyiv, 2–6 November 2026, p. 43.

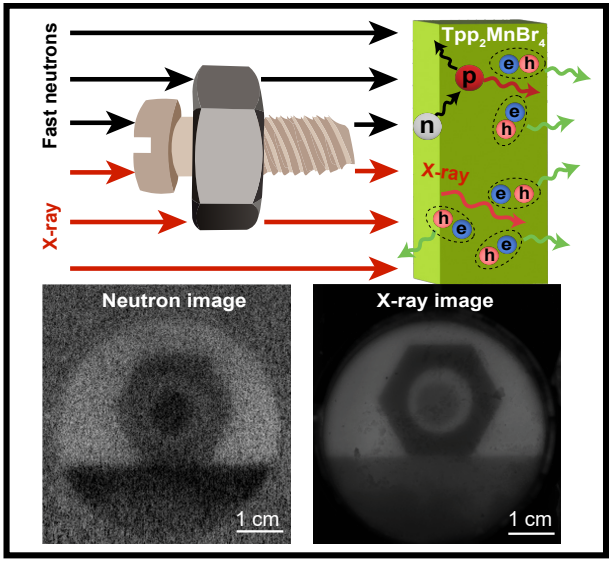


Figure. Schematic of fast-neutron and X-ray detection using a monocompound TPP_2MnBr_4 scintillator, with representative radiographs demonstrating the complementary imaging contrast of a plastic bolt and metal nut. Scale bars: 1 cm.

We4.9 INVITED · WEDNESDAY 16:05 CET · 17:05 KYIV #241

Neutron source at the MAC NSC "KIPT"

E. Rudychev, G. Kovalenko, Ivan Guk, P. Gladkikh, S. Prokhorets
National Science Center "Kharkiv Institute of Physics and Technology", Kharkiv, Ukraine

As can be seen from an overview of the primary, high-intensity neutron sources of various types [1], their characteristics enable research across a wide range of tasks in chemistry, biology, medicine, and solid-state physics. Unfortunately, Ukraine currently lacks neutron sources capable of supporting research in these fields at a sufficiently high level, or of facilitating the training and education of specialists for such work. Consequently, the development and implementation of projects involving high-intensity neutron sources within the country have become an urgent necessity [2].

One such project involves utilizing the 200 MeV electron beam from the multifunctional MAC complex NSC KIPT to create a pulsed neutron source with unique characteristics [2, 3].

In the high-charge mode, the facility's superconducting injector will accelerate electron bunches with a charge of up to 1 nC and a duration of 5 ps at a repetition rate of 500 kHz. In this mode, the average current at the injector output will not exceed 0.5 mA. Following acceleration in the linear accelerator, the electron energy will reach 200 MeV.

As indicated in [1], a single 200 MeV electron generates approximately 0.14 neutrons in a uranium target. The total average neutron flux at the exit of the neutron channel can reach 4.4 $\times 10^{14}$ s^{-1}.

The short length of the electron bunch enables the generation of short neutron pulses at the target, which allows for the use of the time-of-flight technique to measure neutron energy.

To determine the neutron flux at a distance of 10 m from the converter, the interaction of an electron bunch (with a charge of 300 pC and an energy of 205.5 MeV) with a tungsten converter was simulated using the MCNPX code. Targets with diameters of 10, 5, and 1 cm were considered. Based on the simulation results, specifically regarding the optimization of the neutron yield relative to the target parameters, a converter length of approximately 3 cm was found to be the most effective. Reducing the target diameter to 5 cm improves the temporal characteristics of the neutron beam. Calculations indicate that the neutron beam intensity at a distance of 10 m from the converter would decrease by no more than 20% in this case. The total number of neutrons detectable at this location per cm^2 would be 5.804×10^{-9} neutrons per electron. In this geometry, the energy resolution for 10 MeV neutrons would be approximately 8×10^{-3}.

[1] G.D. Kovalenko, I.S. Guk, P.I. Gladkikh, Neutron source based on the multifunctional accelerator complex of the NSC KIPT, // Problems of Atomic Science and Technology. 2023. № 6(148), p. 154-160, https://doi.org/10.46813/2023-148-154.

[2] P. I. Gladkikh, I. S. Guk, G. D. Kovalenko, S. I. Prokhorets, E. V. Rudychev, D. Yu. Shakhov, Multifunctional Accelerator Complex of NSC KIPT (monograph, in Ukrainian), NSC KIPT, Kharkiv: FOP Panov A. M., 2026, 124 pp. https://www.researchgate.net/publication/411425115

[3] P.I. Gladkikh, I.S. Guk, G.D. Kovalenko, S.I. Prokhorets, E.V. Rudychev, Pulsed neutron source at the multifunctional accelerator complex of the national science center "KIPT" // Problems of Atomic Science and Technology. 2025. №6(160), p. 47-49. https://doi.org/10.46813/2025-160-047

Cite as: E. Rudychev et al., “Neutron source at the MAC NSC ‘KIPT’”, in *Book of Abstracts of the 27th Symposium on Photonics and Optics (SPO 2026)*, Kyiv, 2–6 November 2026, p. 45.

We4.10 INVITED · WEDNESDAY 16:20 CET · 17:20 KYIV #287

Subcritical Assembly “Neutron Source” at NSC KIPT: Start-Up Results and Current Status

Andrii Zelinsky

National Science Center “Kharkiv Institute of Physics and Technology”, Kharkiv, Ukraine

Abstract not yet received

Cite as: Andrii Zelinsky, “Subcritical Assembly ‘Neutron Source’ at NSC KIPT: Start-Up Results and Current Status”, in *Book of Abstracts of the 27th Symposium on Photonics and Optics (SPO 2026)*, Kyiv, 2–6 November 2026, p. 47.

Thursday

5 November 2026

Workshop on Laser Processing of Materials for Advanced Optoelectronic Applications

Workshop on Sustainable Materials and Technologies for Optoelectronics and Sensors

Th1 Session 1 · 08:05–09:55 CET · 09:05–10:55 Kyiv

Th1.1	Advances in Efficiency Optimization of Ultrashort Pulse Laser Ablation of Metals	Mindaugas Gedvilas
Th1.2	Direct Laser Writing of Reconfigurable Vanadium Dioxide Devices	Amit Verma
Th1.3	Raman spectroscopy analysis of laser-induced graphene on polymer	Vladyslav Dzhahan
Th1.4	Fabrication, Optical, and Electrical Properties of Laser-reduced Graphene Oxide Films	Danylo Havryliuk
Th1.5	Calibration and Application of Industrial Laser Systems for Thin-Film Optoelectronics	Stanislav Serhiichuk

Th2 Session 2 · 10:15–11:30 CET · 11:15–12:30 Kyiv

Th2.1	Nanosecond laser-driven local synthesis of semiconductors: from 2D materials to supersaturated Ge-based alloys	Enrico Di Russo
Th2.2	Laser-Induced Crystallization of Ge/Sn Multilayer Amorphous Films	Volodymyr Yukhymchuk
Th2.3	Real-time optical inspection and classification of defects in DLW-microstructures	Ievgen Beliak
Th2.4	Deep learning methods for inverse design of diffractive optical elements taking into account technological limitations of direct laser writing	Oleksii Manko

Th3 Session 3 · 12:35–14:35 CET · 13:35–15:35 Kyiv

Th3.1	Element Mixing in Aziridinium based Hybrid Perovskites towards Tunable Optoelectronic Properties	Illia Guralskyi
Th3.2	Cysteine-based Hybrid Perovskite Exhibiting Thermally Tunable Dual-Band Photoluminescence	Valerii Y. Sirenko
Th3.3	Synthesis and Structural Phase Behaviour of B-Site-Mixed Methylammonium Lead–Tin Bromide Perovskites	Hanna Petrosova
Th3.4	Effect of a cationic surfactant on the formation and optical properties of perovskite quantum dots	Dmytro Haleliuk
Th3.5	Structural Diversity and Photocatalytic Properties of Hybrid Ruthenium Coordination Compounds Containing Metal Chloride Anions	Olesia Kucheriv
Th3.6	Thermal energy upconversion using thermally-activated delayed fluorescence materials	Oleg Dimitriev

Th4 Session 4 · 14:55–16:55 CET · 15:55–17:55 Kyiv

Th4.1	Earth-abundant compound semiconductors for solar energy conversion	Galina Gurieva
Th4.2	High-Throughput Robot-Assisted Screening of Sustainable Lead-Free Perovskite Materials for Energy Harvesting Applications	Oleksandr Stroyuk
Th4.3	"Green" Aqueous Synthesis and Understanding the Properties of Cu_2MSnS_4 (M = Zn, Ni, Fe) Nanocrystals	Oleksandra Ivakhno-Tsehelnyk
Th4.4	Controlling phase composition in VOx thin films using getter technologies	Tomash Sabov
Th4.5	CMOS field-effect transistor-based optoelectronic sensors and possible applications	Dovile Cibiraite-Lukenskiene

Th1.1 INVITED · THURSDAY 08:05 CET · 09:05 KYIV #207

Advances in Efficiency Optimization of Ultrashort Pulse Laser Ablation of Metals

Mindaugas Gedvilas

Center for Physical Sciences and Technology (FTMC), Vilnius, Lithuania

Ultrashort pulse laser ablation has become an important technology for precision micro- and nanoprocessing of metals, enabling high spatial resolution, minimal thermal damage, and precise control over surface morphology. However, achieving high processing efficiency while maintaining excellent surface quality remains a major challenge, particularly in industrial applications where high throughput and reproducibility are essential. Understanding the relationships between laser processing parameters, energy deposition, and material removal mechanisms is therefore crucial for optimizing laser ablation processes.

This invited talk presents recent theoretical and experimental advances in ultrashort pulse laser ablation efficiency, with particular emphasis on laser fluence optimization. Analytical modeling, numerical simulations, and experimental results are combined to demonstrate strategies for maximizing ablation efficiency in various laser processing applications, including Gaussian beam laser ablation, thin sheet laser cutting, and laser lift-off.

Special attention is given to the influence of burst-mode irradiation on ablation efficiency and the emergence of bistable ablation regimes. The effects of plasma shielding and attenuation of incident laser radiation by ablation debris are examined to provide deeper insight into the physical mechanisms governing material removal efficiency.

The presented findings contribute to a better understanding of energy-efficient ultrashort pulse laser–matter interactions and provide practical guidelines for optimizing laser processing parameters and facilitating the transfer of ultrafast laser technologies from laboratory research to industrial manufacturing.

Cite as: Mindaugas Gedvilas, "Advances in Efficiency Optimization of Ultrashort Pulse Laser Ablation of Metals", in *Book of Abstracts of the 27th Symposium on Photonics and Optics (SPO 2026)*, Kyiv, 2–6 November 2026, p. 50.

Th1.2 INVITED · THURSDAY 08:35 CET · 09:35 KYIV #297

Direct Laser Writing of Reconfigurable Vanadium Dioxide Devices

Amit Verma

Indian Institute of Technology Kanpur, Kanpur, India

Vanadium dioxide (VO_2) is a phase-transition material which exhibits a reversible structural and an associated insulator-metal phase transition at 68 °C. This phase transition is accompanied with a large change in VO_2 resistivity and dielectric-response properties enabling a host of electromagnetic switching applications from microwave to THz, infrared, and visible wavelengths. Conventional VO_2 device fabrication typically requires VO_2 synthesis in a highly controlled oxygen environment, multiple photolithography steps, film etching, and contact deposition steps. This leads to a significant increase in device development cost due to increased process time and the use of environmentally hazardous chemicals. This talk will discuss a lithography-free, single-step approach for VO_2 synthesis via direct laser-induced oxidation of vanadium thin films under ambient conditions and its application to fabricate VO_2 phase transition based reconfigurable electronic, microwave, infrared, and optical devices.

Cite as: Amit Verma, "Direct Laser Writing of Reconfigurable Vanadium Dioxide Devices", in *Book of Abstracts of the 27th Symposium on Photonics and Optics (SPO 2026)*, Kyiv, 2–6 November 2026, p. 51.

Th1.3 ORAL · THURSDAY 09:05 CET · 10:05 KYIV #276

Raman spectroscopy analysis of laser-induced graphene on polymer

Vladyslav Dzhahan[1], Andriy Korchovyi[2], Petro Lytvyn[2], S. Kondratenko[1], V. Dzhagan[2]

[1]Taras Shevchenko National University of Kyiv, Kyiv, Ukraine [2]V. Lashkaryov Institute of Semiconductor Physics of the National Academy of Sciences of Ukraine, Kyiv, Ukraine

The development of flexible electronics and biomedical sensors requires new materials that combine electrical conductivity, mechanical flexibility, and ease of fabrication. Among the most promising candidates are graphene and its chemical derivatives – graphene oxide (GO) and reduced graphene oxide (rGO). Graphene exhibits exceptionally high carrier mobility and mechanical strength; however, the absence of a bandgap severely limits its use in transistor and sensor structures where a high on/off current ratio is essential. The partially reduced graphene oxide, on the contrary, exhibits dielectric or semiconducting behaviour depending on the oxidation degree. One very popular approach to fabrication of the rGO films and structures is reduction of the preliminarily deposited GO film. The second approach that becomes increasingly popular with the recent development of affordable pulsed laser sources – local formation of graphene-like structures directly on carbon-based materials, such as polymers, paper etc [1]. The advantages of this approach are using no chemicals or deposition equipment, making laser-induced graphene (LIG) a cost-effective and sustainable approach.

Raman spectroscopy is one of the most versatile characterization tools for graphene material, because it can provide information on both the degree of oxidation, structural perfection, and number of monolayers. The key indicators are the D/G intensity ratio, which reflects the defect level, and the shape of the 2D band and its intensity ratio to the G band, indicating number of monolayers and lateral dimensions of graphene structure. The numerous Raman studies reported in the literature so far have demonstrated that the properties of LIG can be tuned in very broad range by using different laser sources and different regimes of their operation. At the same time, most of the studies used CO2 laser for LIG formation on polyimide, while other commercially available pulsed lasers were less studied. Especially attractive for the wide application of LIG technology are commercial laser scanning markers, which has not yet been systematically studied.

In this work, we analyse in detail the Raman spectra of LIG formed on the surface of polyimide (Kapton) formed by ns-pulsed 355 nm and CW 450 nm laser markers with different intensity, scanning speed, repetition rate and other parameters. We established correlations between the LIG structure and laser processing parameters, as well as analyse the properties of UV-induced LIG obtained in this work with the results of the literature, where other laser sources were used.

Establishing clear correlations between laser exposure regimes and rGO properties is an essential foundation for reproducible fabrication of sustainable materials for flexible electronics, biomedical sensors, and micro-energy systems.

Acknowledgement. The work was supported by the NRFU project 2023.05/0022 (Andriy Korchovyi, Volodymyr Dzhagan) and DAAD project "SOMMER!" (Vladyslav Dzhahan, Serhiy Kondratenko).

[1] V. Dzhagan, Y. Azhniuk, O. Dubikovskyi and D.R.T. Zahn. Advances in laser-based lithography and processing of semiconductors and insulators. J. Phys.: Condensed Matter 38 (25) 253001.

Cite as: Vladyslav Dzhahan et al., "Raman spectroscopy analysis of laser-induced graphene on polymer", in *Book of Abstracts of the 27th Symposium on Photonics and Optics (SPO 2026)*, Kyiv, 2–6 November 2026, p. 52.

Th1.4 ORAL · THURSDAY 09:25 CET · 10:25 KYIV #282

Fabrication, Optical, and Electrical Properties of Laser-reduced Graphene Oxide Films

Andriy Korchovyi[2], Anna Yevmenova, Danylo Havryliuk[1], Nazar Mazur[2], Oleksandr Kulbachynskyi[2], Petro Lytvyn[2], Stanislav Serhiichuk[2], V. Dzhagan[2], Volodymyr Yukhymchuk[2], Zinoviia Tsybrii[2]

[1]National University "Zaporizhzhia Polytechnic", Zaporizhzhia, Ukraine [2]V. Lashkaryov Institute of Semiconductor Physics of the National Academy of Sciences of Ukraine, Kyiv, Ukraine

The electrical conductivity and optical properties of graphene oxide are determined by and can be tuned through its degree of reduction, while residual oxygen-containing groups serve as active sites for functionalization and chemical sensing. Reduction is typically achieved via chemical or thermal methods. Laser reduction, by contrast, is a single-step, localized process that requires neither masks nor chemical agents [1].

In this study, a local reduction of graphene oxide films was performed by laser engraver with emission wavelength of 355 nm. For obtaining the initial graphene oxide films, a graphene oxide solution (Merck) was deposited onto quartz substrates via drop-casting and dried at 100°C for 1.5 hours. Several samples were obtained for further investigations, by annealing the as deposited GO films with different regimes of operation of the laser engraver, such as at a frequency of the pulses, a pulse width, and a scanning speed. The obtained samples were characterized by Raman spectroscopy and by four-probe conductivity measurements. On selected samples the thickness of the films was determined by Atomic Force Microscopy. Based on the analysis performed, the following optimal processing parameters were determined: 100 laser passes at a frequency of 130 kHz, and a scanning speed of 2000 mm/s. Under these conditions, the electrical characteristics were measured, revealing a resistance for the reduced graphene oxide (rGO) ranging from 4 kΩ/sq to 5.4 kΩ/sq. The results demonstrate that laser photoreduction of graphene oxide enables the control of surface resistance. Raman spectroscopy was employed to investigate the structural changes in graphene oxide resulting from laser photoreduction. This technique allows for the assessment of the carbon structure's state, the degree of structural ordering, and the presence of defects within the graphene matrix. Particular attention was focused on the characteristic D and G bands, located at approximately 1350 cm^{-1} and 1580 cm^{-1}, respectively. Additionally, the 2D band (~2700 cm^{-1}) was observed and analyzed; its intensity increases noticeably following laser annealing, indicating transformation of a significant part of graphene oxide into graphene.

The results obtained confirm the high potential of laser-induced reduction for the localized formation of electrically conductive thin-film structures and the creation of functional elements for electronic and chemical sensing systems.

Acknowledgement. The work was supported by the National Research Foundation of Ukraine, project # 2023.05/0022.

[1] V. Dzhagan, Y. Azhniuk, O. Dubikovskyi and D.R.T. Zahn. Advances in laser-based lithography and processing of semiconductors and insulators. J. Phys.: Condensed Matter 38 (25), 253001.

Cite as: Andriy Korchovyi et al., "Fabrication, Optical, and Electrical Properties of Laser-reduced Graphene Oxide Films", in *Book of Abstracts of the 27th Symposium on Photonics and Optics (SPO 2026)*, Kyiv, 2–6 November 2026, p. 54.

Th1.5 ORAL · THURSDAY 09:40 CET · 10:40 KYIV #302

Calibration and Application of Industrial Laser Systems for Thin-Film Optoelectronics

Stanislav Serhiichuk[1], Danylo Havryliuk[2], Nazar Mazur[1], Petro Lytvyn[1], Andriy Korchovyi[1], Serhii Levytskyi[1], Volodymyr Yukhymchuk[1], V. Dzhagan[1]

[1]V. Lashkaryov Institute of Semiconductor Physics of the National Academy of Sciences of Ukraine, Kyiv, Ukraine [2]National University "Zaporizhzhia Polytechnic", Zaporizhzhia, Ukraine

Controlling laser-matter interaction is a fundamental prerequisite for the maskless patterning of advanced materials, thin films, and functional optoelectronic architectures. Because modern research frequently relies on high-cost specialized lithographic equipment, industrial laser engravers and markers operating across diverse spectral and temporal regimes present a highly accessible and versatile alternative. However, achieving material modification without uncontrolled thermal damage or phase degradation critically depends on rigorous system calibration and understanding the interrelation between laser parameters.

In this work, we present a comparative methodological study of four industrial laser systems covering a broad spectral range from ultraviolet (UV) to far-infrared (FIR). The practical utility of this multi-system infrastructure was demonstrated through tailored processing protocols for various material classes. The 355 nm UV system enables precise surface ablation and patterning with minimal heat-affected zones due to high photon energy and localized absorption. The 1064 nm NIR fiber laser provides deep photothermal interaction and bulk modification, making it ideal for single-pulse patterning and localized thermal annealing of semiconductor alloys, such as GeSn, VOx, or rGO. The 455 nm diode laser offers controlled continuous-wave thermal treatment and selective reduction of graphene oxide thin films, enabling direct maskless patterning of conductive planar circuits and micro-electrode arrays. Considering the CO_2 system at 10.6 μm, it provides highly efficient photothermal processing of dielectric substrates, oxide materials, and polymers owing to strong infrared absorption.

To ensure reproducible processing conditions, empirical laser power and pulse energy calibration protocols were established using a thermopile power/energy sensor. For the diode-pumped solid-state (DPSS) UV laser operating at 355 nm, the average output power and effective peak pulse power were modeled as non-linear functions of pulse repetition rate and Q-switch interval settings. Calibration of the 455 nm diode system revealed a non-linear optical power response in the low-power domain while maintaining linear scaling of nominal power at higher excitation levels. For the 1064 nm NIR fiber laser, the calibration reveals a distinct lasing threshold near 15% nominal power, above which the real output power increases almost linearly. In the case of the gas CO_2 laser at 10.6 μm, the real power dependence on the nominal setting demonstrates a stable, nearly linear behavior across the entire range (0–100%). Furthermore, pulse repetition frequency variation has a minimal impact on the output power for both IR systems.

Our comparative analysis establishes a practical framework for selecting optimal laser sources, pulse characteristics, and energy density windows, demonstrating that properly calibrated commercial laser markers can substitute expensive lithographic setups for functional prototyping in semiconductor physics and optoelectronics.

Acknowledgement. The work was supported by the National Research Foundation of Ukraine, project # 2023.05/0022.

Cite as: Stanislav Serhiichuk et al., "Calibration and Application of Industrial Laser Systems for Thin-Film Optoelectronics", in *Book of Abstracts of the 27th Symposium on Photonics and Optics (SPO 2026)*, Kyiv, 2–6 November 2026, p. 55.

Th2.1 INVITED · THURSDAY 10:15 CET · 11:15 KYIV #240

Nanosecond laser-driven local synthesis of semiconductors: from 2D materials to supersaturated Ge-based alloys

Enrico Di Russo

University of Padova, Padova, Italy

The precise, localized control of semiconductor properties is a central challenge in the development of next-generation nanoelectronics, optoelectronics, and photonic devices. Among the available processing techniques, nanosecond pulsed laser processing has emerged as a uniquely powerful tool, offering spatial and temporal confinement of energy deposition, compatibility with existing Si CMOS infrastructure, and the ability to drive materials far from thermodynamic equilibrium. In this work, we demonstrate two complementary laser-based routes to engineer semiconductor thin films: nanosecond UV pulsed laser annealing (PLA) for the crystallization of sputter-deposited MoS_2, and nanosecond pulsed laser melting (PLM) for the fabrication of supersaturated GeSn alloys.

Wafer-scale synthesis of high-quality layered transition metal dichalcogenides (TMDs) remains a key bottleneck for their integration into functional devices. Sputtering offers a scalable and reproducible route to large-area MoS_2 films; however, as-deposited layers are amorphous and require post-deposition crystallization. Here, we present a two-step process in which stoichiometric MoS_2 films are sputter-deposited on Si/SiO_2 substrates and subsequently irradiated with nanosecond UV (248 nm) laser pulses in a N_2-rich atmosphere [1]. By systematically varying the number of pulses and the energy density, we identify the processing window yielding (002)-oriented nanocrystalline 2H-MoS_2 films with uniform coverage, characterized by Raman spectroscopy, XRD, RBS, AFM, and TEM. Heat flow simulations confirm that laser energy confinement keeps the Si/SiO_2 substrate temperature well below the back-end-of-line thermal budget limit of Si CMOS technology (770 K), enabling direct integration with existing device platforms.

Building on the concept of laser-driven non-equilibrium processing, we further exploit nanosecond PLM to fabricate GeSn alloys with Sn concentrations far exceeding the equilibrium solid solubility in Ge. Above ~8 at.% Sn, GeSn alloys undergo an indirect-to-direct bandgap transition, enabling mid-infrared light emission. Using a two-step ex-situ approach, thin Sn films (<50 nm) are deposited by DC magnetron sputtering onto Ge(100) and Ge-on-Si substrates. Subsequent nanosecond PLM melts the near-surface region, enabling rapid Sn diffusion and incorporation up to 20 at.% [2,3]. SIMS depth profiles confirm box-like, uniform Sn distributions, while TEM reveals Sn segregation along threading dislocations at the GeSn/Ge interface. The substitutional Sn fraction correlates with regrowth velocity: lower energy densities favor substitutional incorporation, while a low-energy corrective pulse (300–400 mJ/cm^2) restores substitutional Sn in samples processed at higher fluences (800 mJ/cm^2). Reciprocal space maps reveal tensile strain from thermal mismatch, lowering the Sn threshold for the direct bandgap transition.

Together, these results establish nanosecond pulsed laser processing as a versatile and CMOS-compatible platform for the local, tunable synthesis of advanced semiconductors, with direct implications for 2D material integration, mid-infrared photonics, and beyond.

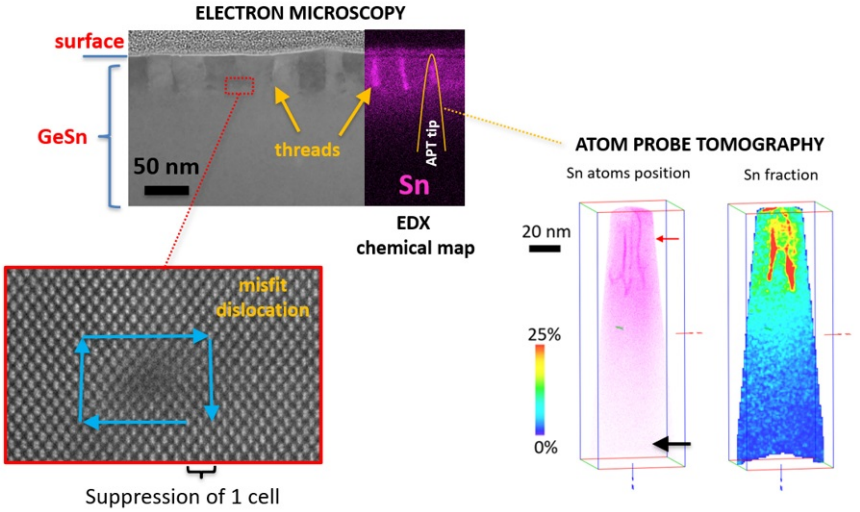


Figure. TEM micrograph and APT 3D reconstruction of the GeSn sample, illustrating the material structure and local Sn distribution.

[1] E. Di Russo et al., Synthesis of Large-Area Crystalline MoS_2 by Sputter Deposition and Pulsed Laser Annealing. ACS Appl. Electron. Mater. 5 (5) 2862 (2023).

[2] E. Di Russo et al., Synthesis of relaxed Ge0.9Sn0.1/Ge by nanosecond pulsed laser melting. Applied Surface Science 612, 155817 (2023).

[3] D. Fontana et al., Ex-situ n-type heavy doping of Ge1-xSnx epilayers by surface Sb deposition and pulsed laser melting. Applied Surface Science 600, 154112 (2022).

Cite as: Enrico Di Russo, "Nanosecond laser-driven local synthesis of semiconductors: from 2D materials to supersaturated Ge-based alloys", in *Book of Abstracts of the 27th Symposium on Photonics and Optics (SPO 2026)*, Kyiv, 2–6 November 2026, p. 57.

Th2.2 ORAL · THURSDAY 10:45 CET · 11:45 KYIV #245

Laser-Induced Crystallization of Ge/Sn Multilayer Amorphous Films

Volodymyr Yukhymchuk[1], Petro Lytvyn[1], M. V. Mazur[1], Serhii Antonin[1], Olga Kapush[1], Oksana Isaieva[1], Oleksandr Gudymenko[1], Volodymyr Dzhagan[1], Andriy Dmytruk[2]

[1] V. Lashkaryov Institute of Semiconductor Physics of the National Academy of Sciences of Ukraine, Kyiv, Ukraine [2] Institute of Physics of the National Academy of Sciences of Ukraine, Kyiv, Ukraine

GeSn alloy thin films grown on silicon substrates attract significant attention in infrared optoelectronics. The primary advantage of GeSn is transforming indirect-bandgap germanium into a direct-bandgap semiconductor through substitutional incorporation of 8–10 at.% tin atoms into the Ge lattice. Since the equilibrium solubility of Sn in Ge at room temperature does not exceed 1 at.%, nonequilibrium growth methods and ultrafast processing are required to form metastable solid solutions. This work presents a comparative study of the crystallization of 150-nm-thick multilayer amorphous Ge/Sn films (10 periods: 12.8 nm Ge / 2.2 nm Sn) on a Ge/Si(100) buffer layer under pulsed nanosecond (355 nm, 22 ns) and femtosecond (800 nm,150 fs) laser irradiation.

Multilayer heterostructures were deposited via vacuum thermal evaporation of Ge and Sn targets. The resulting samples were subjected to laser annealing: nanosecond UV scanning with pulse energy density from 0.1 to 0.6 J/cm2 and a femtosecond Ti: sapphire laser system with varying cumulative energy density. Structural, morphological, and optical characterization of the polycrystalline films was performed using Raman spectroscopy, X-ray diffraction (XRD), scanning electron microscopy (SEM), and time-of-flight secondary ion mass spectrometry (ToF-SIMS).

Multilayer heterostructures were deposited via vacuum thermal evaporation of Ge and Sn targets.

According to Raman and XRD data, pulsed nanosecond annealing within a pulse energy density range of 0.2-0.3 J/cm2 induces the most effective solid-phase crystallization. At 0.2 J/cm2, a maximum substitutional tin concentration of ≈10 at.% Sn is achieved. The average nanocrystal size, determined via the Scherrer equation from the (111) reflection, is ≈13 nm. Increasing energy density above 0.35 J/cm2 accelerates Sn segregation, and 0.6 J/cm2 leads to film ablation. At the laser spot periphery (2-3 μm), lateral thermal wave propagation promotes an atomically smooth surface without melting. For femtosecond laser annealing (800 nm), a regime with low energy density per individual pulse was selected; therefore, a cumulative effect (≈10^4 pulses) was utilized to crystallize the amorphous layer. The optimal absorbed energy density is 150 J/cm2, enabling incorporation of up to 7.5 at.% Sn. Higher cumulative energy leads to Sn precipitation out of lattice sites. Contrary to theoretical expectations of higher efficiency for femtosecond annealing due to ultrafast Sn freezing, nanosecond treatment yields a higher substitutional Sn fraction (10 at.% vs. 7.5 at.%). ToF-SIMS depth profiles explain this: femtosecond annealing induces interfacial atomic intermixing across the boundary between the GeSn film and Ge buffer layer. SEM showed that the surface morphology of the films under these two types of laser processing also differs substantially; in particular, femtosecond annealing causes self-organization of laser-induced periodic surface structures (LIPSS), promising for textured optoelectronic applications. Consequently, it can

be concluded that pulsed nanosecond laser annealing (0.2–0.3 J/cm^2) is the optimal method for producing planar polycrystalline GeSn films with a direct-bandgap structure.

Acknowledgement. This work was supported by the National Research Foundation of Ukraine under Project No. 2023.03/0186 “Strain Engineering of the Electronic Structure of GeSn Thin Films for Next-Generation IR Optoelectronics”.

Cite as: Volodymyr Yukhymchuk et al., “Laser-Induced Crystallization of Ge/Sn Multilayer Amorphous Films”, in *Book of Abstracts of the 27th Symposium on Photonics and Optics (SPO 2026)*, Kyiv, 2–6 November 2026, p. 59.

Th2.3 ORAL · THURSDAY 11:00 CET · 12:00 KYIV #248

Real-time optical inspection and classification of defects in DLW-microstructures

Ievgen Beliak, Yuriy Chehil

Institute for Information Recording of the National Academy of Sciences of Ukraine, Kyiv, Ukraine

Direct Laser Writing (DLW) enables the fabrication of micro- and submicron structures with predefined geometries directly on the surface of photosensitive and functional materials. At the same time, variations in laser irradiation parameters, non-uniformity of thin-film properties, and instability of individual fabrication stages can result in local defects that affect the geometrical and functional characteristics of the fabricated structures.

Optical microscopy provides non-destructive inspection of direct-laser-written structures; however, manual analysis of a large number of fabricated elements is time-consuming and depends on subjective operator assessment. Computer vision and automated image analysis make it possible to move from visual identification of individual imperfections to systematic defect detection, classification, and quantitative evaluation directly during inspection of the fabrication process.

An approach to automated optical inspection of DLW-fabricated microstructures is proposed, comprising the following stages: (1) acquisition and preprocessing of optical images or video sequences of the fabricated areas; (2) development of a taxonomy of characteristic defects based on their morphological features and deviations from the target geometry; (3) automated detection and localization of defective regions using computer vision methods and their assignment to predefined defect classes; (4) quantitative evaluation of defect parameters, including their dimensions, number, spatial distribution, and degree of deviation from the reference structure; and (5) correlation of the detected defects with their probable physical and technological origins to provide feedback to the direct laser writing process.

The proposed approach enables a transition from post-process visual inspection to automated analysis of fabricated microstructures under near-real-time conditions. The obtained results can be used for objective assessment of direct laser writing quality, accumulation of statistical data on characteristic defects, and further adaptive correction of technological parameters during the fabrication of micro- and submicron structures.

Cite as: Ievgen Beliak et al., "Real-time optical inspection and classification of defects in DLW-microstructures", in *Book of Abstracts of the 27th Symposium on Photonics and Optics (SPO 2026)*, Kyiv, 2–6 November 2026, p. 61.

Th2.4 ORAL · THURSDAY 11:15 CET · 12:15 KYIV #227

Deep learning methods for inverse design of diffractive optical elements taking into account technological limitations of direct laser writing

Oleksii Manko, Ievgen Beliak

Institute for Information Recording of the National Academy of Sciences of Ukraine, Kyiv, Ukraine

Direct Laser Writing (DLW) is the basis of maskless photolithography for the fabrication of high-resolution diffractive optical elements (DOEs) and coded structures for long-term storage media. Traditional DOE design relies on analytical calculations, electromagnetic modeling, and iterative parameter optimization. For free-form geometries, the configuration space grows rapidly, which leads to significant computational costs and complicates the search for structures that simultaneously satisfy optical and technological requirements.

Inverse design based on machine and deep learning allows replacing repeated iterative search by building a relationship between the target optical response and the geometry of the element. Such methods (tandem networks, generative-adversarial networks, conditional diffusion models) are successfully used in integrated photonics and metasurfaces. At the same time, they have not been adapted to the technological context of DLW for optical information storage.

The development of deep learning methods and models for automated inverse design of DOE geometry taking into account the constraints of the real recording process is a relevant task. The following stages were proposed: (1) selection of a DOE class compatible with DLW equipment and formalization of target characteristics (diffraction efficiency, angular intensity distribution) as optimization problems; (2) construction of a direct diffraction model and formation of a dataset of "geometry - optical response" pairs; (3) formalization of DLW technological limitations as model constraints or components of the loss function, which combines the deviation of the optical response from the target with a penalty for violating technological limitations; (4) comparison of a tandem network, a generative-adversarial network, and a conditional diffusion model with a physically informed component in terms of response reproduction accuracy, speed, and variety of solutions relative to classical methods; (5) manufacturing prototypes on the DLW installation, measuring their optical response, and correcting the direct and inverse models in a closed loop of "design → manufacturing → measurement → correction".

The proposed approach is expected to substantially reduce the design cycle of new DOEs by replacing repeated manual optimization with automated generation and subsequent verification. It can also expand the range of accessible geometries through free-form design and provide a reproducible set of data and models for further development, in particular for increasing the recording density of long-term optical storage media.

Cite as: Oleksii Manko et al., "Deep learning methods for inverse design of diffractive optical elements taking into account technological limitations of direct laser writing", in *Book of Abstracts of the 27th Symposium on Photonics and Optics (SPO 2026)*, Kyiv, 2–6 November 2026, p. 62.

Th3.1 INVITED · THURSDAY 12:35 CET · 13:35 KYIV #224

Element Mixing in Aziridinium based Hybrid Perovskites towards Tunable Optoelectronic Properties

Illia Guralskyi, Danylo Kreiman, Dmytro Haleliuk, Hanna Petrosova, Olesia Kucheriv

Taras Shevchenko National University of Kyiv, Kyiv, Ukraine

Hybrid organic-inorganic metal halide perovskites are promising semiconductors for photovoltaic and light-emitting applications owing to their compositional flexibility and tunable optoelectronic properties. In this presentation, aziridinium-based three-dimensional perovskites are discussed as a versatile platform for band-gap engineering through halide substitution and B-site metal alloying.

Three series were studied: mixed bromide–iodide $(AzrH)PbBr_xI_{3-x}$, mixed chloride–bromide $(AzrH)PbBr_xCl_{3-x}$, and mixed lead–tin $(AzrH)Pb_xSn_{1-x}Br_3$ perovskites, where AzrH denotes the aziridinium cation. Their structural and optical properties were investigated using single-crystal and powder X-ray diffraction, diffuse reflectance spectroscopy, and photoluminescence measurements, complemented by density functional theory (DFT) calculations.

All investigated systems demonstrate substantial compositional control over their structural and electronic properties. Halide substitution preserves the cubic perovskite framework while modifying lattice parameters and optical band gaps. In the mixed bromide-iodide series, the band gap can be tuned from 1.57 to 2.23 eV. The chloride-bromide compounds exhibit systematic band-gap variation accompanied by composition-dependent photoluminescence, with emission maxima shifting from 445 to 504 nm as the bromide content increases. In both systems, preferential incorporation of one halide relative to its precursor proportion highlights the importance of verifying the final material composition. Complementarily, Pb–Sn alloying enables effective band-gap reduction from 2.41 eV for $(AzrH)SnBr_3$ to 1.95 eV for the equimolar composition, demonstrating pronounced band-gap bowing associated with interactions between Pb- and Sn-derived electronic states. The mixed-metal compounds retain a cubic structure at room temperature across the investigated composition range, while exhibiting composition-dependent temperature-induced phase transitions.

These findings establish aziridinium-based perovskites as a versatile materials platform for tailoring semiconductor properties through complementary anion and cation-site engineering. The demonstrated control over crystal structure, optical absorption, and emission provides a foundation for developing hybrid perovskites with targeted properties for next-generation optoelectronic applications.

Cite as: Illia Guralskyi et al., "Element Mixing in Aziridinium based Hybrid Perovskites towards Tunable Optoelectronic Properties", in *Book of Abstracts of the 27th Symposium on Photonics and Optics (SPO 2026)*, Kyiv, 2–6 November 2026, p. 63.

Th3.2 ORAL · THURSDAY 13:05 CET · 14:05 KYIV #231

Cysteine-based Hybrid Perovskite Exhibiting Thermally Tunable Dual-Band Photoluminescence

Valerii Y. Sirenko[1], Olesia Kucheriv[1], Sergiu Shova[2], Illia Guralskyi[1]

[1] *Taras Shevchenko National University of Kyiv, Kyiv, Ukraine* [2] *"Petru Poni" Institute of Macromolecular Chemistry, Iași, Romania*

Hybrid organic–inorganic perovskites offer versatile platforms for tuning light emission through their chemical composition and structural dimensionality. However, achieving tunable broadband emission in single-phase lead iodide systems remains challenging. In this work, we present the synthesis, structural characterization, and optical properties of a two-dimensional hybrid perovskite, (L-cysH)$PbI_3 \cdot H_2O$, incorporating L-cysteinium cations (L-CysH). Its crystal structure comprises inorganic layers of corner- and edge-sharing PbI_6 octahedra, separated by organic cations and water molecules connected through an extensive hydrogen-bonding network. Optical absorption measurements yield a band gap of 2.53 eV. Under 377 nm excitation at 78 K, the compound exhibits dual-band photoluminescence comprising a relatively narrow peak near 473 nm and a broad band centered at approximately 534 nm, tentatively attributed to free and self-trapped excitons, respectively. Cooling from 238 to 78 K increases the integrated emission intensity approximately 27-fold and shifts the CIE chromaticity coordinates from (0.342, 0.399) to (0.385, 0.473), demonstrating thermally tunable emission. Arrhenius analysis yields a thermal-quenching activation energy of 72.3 meV. Density functional theory calculations reveal an indirect fundamental band gap with a nearby direct transition and band-edge states predominantly derived from the inorganic lead iodide framework. The combined results highlight amino-acid-based hybrid perovskites as a platform for exploring temperature-responsive luminescence without halide mixing or extrinsic luminescent dopants.

[1] Sirenko, V. Y., Kucheriv, O. I., Shova, S. & Gural'skiy, I. A. Cysteine-Based Hybrid Perovskite Exhibiting Thermally Tunable Dual-Band Photoluminescence. Inorg. Chem. 65, 21837–21848 (2026).

Cite as: Valerii Y. Sirenko et al., "Cysteine-based Hybrid Perovskite Exhibiting Thermally Tunable Dual-Band Photoluminescence", in *Book of Abstracts of the 27th Symposium on Photonics and Optics (SPO 2026)*, Kyiv, 2–6 November 2026, p. 64.

Th3.3 ORAL · THURSDAY 13:20 CET · 14:20 KYIV #237

Synthesis and Structural Phase Behaviour of B-Site-Mixed Methylammonium Lead–Tin Bromide Perovskites

Hanna Petrosova, Olesia Kucheriv, Illia Guralskyi
Taras Shevchenko National University of Kyiv, Kyiv, Ukraine

Compositional engineering through metal mixing is an important strategy for tailoring the structural and functional properties of hybrid metal halide perovskites.[1] While extensive research has focused on mixing organic cations at the A-site and halide anions at the X-site,[2] the effects of B-site mixing on phase stability and structural transitions remain less explored. In this work, we investigate a series of methylammonium lead–tin bromide perovskites, $MAPb_{1-x}Sn_xBr_3$, to establish the relationship between metal composition, crystal structure, and temperature-dependent phase behaviour.[3]

Mixed-metal perovskites with different Sn contents were synthesized, and their compositions and structural characteristics were examined using powder X-ray diffraction (PXRD) and scanning electron microscopy coupled with energy-dispersive X-ray spectroscopy (SEM–EDX). These complementary methods enabled the assessment of phase formation, changes in the crystal lattice, and the incorporation of tin into the lead-based perovskite framework. The systematic evolution of the diffraction patterns with increasing Sn content demonstrates the structural compatibility of the two end-member compounds and the formation of mixed-metal compositions.

Temperature-dependent studies, including differential scanning calorimetry (DSC), were used to investigate phase transitions across the compositional series. The results were combined with dielectric spectroscopy measurements to construct a temperature–composition phase diagram and evaluate the influence of B-site mixing on the structural phase behaviour. The introduction of tin slightly stabilizes the cubic phase, while the overall changes in structural transition temperatures remain relatively modest compared with those commonly associated with A-site or X-site mixing. Nevertheless, metal mixing affects the ordering and dynamics of the methylammonium cations, highlighting the interplay between the inorganic framework and the organic sublattice.

This study demonstrates the feasibility of preparing mixed Pb–Sn bromide perovskites across a broad compositional range and emphasizes the importance of systematic compositional and temperature-dependent characterization. Understanding how B-site mixing influences phase stability provides a basis for the rational design of hybrid perovskites with tailored structural and functional properties, relevant to the development of optoelectronic materials.

[1] D. S. Kreiman, O. I. Kucheriv, B. Laurentiu, S. Shova and I. A. Gural'skiy, Mater. Chem. Front., 2026, 10, 3056–3067.

[2] O. I. Kucheriv, D. A. Haleliuk, S. Shova and I. A. Gural'skiy, Dalt. Trans., 2025, 54, 1618–1624.

[3] G. Rimkus, S. Balčiūnas, H. R. Petrosova, O. I. Kucheriv, R. Lemežis, V. Klimavičius, V. Kalendra, J. Banys, I. A. Gural'skiy and M. Šimėnas, Chem. Mater., 2025, 37, 1314–1320.

Cite as: Hanna Petrosova et al., "Synthesis and Structural Phase Behaviour of B-Site-Mixed Methylammonium Lead–Tin Bromide Perovskites", in *Book of Abstracts of the 27th Symposium on Photonics and Optics (SPO 2026)*, Kyiv, 2–6 November 2026, p. 65.

Th3.4 ORAL · THURSDAY 13:35 CET · 14:35 KYIV #230

Effect of a cationic surfactant on the formation and optical properties of perovskite quantum dots

Dmytro Haleliuk[1], Illia Guralskyi[1], Sergiu Shova[2]

[1] Taras Shevchenko National University of Kyiv, Kyiv, Ukraine [2] "Petru Poni" Institute of Macromolecular Chemistry, Iași, Romania

Hybrid organic-inorganic perovskites (HOIPs) have attracted considerable attention in recent years. These materials are characterized by the general formula ABX_3 (where A is an organic cation, B is a metal cation, and X is a halide anion) and exhibit unique semiconducting properties. Driven by extensive research, these compounds have been successfully integrated as active layers in solar cells, light-emitting diodes, lasers, and photodetectors [1]. A highly promising direction in HOIP research focuses on quantum dots (QD) – semiconductor nanoparticles characterized by a high photoluminescence quantum yield and a size-tunable optical bandgap [2].

In this study, $MAPbBr_3$ (MA = methylammonium) quantum dots were synthesized using varying amounts of a cationic surfactant, cetyltrimethylammonium bromide (CTAB). The synthesis was based on the ligand-assisted reprecipitation method. The photoluminescence and absorption spectra of the synthesized quantum dot colloids were acquired and analyzed. The results revealed that with increasing CTAB concentration, the photoluminescence intensity reaches a maximum at 3.5 equivalents of CTAB, accompanied by a slight widening of the optical bandgap from 2.3 to 2.4 eV.

Furthermore, the morphology of the quantum dot samples was investigated using transmission electron microscopy. Powder X-ray diffraction analysis revealed that an excess of the surfactant leads to the formation of a two-dimensional (2D) perovskite incorporating the CTAB cation. This 2D perovskite was successfully isolated as a single crystal, and its crystal structure was unambiguously determined via single-crystal X-ray diffraction. The presented findings open up new avenues for the application of these nanomaterials in the development of advanced optoelectronic devices.

[1] K. Zhou, B. Qi, Z. Liu, X. Wang, Y. Sun and L. Zhang. Advanced Organic–Inorganic Hybrid Materials for Optoelectronic Applications. Adv. Funct. Mater. 2024, 34, 2411671.

[2] D. S. Kreiman, O. I. Kucheriv, L. Baltag, S. Shova and I. A. Gural'skiy. Bandgap Engineering via Halide Mixing in Aziridinium Lead Perovskites: towards Tunable Quantum Dots. Mater. Chem. Front. 2026, 10 (17), 3056–3067.

Cite as: Dmytro Haleliuk et al., "Effect of a cationic surfactant on the formation and optical properties of perovskite quantum dots", in *Book of Abstracts of the 27th Symposium on Photonics and Optics (SPO 2026)*, Kyiv, 2–6 November 2026, p. 67.

Th3.5 ORAL · THURSDAY 13:50 CET · 14:50 KYIV #233

Structural Diversity and Photocatalytic Properties of Hybrid Ruthenium Coordination Compounds Containing Metal Chloride Anions

Olesia Kucheriv[1], Valerii Y. Sirenko[1], Igor O. Fritsky[1], Illia Guralskyi[1], Sergiu Shova[2]

[1] Taras Shevchenko National University of Kyiv, Kyiv, Ukraine [2] "Petru Poni" Institute of Macromolecular Chemistry, Iași, Romania

Ten new hybrid coordination compounds containing the octahedral tris(2,2′-bipyridine)ruthenium(II) cation and structurally diverse metal chloride anions were synthesized and characterized by single-crystal X-ray diffraction. The inorganic components exhibit remarkable structural diversity; the formation of discrete tetrahedral anions $[CoCl_4]^{2-}$, $[CdCl_4]^{2-}$, oligomeric units $[Zn_2Cl_6]^{2-}$, $[Cu_2Cl_6]^{2-}$, $[Cd_4Cl_{12}]^{4-}$, $[Fe_2Cl_6O]^{2-}$, $[Bi_4Cl_{16}]^{4-}$ and polymeric chains $[Sb_6Cl_{22}]_n^{4n-}$, $[Sb^{III}{}_6Sb^{V}Cl_{27}]_n^{4n-}$ and $[Pb_7Cl_{22}DMF]_n^{8n-}$ is observed. The metal chloride anions display a wide range of coordination environments, including tetrahedral, trigonal-bipyramidal, square-pyramidal, and octahedral geometries, often with substantial distortions and pronounced differences in metal–chloride bond lengths. These coordination polyhedra are connected through edge- and corner-sharing to form diverse inorganic architectures, with particularly complex arrangements observed for antimony- and lead-containing compounds. In several structures, the inorganic substructures are further distinguished by mixed oxygen/chlorine coordination, coordinated solvent molecules, or additional interpolyhedral contacts.

The optical and photocatalytic properties of two selected compounds containing cobalt(II) and cadmium(II) chloride species were investigated. Both compounds exhibit similar visible-light absorption dominated by the common ruthenium-based chromophore. However, differences in their emission characteristics indicate that the inorganic component influences the relaxation of photoexcited states.

The photocatalytic activity of both compounds was evaluated by monitoring the degradation of 2-mercaptobenzothiazole under visible-light irradiation. Both materials promoted degradation, whereas negligible changes were observed in control experiments conducted without either illumination or catalyst. The cobalt-containing compound exhibited substantially higher photocatalytic activity than its cadmium-containing analogue, achieving complete disappearance of the characteristic absorption band of the organic substrate within the investigated irradiation period. This difference suggests that the inorganic component plays an important role in determining photocatalytic performance. The accessible redox chemistry of cobalt(II) may contribute to electron-transfer processes following excitation of the ruthenium-based chromophore, whereas cadmium(II) is more likely to influence the reaction through structural, electrostatic, or adsorption-related effects.

These results demonstrate that combining the same molecular photosensitizing component with different metal chloride species provides an effective strategy for generating hybrid materials with diverse crystal architectures and tunable optical and photocatalytic properties. The findings highlight the importance of inorganic substructure design in establishing relationships between crystal structure, photophysical behaviour, and photocatalytic performance.

Cite as: Olesia Kucheriv et al., “Structural Diversity and Photocatalytic Properties of Hybrid Ruthenium Coordination Compounds Containing Metal Chloride Anions”, in *Book of Abstracts of the 27th Symposium on Photonics and Optics (SPO 2026)*, Kyiv, 2–6 November 2026, p. 68.

Th3.6 INVITED · THURSDAY 14:05 CET · 15:05 KYIV #217

Thermal energy upconversion using thermally-activated delayed fluorescence materials

Oleg Dimitriev[1], Alexander Fedoryak[1], Chih-Hao Chang[2], Dovydas Blazevicius[3], Fu-Chuan Fan[2], Gintare Krucaite[3], Petro Smertenko[1], Saulius Grigalevicius[3], Shih-Wei Huang[2]

[1] V. Lashkaryov Institute of Semiconductor Physics of the National Academy of Sciences of Ukraine, Kyiv, Ukraine [2] Yuan Ze University, Taoyuan, Taiwan [3] Kaunas University of Technology, Kaunas, Lithuania

Heat and thermal radiation are large components of energy provided by direct sun radiation (where infrared constitutes a significant portion), terrestrial radiation, byproducts of industrial and agricultural activity, physical, chemical and biological processes in nature as well. However, a subsequent conversion of thermal energy into other useful forms such as electricity or mechanical work is associated with significant irreversible losses and generally low efficiencies if operating at modest temperature differences. Therefore, novel principles of thermal energy conversion into convenient forms, which are less dependent on high temperatures and temperature gradients as well as on spontaneous discharge, are still of great demand. Thermally activated delayed fluorescence (TADF) is an interesting option for thermal energy upconversion into the visible light, where the latter can be further used for solar cell operation to produce electricity or for direct lighting. In TADF process, the thermal activation step is needed to fulfill an electronic transition from the triplet to singlet energy level of the TADF emitter, from which radiative relaxation of the excited electron occurs, where heat might be exploited as a side energy assisting luminescence. In this work, the potential of heat upconversion to visible light through thermal management of OLEDs of the third generation is demonstrated. We show that the performance of OLEDs based on specific TADF emitters can be effectively enhanced by heating. In particular, enhancement of electroluminescence by 9-12 times was achieved when operating near the turn-on voltage and heating the device to 50 °C, while enhancement decreases at higher applied biases. Upon heating, enhancement of the external quantum efficiency and power efficiency of the devices was achieved by factors of up to one order of magnitude and 13-16%, respectively. Power upconversion efficiency of low-energy heat to light energy was estimated to be low, of the order of 0.1%, but being feasible due to abundance of the waste heat. From the practical point of view, exploiting OLEDs at high temperatures may still be a challenging task due to the potentially negative long-term impact of heat on device performance, which should be prevented as well. By overcoming the related problems, the thermal management of emissions and the energy upconversion of TADF-based OLEDs promise potential application of this phenomenon for heat harvesting and energy-saving applications.

Cite as: Oleg Dimitriev et al., "Thermal energy upconversion using thermally-activated delayed fluorescence materials", in *Book of Abstracts of the 27th Symposium on Photonics and Optics (SPO 2026)*, Kyiv, 2–6 November 2026, p. 70.

Th4.1 INVITED · THURSDAY 14:55 CET · 15:55 KYIV #232

Earth-abundant compound semiconductors for solar energy conversion

Galina Gurieva, Susan Schorr

Helmholtz-Zentrum Berlin für Materialien und Energie, Berlin, Germany

The need of handling eco-friendly and cheap compound semiconductors in thin film photovoltaics (PV) has constantly pushed the research towards more environmentally friendly materials, such as Kesterite-type compound semiconductors Cu2ZnSnS4 (CZTS), Cu2ZnSnSe4 (CZTSe) and Cu2ZnSn(S,Se)4 (CZTSSe). They present the only critical raw material (CRM) free thin film PV technology with tunable band gap energy and excellent long-term stability. The current record efficiency for CZTSSe solar cells of 16.5 %[1] highlights the great potential of these abundant chalcogenides to support a sustainable energy transition. Additionally, finding alternative semiconductor materials with suitable properties remains a task of utmost importance for the widespread use of renewable energies.

In record devices these chalcogenide absorber materials generally show a non-stoichiometric composition which is possible due to a remarkable flexibility of their crystal structure. This ability to accept deviations from stoichiometry is correlated to the formation of intrinsic point defects [2]. The formation of such defects, like vacancies, antisites and interstitials, is driven thermodynamically by minimizing the Gibbs free energy of the crystal. The key issue for kesterite solar cells is the large open-circuit voltage deficit which is caused by three main factors: (i) a non-homogeneous absorber composition resulting in bandgap fluctuations [3] and formation of secondary phases, (ii) structural disorder like Cu/Zn disorder [4] or intrinsic point defects[2] causing strong band tailing [3] and (iii) the multi-element composition and the variable valence of Sn resulting in complicated defect properties[5].

Ternary nitrides ZnGeN2 and ZnSnN2 are being considered as promising candidates for photovoltaic absorber materials, containing uniquely elements of low toxicity and low resource criticality. Further to bandgap tuning by alloying, we have shown that these compounds possess a second mechanism for bandgap tuning through cation disorder [6].

The presentation will discuss the potential of point defect engineering to optimize the key factors limiting the open circuit voltage of the potential solar cell. Based on the off-stoichiometry type model for quaternary chalcogenides [2] correlating chemical composition and occurring intrinsic point defects in these compound semiconductors, a compositional region for highly efficient devices can be revealed. Changing the degree of Cu/Zn disorder varies the band gap energy as well as the value of PLmax[7]. The Cu/Zn disorder can be influenced by a thermal annealing process [8] nowadays technologically applied as post-deposition treatment. Cation disorder is also important for the bandgap engineering in ZnGeN2, showing an interplay with the unavoidable oxygen content in the material[6].

The presentation is based on our systematic experimental studies of quaternary compound semiconductors applying advanced analytical methods like neutron and synchrotron X-ray diffraction, photoluminescence and UV-Vis spectroscopy.

[1] https://www.nlr.gov/pv/cell-efficiency

[2] S.Schorr et al., J. Phys.: Energy 2 (2020) 012002

[3] T.Gokmen et al., Appl. Phys. Lett. 103 (2013) 103506

[4] S.Schorr et al., Europ. J. Mineral. 19 (2007) 65

[5] R.Fonoll-Rubio et al., Energy Environ. Sci. 14 (2021) 507

[6] Z.Wang et al., J. Mat. Chem. C 12 (2024) 1124

[7] G.Gurieva et al., Sol. En. Mat. Sol. Cells 248 (2022) 112009

[8] D.Toebbens et al., Phys. Stat. Solidi B 253 (2016) 1890

Cite as: Galina Gurieva et al., "Earth-abundant compound semiconductors for solar energy conversion", in *Book of Abstracts of the 27th Symposium on Photonics and Optics (SPO 2026)*, Kyiv, 2–6 November 2026, p. 71.

Th4.2 INVITED · THURSDAY 15:25 CET · 16:25 KYIV #298

High-Throughput Robot-Assisted Screening of Sustainable Lead-Free Perovskite Materials for Energy Harvesting Applications

Oleksandr Stroyuk

Helmholtz Institute Erlangen-Nürnberg for Renewable Energy (HI ERN), Forschungszentrum Jülich GmbH, Erlangen, Germany

Abstract not yet received

Cite as: Oleksandr Stroyuk, "High-Throughput Robot-Assisted Screening of Sustainable Lead-Free Perovskite Materials for Energy Harvesting Applications", in *Book of Abstracts of the 27th Symposium on Photonics and Optics (SPO 2026)*, Kyiv, 2–6 November 2026, p. 73.

Th4.3 ORAL · THURSDAY 15:55 CET · 16:55 KYIV #236

"Green" Aqueous Synthesis and Understanding the Properties of Cu_2MSnS_4 (M = Zn, Ni, Fe) Nanocrystals

Oleksandra Ivakhno-Tsehelnyk[1], L. Hertling[1], H. Thomas[1], V. Dzhagan[2], S. Kondratenko[3], D. R. T. Zahn[1]

[1] Chemnitz University of Technology, Chemnitz, Germany [2] V. Lashkaryov Institute of Semiconductor Physics of the National Academy of Sciences of Ukraine, Kyiv, Ukraine [3] Taras Shevchenko National University of Kyiv, Kyiv, Ukraine

Quaternary chalcogenides based on Cu_2ZnSnS_4 (CZTS) are attracting attention as earth-abundant, low-cost semiconductor materials for thin-film photovoltaics (PV) and thermoelectric (TE) applications. Substituting Zn with transition metals such as Ni, Fe, and Co offers opportunities to modify cation distribution, defect structure and electronic properties.

The "green" aqueous synthesis protocol originally developed for CZTS [1], was used to explore the possibility of synthesising Cu_2MSnS_4 (M = Zn, Ni, Fe, Co) nanocrystals (NCs). Protocol modifications have enabled the synthesis of different compositions, particularly Cu_2NiSnS_4 (CNTS), while the synthesis of Fe- and Co-containing compounds remains challenging. This study demonstrates that CZTS and CNTS NCs can be synthesised and size-selected under the same temperature, pressure and atmospheric conditions.

The combination of X-ray diffraction, Raman spectroscopy, ultraviolet-visible (UV-vis) spectroscopy and photoemission/inverse photoemission (UPS/IPES) spectroscopies facilitates the analysis of the influence of NCs size, crystallinity and secondary phases on the structural and electronic properties of these materials. The differences in the main A_1 Raman mode for CZTS and CNTS are discussed in particular. According to DFTB+ phonon calculations, these differences are likely from the distinct sensitivity of the CZTS and CNTS phonon spectra to defect type and stoichiometry.

The results obtained demonstrate the potential of environmentally friendly synthesis for creating CZTS-like nanomaterials, and highlight the necessity of combining experimental methods with modelling in order to reliably establish the relationship between structure and properties.

Acknowledgement. DFG Project ZA 146/59-1 and DAAD "SOMMER!"

[1] Stroyuk, O., Raevskaya, A., Selyshchev, O. et al. Sci Rep 8, 13677 (2018).

Cite as: Oleksandra Ivakhno-Tsehelnyk et al., "'Green' Aqueous Synthesis and Understanding the Properties of Cu_2MSnS_4 (M = Zn, Ni, Fe) Nanocrystals", in *Book of Abstracts of the 27th Symposium on Photonics and Optics (SPO 2026)*, Kyiv, 2–6 November 2026, p. 74.

Th4.4 ORAL · THURSDAY 16:10 CET · 17:10 KYIV #253

Controlling phase composition in VOx thin films using getter technologies

Oleksandr Dubikovskyi, Oleksiy Efremov, Tomash Sabov, Volodymyr Dzhagan, Boris Romanyuk, Denys Maziar, Ihor Danylenko, Serhii Antonin

V. Lashkaryov Institute of Semiconductor Physics of the National Academy of Sciences of Ukraine, Kyiv, Ukraine

Vanadium oxide (VOX) thin films of different phase composition and stoichiometry (1.5< x< 2.5) are widely used in nano- and micro-electronics, sensors, applied optics, and energy-saving technologies. There are about 20 phases of vanadium-oxygen system including main (VO, V2O3, V3O5, VO2, V2O5) and defective (VnO2n-1, VnO2n+1, etc) phases. Of particular interest are the VO2 phase, which have rapid reversible metal-insulator phase transition (MIT). The main issue is the simultaneous formation of different phases during VOx thin film growth. Therefore, despite the experience of several decades, during which many methods of synthesis of VO2 and other useful phases of VOx were developed, the problem of obtaining precisely the target phase, not only of a given stoichiometry (x=2) still remains. Accumulated experience has shown that, mainly, it is not possible to synthesize a VOX film of the required stoichiometry, phase composition and crystal structure in one step. To form a film with one dominant phase the usage of corrective post-treatments, like post low temperature annealing (under 450 oC) which leading to VO2 phase crystallisation in amorphous VOx films.

This work presents a new method of post-growth control of oxygen content in VOx thin films by gettering. It is implemented through an ultrathin intermediate aluminium layer deposited on the substrate before the VOx film deposition. During annealing the system in an inert environment, gradual diffusion of oxygen from the VOx film towards Al and its oxidation takes place. The 200 nm VO_x/Al/Si heterosystem was subject to thermodynamic analysis and investigated experimentally. The films were deposited by reactive RF magnetron sputtering using O2/Ar gas mixture, followed by annealing in Ar atmosphere. The crystalline structure of VOx thin films was investigated using X-Ray diffraction. The chemical state of the surface was analysed using X-Ray photoelectron spectroscopy. The redistribution of elemental composition in VO_x>$_2$/Al heterostructures during thermal oxygen gettering were investigated using secondary ion mass spectrometry (SIMS) depth profiling. A new cluster-ion analysis of VOx films was proposed. The results show that gettering promoted the V_2O_5-to-VO_2 transformation and incorporated Al as bridging Al–O–Al complexes replacing V–V dimers.

Acknowledgement. This work was partly supported by priority research program of NAS of Ukraine, project #0125U000799 “New physical principles and technologies for the development of the component base of modern infrared optoelectronics”

Cite as: Oleksandr Dubikovskyi et al., “Controlling phase composition in VOx thin films using getter technologies”, in *Book of Abstracts of the 27th Symposium on Photonics and Optics (SPO 2026)*, Kyiv, 2–6 November 2026, p. 75.

Th4.5 INVITED · THURSDAY 16:25 CET · 17:25 KYIV #209

CMOS field-effect transistor-based optoelectronic sensors and possible applications

Dovile Cibiraite-Lukenskiene[1], Alvydas Lisauskas[2], Patricija Ivanauskaite[1], Ricardas Petkus[1]

[1]Center for Physical Sciences and Technology (FTMC), Vilnius, Lithuania [2]Vilnius University, Vilnius, Lithuania

The nominal cut-off frequency of a semiconductor transistor does not necessarily mark the end of its potential for radio-frequency and terahertz applications. This talk explores the physics, development, and performance of antenna-coupled field-effect transistor detectors (TeraFETs) fabricated in CMOS technology, highlighting how nonlinear effects enable detection far beyond conventional transistor operating limits. Key aspects include the operating principles of TeraFETs, sensitivity limits across different semiconductor technologies, and the challenges of predicting device performance at frequencies above 2 THz. Examples of demonstrated applications in terahertz imaging, broadband and selective spectroscopy, gas sensing, and passive room-temperature detection will be presented. The talk will conclude with an outlook on the remaining scientific challenges and the potential of FET-based technologies for future terahertz sensing systems.

Cite as: Dovile Cibiraite-Lukenskiene et al., "CMOS field-effect transistor-based optoelectronic sensors and possible applications", in *Book of Abstracts of the 27th Symposium on Photonics and Optics (SPO 2026)*, Kyiv, 2–6 November 2026, p. 76.

Friday

6 November 2026

Conference on Optics and High Technology Material Science

Fr1 Session 1 · 08:10–09:40 CET · 09:10–10:40 Kyiv

Fr1.1	Generation, propagation and remote action of laser radiation	Liudmyla Derzhypolska
Fr1.2	Lasing of dye-doped mesostructured hybrid films in the critical (near-cutoff) regime: guided and Lummer–Gehrcke modes	Artem Podshebiakin
Fr1.3	Mie-Theory-Based Modeling of Light Extinction Spectra for Size and Shell-Thickness Estimation of Photochemically Synthesized pNIPAM-Coated Silver Nanoparticles	Andrii Lopatynskyi
Fr1.4	Renaissance of Magneto-Optics, or New Challenges – Old Methods	Mariia Pashchenko

Fr2 Session 2 · 10:00–11:45 CET · 11:00–12:45 Kyiv

Fr2.1	Molten Salts: A Versatile Platform for Engineering Functional Glasses and Crystalline Materials	Kateryna Terebilenko
Fr2.2	Effect of Cesium Doping on the Structural, Electronic, and Optical Properties of BaSnO3: A First-Principles Study for Photovoltaic Applications	Younes Elalaoui
Fr2.3	Electronic properties of inhomogeneous polar textures in $BaTiO_3$: A second-principles study	Binayak Mukherjee
Fr2.4	MgO-Mediated Densification and Electromechanical Hardening in BNT-BT-KNN Lead-Free Piezoceramics: Decoupling Porosity from Acceptor Effects	Saicharen Lakshmanan
Fr2.5	Effect of Graphite Inclusions on the Mechanical Properties of Silicon Carbide Ceramics	Rostyslav Vazhnenko
Fr2.6	Functionally Graded Polymer-Inorganic Composites as Advanced Wideband Microwave Absorbers	Oleksandr Zaichenko

Fr3 Session 3 · 13:00–13:45 CET · 14:00–14:45 Kyiv

Fr3.1	Structural and optical properties of undoped and Sn-doped β-Ga2O3 thin films deposited by ultrasonic spray pyrolysis	Polina Shamrovska
Fr3.2	Exhibition of spatial dispersion in optical properties of lattices of plasmonic nanoparticles	Eugene Bortchagovsky
Fr3.3	Effect of Nanoconfinement on Thermal Transport in Porous Silicon / Phase Change Material Composites	Vladyslav Tsehelnyi

Fr4 Session 4 · 13:45–14:33 CET · 14:45–15:33 Kyiv

Fr4.1	Hydrostatic Piezopotential in Unpoled Polycrystalline Particles: Finite Element Analysis of Grain Disorder, Cavitation Loading and Electrolyte Screening in Lead-Free Piezocatalysts	Saicharen Lakshmanan
Fr4.2	Alkali Volatilization as a Hidden Compositional Variable in Ta-Modified KNN: Electrical Characterisation and Preliminary Pencil-Lead-Break Response	Ayush K. Samal
Fr4.3	Sintering temperature influence on phase stability of scandium-stabilized ZrO_2 ceramics	Vita Prosolenko
Fr4.4	Dispersion analysis of IR spectra of $Mg_xZn_{1-x}O$ ceramics: phonon behaviour and phase composition	Viktor Bardakov
Fr4.5	Effect of ZnO electrical conductivity on the composition of hexagonal and cubic phases in MgxZn1-xO ceramics	Oleksandr Melnichuk
Fr4.6	Frustrated total internal reflection (Otto geometry) in a ZnO/6H-SiC structure: coupling through an air gap, a simulation study	Oleksii Sakhniuk
Fr4.7	Effect of Fluoride Modification on the Structure and Luminescence of Europium-Doped Phosphomolybdate Glasses	Kateryna Terebilenko
Fr4.8	Optical and electrophysical properties of some porous phosphate-molybdate glasses	Vasyl Cherevyshnyi
Fr4.9	Optical and dielectric properties of gelatin incorporated with K2Eu(PO4)(WO4) microcrystals	Vitalii Chornii
Fr4.10	Mechanical properties of a Ti–Cu nanocomposite prepared by mechanical alloying	Mykola Melnichenko
Fr4.11	Order in nanoparticles-doped liquid crystals	R. Karapinar
Fr4.12	Optical Absorption as a Probe of Fluorination and Crystalline Phase in P(VDF-TrFE): A Density Functional Theory Study	Zakhar Baranchykov

Fr5 Session 5 · 14:33–15:09 CET · 15:33–16:09 Kyiv

Fr5.1	Comparison of Theoretical and Experimental Raman and Infrared Spectra of P(VDF-TrFE): Phase and Composition Sensitivity	Dmytro Zaporoshchenko
Fr5.2	Aziridinium Cation based Cadmium Halide Hybrids	Danylo Kreiman
Fr5.3	Band-structure evolution in Cs2AgxNa1-xInCl6 double perovskites and its manifestation in VUV-excited photoluminescence	Denys Orlov
Fr5.4	Singlet Oxygen Generation by Different Types of MXenes ($Ti_3C_2T_x$) and Ti_3AlC_2 and Ti_3SiC_2 MAX Phases under Near-IR Excitation	Nazarii Tkach
Fr5.5	Optical Properties and Singlet Oxygen Generation in Tryptanthrin/MoS_2 Nanosystems	Nazarii Tkach
Fr5.6	Silicon incorporation and dislocation-related traps in GeSn and GeSiSn layers on Si: an impedance and photocurrent study	Andrii Pocherpailo
Fr5.7	Investigation of the influence of natural scenes conditions on thermal contrast and detection range of phase-change materials	Yevhen Melezhyk
Fr5.8	Low-Cost Real-Time Frame-to-Event Converter for Prototyping Event-Based Obstacle Detection	Vitalii Bortnik
Fr5.9	Water in Structures and Vibrations of Cellulose and Methylcellulose	Danylo Morozov

Fr6 Session 6 · 15:30–16:26 CET · 16:30–17:26 Kyiv

Fr6.1	Formation and properties of barrier structures based on p-CdTe:Cl fabricated by laser-induced indium doping	Serhii Levytskyi
Fr6.2	Deep Level Admittance Spectroscopy of PEDOT:PSS/Si Heterostructure	Oleh Bozhko
Fr6.3	Heterogeneity and oxidation of layered porous silicon studied by spectroscopic ellipsometry	Taras Veremeichyk
Fr6.4	Electrical Tuning of the Graphene Mode in a One-Dimensional Terahertz Photonic Microcavity with a Multilayer Graphene Stack: Effects of Gate Voltage and Number of Layers	Solmaz Salary
Fr6.5	Sub-Terahertz Penetration Loss Measurements at 131.6 GHz for Indoor Environments	Andrii Shekera
Fr6.6	Concepts for propagation-invariant spatiotemporal optical vortex formation	Dmytro Ivanskyi
Fr6.7	High-resolution fabrication of diffractive optical elements by direct laser writing	Dmytro Manko
Fr6.8	Tracking the thermostimulated diffusion in the structures 'Ag–$As_{40}S_{60}$ superthin film' with surface plasmon-polaritons	Sergii Mamykin
Fr6.9	Automatic Control System for a Precision Diffuse Optical Emitter	Viktor Shyshkin
Fr6.10	The influence of spectral composition and intensity of LED phytolighting on the growth of higher and lower plants	Praskoviya Boltovets
Fr6.11	Optical–Digital Analysis of Leaf Venation: Integrating Light and Scanning Electron Microscopy with Digital Morphometry	Oksana Futorna
Fr6.12	Structural properties of chitosan and chitosan-based composites	Diana Hurova
Fr6.13	Quantitative Assessment of Tryptophan Content in the Blood Plasma of Oropharyngeal Cancer Patients	Tymur Isokov
Fr6.14	Effect of Si doping and annealing on optical properties of MOCVD-grown β-Ga_2O_3 thin films	Andrii Kozak

Fr1.1 INVITED · FRIDAY 08:10 CET · 09:10 KYIV #299

Generation, propagation and remote action of laser radiation

Liudmyla Derzhypolska

Institute of Physics of the National Academy of Sciences of Ukraine, Kyiv, Ukraine

The efficiency of remote action of laser radiation is determined by the entire "source – channel – target" chain rather than by the laser alone. The report presents recent results of our group for each of its links.

At the source, two compact solid-state lasers are being developed: a diode-pumped Nd:YAG laser and an air-cooled thin-disk laser. The key element of both is a passive Q-switch based on a dye-doped polyurethane matrix. It uses the IR-1061 dye, whose absorption cross-section at 1064 nm is 22 times larger than that of BDN. With this Q-switch, a test Nd:YAG laser delivered single pulses of 0.96 J and 11 ns.

The energy that reaches a distant target, however, depends on how the beam is delivered through the atmosphere. It is shown that the optimal focusing condition corresponds to the minimum spot size rather than to the beam waist. The predicted linear growth of the minimum spot with distance has been verified on open atmospheric paths of up to 1 km. Turbulence effects are described within the kinetic photon distribution approach.

At the target, optoelectronic devices are considered. Their optical systems reflect part of the incident radiation back toward the source (the cat-eye effect). The effect is strongly enhanced by the image sensor located in the focal plane of the camera lens. On this basis, a model of camera detection under daylight background is proposed, and hidden cameras with apertures of 2–20 mm have been detected at about 100 m. At the same time, the lens concentrates the laser energy on the sensor and thus makes it vulnerable. Damage thresholds of CMOS image sensors at 1064 nm have been determined. Below 0.14 mJ in the camera aperture, only temporary blinding occurs, whereas above 1.7 mJ the camera fails irreversibly.

Acknowledgement. The work was carried out at the Institute of Physics, NAS of Ukraine, with the support of the Ministry of Education and Science of Ukraine within the initiative research project Pt/2026.2 "Development and study of energy-efficient methods and laser sources for remote action of laser radiation on moving objects".

Cite as: Liudmyla Derzhypolska, "Generation, propagation and remote action of laser radiation", in *Book of Abstracts of the 27th Symposium on Photonics and Optics (SPO 2026)*, Kyiv, 2–6 November 2026, p. 80.

Fr1.2 ORAL · FRIDAY 08:40 CET · 09:40 KYIV #260

Lasing of dye-doped mesostructured hybrid films in the critical (near-cutoff) regime: guided and Lummer–Gehrcke modes

Artem Podshebiakin[1], V. P. Yashchuk[1], E. V. Leonenko[2], E. A. Tikhonov[2], O. Liamets[2]

[1] *Taras Shevchenko National University of Kyiv, Kyiv, Ukraine* [2] *Institute of Physics of the National Academy of Sciences of Ukraine, Kyiv, Ukraine*

Integrated photonics needs film lasers as thin as possible, yet an asymmetric planar waveguide guides light only above the cutoff thickness h_c of its fundamental mode. We examine lasing in the critical regime, $h \approx h_c$, where the TE_0 effective index N approaches the substrate index n_s, and show that Lummer–Gehrcke (LG) modes [1] are its sub-cutoff special case.

The samples are sol–gel mesostructured TiO_2/Pluronic P123 and SiO_2/P123 films doped with rhodamine 6G on glass ($n_s = 1.515$). Dye in ∼12-nm micellar pores avoids concentration quenching up to 5 mmol/L, while the inorganic network sets n_f from 1.45–1.52 (SiO_2) to 1.56–1.69 (TiO_2). For $n_f = 1.565$, $h_c = 291$ nm ($\lambda = 580$ nm), so TiO_2 films of 200 nm ($0.69h_c$) and 340 nm ($1.17h_c$) bracket the cutoff, while SiO_2 films ($n_f \lesssim n_s$) have no guided mode.

Films were pumped transversely (532 nm, 15 ns, $\approx 3 \times 0.5$ mm^2 stripe). Imaging the end face across the spectrograph slit gave film and substrate spectra simultaneously; far-field spots, end masking and substrate immersion completed the measurements.

The 340-nm film is single-mode: $N - n_s = 1.6 \times 10^{-3}$, confinement factor 0.26, 73.5% of the mode power in the substrate. It lases with a sharp threshold (FWHM 60→5 nm) into a beam with interference fringes, whose divergence normal to the film, 6.3°, is fixed by the evanescent tail, $\theta_\perp \approx 2\sqrt{N^2 - n_s^2}$. Hence $N - n_s \approx 1.0 \times 10^{-3}$: the mode runs only 0.15° above the critical angle, and the divergence gauges cutoff proximity.

The 200-nm film shows a sharp threshold (FWHM 39→6.6 nm, twofold rebroadening above it), emitting from both film and substrate ends. Both channels narrow identically, whereas lateral emission stays ASE-like. As the pump grows 20-fold (0.007→0.15 MW/mm^2), the film output rises superlinearly and the substrate output linearly, concentrating energy in the film; immersion, which removes the reflection at the free substrate face, suppresses the substrate peak. The SiO_2 film needs an order of magnitude higher pump.

We attribute the substrate channel to LG modes. Below cutoff the film, bounded by total reflection at the air side and partial near-critical reflection at the substrate side, behaves as an LG plate: along the pumped stripe it releases coherent partial beams into the substrate at the grazing angle θ_s that maximises their gain path in the film [2,3]. Transfer-matrix calculations show that, as $h \to h_c$, this gain path grows from $\approx 14h$ (200 nm) to $\approx 100h$ ($0.96h_c$), while the beams' exit angle from the substrate end, $\arcsin\sqrt{n_s^2 - N^2}$ with $N = n_s \sin\theta_s$, falls from 12° to ≈ 1°; above h_c the LG mode turns continuously into TE_0. Near h_c the two lobes become collinear and mutually coherent, which explains the fringes and the narrow (9–11°) substrate-end spot of the 340-nm film.

The critical regime combines a nanoscale gain layer, mirrorless feedback and an output direction programmable by h or n_f; we discuss ultrathin lasers with substrate output coupling, divergence-based metrology of $N - n_s$ and index sensing at the substrate side.

FRI

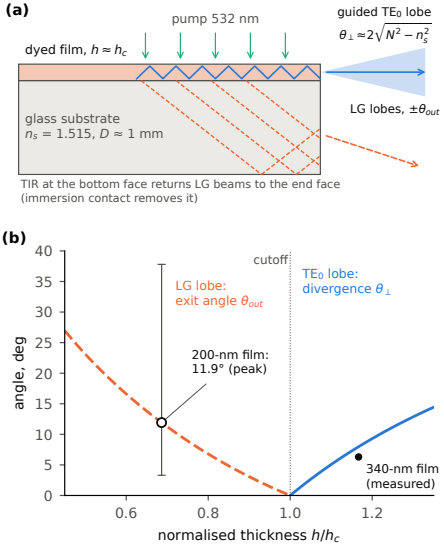


Figure. (a) Guided TE_0 and Lummer–Gehrcke (LG) emission channels near cutoff. (b) Calculated TE_0 divergence and LG exit angle versus h/hc (TiO_2, nf=1.565); filled dot – measured 340-nm film, open dot – predicted 200-nm film.

[1] E.A. Tikhonov et al., Laser Phys. 28, 045801 (2018).

[2] A. Penzkofer et al., Opt. Commun. 229, 279 (2004).

[3] J. Peter et al., J. Appl. Phys. 117, 015301 (2015).

Cite as: Artem Podshebiakin et al., "Lasing of dye-doped mesostructured hybrid films in the critical (near-cutoff) regime: guided and Lummer–Gehrcke modes", in *Book of Abstracts of the 27th Symposium on Photonics and Optics (SPO 2026)*, Kyiv, 2–6 November 2026, p. 81.

Fr1.3 ORAL · FRIDAY 08:55 CET · 09:55 KYIV #270

Mie-Theory-Based Modeling of Light Extinction Spectra for Size and Shell-Thickness Estimation of Photochemically Synthesized pNIPAM-Coated Silver Nanoparticles

Mariia Khutko, Vitalii Lytvyn, Petro Demydov, Volodymyr Chegel, Andrii Lopatynskyi

V. Lashkaryov Institute of Semiconductor Physics of the National Academy of Sciences of Ukraine, Kyiv, Ukraine

Silver nanoparticles (AgNPs) coated with stimuli-responsive polymers are promising hybrid nanomaterials for plasmonic and sensing applications [1]. Polymer shells provide steric stabilization and allow the nanoparticle surface to be functionalized [2]. In this work, AgNPs coated with poly(N-isopropylacrylamide) (pNIPAM) were synthesized by a photochemically assisted method. The order in which reagents were added and the UV irradiation time were varied to optimize nanoparticle formation and shell growth.

Atomic force microscopy confirmed the formation of well-defined nanoparticles. Dynamic light scattering gave hydrodynamic size distributions consistent with the presence of a polymer coating. Light extinction spectra showed the localized surface plasmon resonance band characteristic of AgNPs.

To interpret the spectra quantitatively, we developed a computer model that estimates distributions of core size and polymer shell thickness from extinction measurements. The modeling had two stages:

1. **Spectrum generation.** Extinction spectra were calculated for bare and pNIPAM-coated AgNPs and for pure pNIPAM particles, covering a range of core sizes and shell thicknesses. The calculations used Mie theory for coated spheres [3] with the optical constants of bulk Ag were approximated by high-order polynomials and corrected for size-dependent electron relaxation, using the bulk relaxation time, plasma frequency, and Fermi velocity of silver. The refractive index of pNIPAM was taken as 1.52.
2. **Spectrum fitting.** The simulated spectra were combined with weighting coefficients chosen by Monte Carlo enumeration. The summed spectrum was then fitted to the experimental data by a least-squares technique.

The simulated spectra agreed well with the experimental ones and allowed the structural parameters of the nanoparticles to be estimated. The proposed photochemical method yields stable colloids with a controlled size distribution. These nanoparticles are promising in fabricating nanocontainers for drug delivery and as signal enhancers in plasmon-enhanced spectroscopy.

[1] Diehl, F., Hageneder, S., Fossati, S., Auer, S. K., Dostalek, J., & Jonas, U. (2022). Plasmonic nanomaterials with responsive polymer hydrogels for sensing and actuation. *Chemical Society Reviews*, 51(10), 3926-3963.

[2] Duan, H., Muhuri, D., & He, J. (2024). Polymers on plasmonic metal nanoparticles: From symmetric coating to asymmetric surface patterning. *Polymer*, 303, 127115.

[3] Lopatynskyi, A. M., Lopatynska, O. G., Guo, L. J., & Chegel, V. I. (2010). Localized surface plasmon resonance biosensor—Part I: Theoretical study of sensitivity—Extended Mie approach. *IEEE Sensors Journal*, 11(2), 361-369.

Cite as: Mariia Khutko et al., "Mie-Theory-Based Modeling of Light Extinction Spectra for Size and Shell-Thickness Estimation of Photochemically Synthesized pNIPAM-Coated Silver Nanoparticles", in *Book of Abstracts of the 27th Symposium on Photonics and Optics (SPO 2026)*, Kyiv, 2–6 November 2026, p. 83.

Fr1.4 INVITED · FRIDAY 09:10 CET · 10:10 KYIV #289

Renaissance of Magneto-Optics, or New Challenges – Old Methods

Mariia Pashchenko

Institute of Physics of the Czech Academy of Sciences, Prague, Czech Republic

Magneto-optical effects, arising from the interaction of polarized light with exchange splitting and spin-orbit coupling, have long been powerful tools for investigating the electronic structure and magnetic domains of magnetically ordered materials. In this lecture, we will revisit the fundamental principles of magneto-optical phenomena and review their main types, including transmission effects (Faraday and Voigt effects) and reflection effects (polar, longitudinal, and transverse magneto-optical Kerr effects, MOKE).

We will compare these techniques, discuss their respective advantages and limitations, and examine the types of information that can be obtained from each of them. Finally, we will show why magneto-optics is currently experiencing a renaissance. Recent discoveries of unconventional magnetic orders, particularly in altermagnets and compensated ferrimagnets, have created new experimental challenges that often cannot be addressed by conventional techniques alone. We will discuss how modern magneto-optical methods are helping to overcome these challenges and are opening new avenues for the study of magnetic materials.

Cite as: Mariia Pashchenko, "Renaissance of Magneto-Optics, or New Challenges – Old Methods", in *Book of Abstracts of the 27th Symposium on Photonics and Optics (SPO 2026)*, Kyiv, 2–6 November 2026, p. 85.

Fr2.1 INVITED · FRIDAY 10:00 CET · 11:00 KYIV #251

Molten Salts: A Versatile Platform for Engineering Functional Glasses and Crystalline Materials

Kateryna Terebilenko[1], Serhii Nedilko[1], Vitalii Chornii[2]

[1]Taras Shevchenko National University of Kyiv, Kyiv, Ukraine [2]National University of Life and Environmental Sciences of Ukraine, Kyiv, Ukraine

Science and innovation are essential drivers of technological development, national resilience, and post-war recovery. In this context, the chemistry of melts offers significant opportunities for developing advanced functional materials while improving the efficiency of technological processes and the sustainable use of limited resources. This contribution explores fundamental and applied aspects of melt-based synthesis, focusing on the development of luminescent glass-ceramics for modern optoelectronic applications.

Conventional white light-emitting diodes (LEDs) commonly rely on blue-emitting semiconductor chips combined with phosphor-containing polymer coatings that convert part of the emitted radiation into longer wavelengths. Despite their technological simplicity, polymer matrices are susceptible to photochemical and thermal degradation, which can impair optical performance during prolonged operation. Inorganic glass matrices represent a promising alternative owing to their enhanced thermal and chemical stability. However, conventional silicate-based approaches often require high processing temperatures, potentially exceeding 1600 °C, and may involve complex processing procedures to achieve a homogeneous distribution of the luminescent phase.

An alternative strategy involves the use of modified phosphate glasses with tailored compositions that enable lower-temperature processing and the formation of luminescent phases in situ. In this approach, the functional material is engineered by controlling the composition of the initial melt, allowing the luminescent crystalline phase to form directly within the glass matrix during thermal treatment through nucleation and crystallization. This eliminates the need to synthesize the phosphor separately and subsequently disperse it in the glass. The resulting glass-ceramic structure combines the isotropic, protective matrix of the amorphous phase with the efficient light emission of crystalline phosphors. Controlling the nucleation process, crystallite size, and spatial distribution of the crystalline phase is essential for achieving homogeneous optical properties and improving the stability and reproducibility of the resulting materials.

From a fundamental perspective, the proposed approach exploits the interplay between structural disorder and long-range order during melt cooling. Depending on composition and thermal history, crystallization may be suppressed, leading to glass formation, or promoted, resulting in the development of crystalline phases. By deliberately controlling these competing processes, it becomes possible to combine the advantages of both structural states within a single functional material. Thus, melt chemistry provides a versatile platform for engineering luminescent glass-ceramics with tailored structural and optical properties, offering promising opportunities for more durable and efficient optoelectronic devices.

Cite as: Kateryna Terebilenko et al., "Molten Salts: A Versatile Platform for Engineering Functional Glasses and Crystalline Materials", in *Book of Abstracts of the 27th Symposium on Photonics and Optics (SPO 2026)*, Kyiv, 2–6 November 2026, p. 86.

Fr2.2 ORAL · FRIDAY 10:30 CET · 11:30 KYIV #210

Effect of Cesium Doping on the Structural, Electronic, and Optical Properties of BaSnO3: A First-Principles Study for Photovoltaic Applications

Younes Elalaoui, Rhma Adhiri, Touria Lachhab
Hassan II University of Casablanca, Casablanca, Morocco

Oxide perovskites have attracted increasing interest for photovoltaic applications due to their structural stability, tunable electronic properties, and potential for optoelectronic devices. Among these materials, barium stannate ($BaSnO_3$) exhibits promising characteristics, including a cubic crystal structure and high electron mobility. However, its wide band gap limits its absorption of the visible portion of the solar spectrum. In this context, doping represents a promising strategy for improving its physical and optical properties. This study aims to investigate the influence of cesium (Cs) doping, introduced at the barium sites, on the structural, electronic, and optical properties of $BaSnO_3$ at different doping concentrations, corresponding to the compositions $Cs_xBa_{1-x}SnO_3$ (x = 0.125, 0.25, and 0.375). The calculations are performed within the framework of density functional theory (DFT) using the Quantum ESPRESSO code. Structural optimization is carried out to evaluate the evolution of the lattice parameter as a function of cesium concentration. The electronic properties are analyzed through the band structures and density of states, while the optical properties are investigated using the dielectric functions and the related optical quantities. The obtained results show an increase in the lattice parameter and a decrease in the band gap with increasing cesium concentration. This band-gap reduction could promote the absorption of a broader portion of the solar spectrum and enhance the optoelectronic potential of the material. This study therefore contributes to a better understanding of the effect of cesium doping on the properties of $BaSnO_3$ and to the assessment of its potential for photovoltaic applications.

Cite as: Younes Elalaoui et al., "Effect of Cesium Doping on the Structural, Electronic, and Optical Properties of BaSnO3: A First-Principles Study for Photovoltaic Applications", in *Book of Abstracts of the 27th Symposium on Photonics and Optics (SPO 2026)*, Kyiv, 2–6 November 2026, p. 88.

Fr2.3 ORAL · FRIDAY 10:45 CET · 11:45 KYIV #234

Electronic properties of inhomogeneous polar textures in $BaTiO_3$: A second-principles study

Binayak Mukherjee[1], Fernando Gomez-Ortiz[1], Xu He[1], Pablo García-Fernández[2], Javier Junquera[2], Philippe Ghosez[1]

[1] *University of Liège, Liège, Belgium* [2] *University of Cantabria, Santander, Spain*

Second-principles lattice models have recently enabled large-scale simulations of complex polar textures in ferroelectric perovskite oxides, including vortices, skyrmions, merons and related inhomogeneous domain structures [1-3]. In displacive compounds, it is known that extra charge can induce local tuning of displacive motions, being for instance at the origin of anti-distortive polarons [4]. It might therefore be questioned if, reciprocally, the intrinsic inhomogeneity of distortions inherent to polar textures can locally tune the electronic properties and produce unexpected phenomena.

In practice, the electronic properties of large-scale systems are hardly accessible from first-principles calculations while second-principles lattice models integrate out the electronic degrees of freedom, so preventing direct access to them. To overcome this limitation, a methodology has been proposed to explicitly and self-consistently reintroduce selected electronic degrees of freedom within pre-existing lattice models [5,6]. Following this methodology, we report the construction of a Wannier-based second-principles electronic model for $BaTiO_3$ from first-principles calculations. We benchmark its accuracy against reference first-principles calculations across multiple structural configurations, including both pristine and doped systems, using the electronic band structure as the primary metric

Subsequently, we combine this electronic model with its lattice counterpart to explore the electronic properties of nanoscale topological textures in $BaTiO_3$. Focusing on topologically non-trivial polar textures obtained from the corresponding lattice model [2,3], we analyze how these inhomogeneous polar distortions reshape the local electronic structure.

Acknowledgement. Binayak Mukherjee was supported by IPD-STEMA grant from the University of Liege.

[1] J. Junquera, et al, "Topological phases in polar oxide nanostructures," Rev. Mod. Phys. 95, 025001 (2023).

[2] L. Bastogne, F. Gomez-Ortiz, S. Anand and Ph. Ghosez, Dynamical manipulation of polar topologies from acoustic phonon excitations, Nano Lett. 24, 13783 (2024).

[3] F. Gómez-Ortiz, L. Bastogne, S. Anand, M. Yu, X. He, and P. Ghosez, "Switchable skyrmion – antiskyrmion tubes in rhombohedral $BaTiO_3$ and related materials," Phys. Rev. B 111, L180104 (2025).

[4] H. Hassani, E. Bousquet, X. He, B. Partoens, and P. Ghosez, "The anti-distortive polaron as an alternative mechanism for lattice-mediated charge trapping," Nat. Commun. 16, 1688 (2025).

[5] P. García-Fernández, J. C. Wojdeł, J. Íñiguez, and J. Junquera, "Second-principles method for materials simulations including electron and lattice degrees of freedom," Phys. Rev. B 93, 195137 (2016).

[6] N. Carral-Sainz, T. Fernández-Ruiz, J. Íñiguez-González, J. Junquera, and P. García-Fernández, "Systematic generation of electron models for second-principles density functional theory methods," Phys. Rev. B 112, 155146 (2025).

Cite as: Binayak Mukherjee et al., "Electronic properties of inhomogeneous polar textures in $BaTiO_3$: A second-principles study", in *Book of Abstracts of the 27th Symposium on Photonics and Optics (SPO 2026)*, Kyiv, 2–6 November 2026, p. 89.

Fr2.4 ORAL · FRIDAY 11:00 CET · 12:00 KYIV #199

MgO-Mediated Densification and Electromechanical Hardening in BNT-BT-KNN Lead-Free Piezoceramics: Decoupling Porosity from Acceptor Effects

Swarup Kundu, Kiran K. Padhi, Saicharen Lakshmanan
Sri Sathya Sai Institute of Higher Learning, Puttaparthi, India

Acceptor doping is the standard route to raising the mechanical quality factor Q_m of lead-free piezoceramics for high-power and resonant applications, but in solid-state processed ceramics the same additive also changes sintering behaviour, so gains in Q_m are often confounded with changes in porosity. We separate these two effects in BNT-BT-KNN ceramics modified with 0 to 0.5 wt% MgO and prepared by conventional solid-state reaction.

X-ray diffraction with Rietveld refinement confirms a perovskite structure for all compositions, and SEM shows grain sizes of about 1.8 to 2.0 µm. Relative density peaks at 0.3 wt% MgO, whereas Q_m, determined by resonance and anti-resonance impedance spectroscopy following IEEE 176, rises monotonically from 67 for the undoped ceramic to 350 at 0.5 wt%. Because densification and hardening peak at different compositions, the five-fold rise in Q_m cannot be attributed to reduced porosity and is consistent with intrinsic acceptor hardening by Mg on the B site. The planar coupling factor stays close to 0.2 across the series, while d_{33} falls from 200 to 110 pC/N and the voltage coefficient g_{33} falls from 29.7 to 14.1 mV·m/N. The undoped ceramic's g_{33} exceeds those of commercial PZT-5A and PZT-5H. Compositions above 0.5 wt% showed dielectric breakdown below 20 kV/cm and could not be poled.

The series therefore offers a tunable trade-off between voltage output and mechanical quality factor within a single lead-free system: low MgO contents suit sensing and energy harvesting, and higher contents suit resonant actuation and impedance-based structural health monitoring. Dielectric and ferroelectric characterisation are discussed in relation to the proposed defect-dipole mechanism.

Cite as: Swarup Kundu et al., "MgO-Mediated Densification and Electromechanical Hardening in BNT-BT-KNN Lead-Free Piezoceramics: Decoupling Porosity from Acceptor Effects", in *Book of Abstracts of the 27th Symposium on Photonics and Optics (SPO 2026)*, Kyiv, 2–6 November 2026, p. 90.

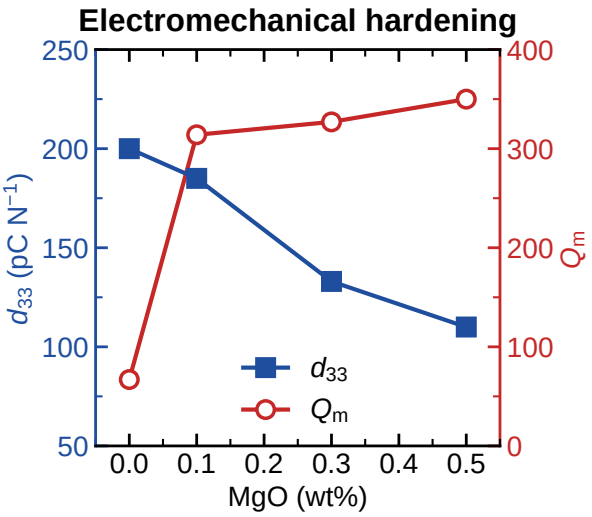


Figure. Piezoelectric coefficient d33 and mechanical quality factor Qm of 0.91BNT-0.05BT-0.04KNN ceramics as a function of MgO content: acceptor hardening raises Qm five-fold while d33 falls.

Fr2.5 ORAL · FRIDAY 11:15 CET · 12:15 KYIV #262

Effect of Graphite Inclusions on the Mechanical Properties of Silicon Carbide Ceramics

Rostyslav Vazhnenko[1], Vadym Shvernyk[1], Hanna Pshenychna[1], Oleksii Popov[2]

[1] *Taras Shevchenko National University of Kyiv, Kyiv, Ukraine* [2] *Institute of Applied Physics of the National Academy of Sciences of Ukraine, Sumy, Ukraine*

Silicon carbide (SiC) ceramics are widely recognized for their high hardness, excellent thermal stability, and chemical inertness. However, the inherent brittleness of pure (SiC) matrix remains a primary limitation for demanding structural and armour applications. In this study, the effect of graphite inclusions on the mechanical performance and sintering behavior of SiC-based ceramics was investigated. Ceramic samples with varying graphite concentrations (ranging from 10% to 30%) were fabricated to establish the structure-property relationships.

Mechanical testing revealed that low to moderate graphite additions substantially modify the failure mechanism of the material. Specifically, the incorporation of minor graphite inclusions in the range of 10–20% significantly improves the fracture toughness of the matrix. This enhancement is primarily attributed to the presence of the soft secondary phase, which effectively deflects the crack front and dissipates crack energy. Conversely, increasing the graphite content up to approximately 30% results in a pronounced degradation of overall mechanical strength. Such deterioration is caused by material oversaturation with the soft graphitic phase.

Beyond mechanical properties, the influence of graphite addition on the technological parameters of synthesis was evaluated. The introduction of graphite into the initial powder batch was found to exert a positive effect on the linear shrinkage of the final ceramic product.

Consequently, optimizing the graphite content within 10–20% offers a balanced combination of enhanced fracture toughness, controlled shrinkage, and acceptable mechanical properties.

Cite as: Rostyslav Vazhnenko et al., "Effect of Graphite Inclusions on the Mechanical Properties of Silicon Carbide Ceramics", in *Book of Abstracts of the 27th Symposium on Photonics and Optics (SPO 2026)*, Kyiv, 2–6 November 2026, p. 92.

Fr2.6 ORAL · FRIDAY 11:30 CET · 12:30 KYIV #247

Functionally Graded Polymer-Inorganic Composites as Advanced Wideband Microwave Absorbers

Oleksandr Zaichenko[1], Vladimir Tuz[2], Yevhen Yashchyshyn[3], Ivan Demydov[1], Khrystyna Harhay[1], Konrad Godziszewski[3], Nataliya Mitina[1], Oleh Izhyk[4], Roman Nebesnyi[1], Volodymir Storozh[1]

[1]Lviv Polytechnic National University, Lviv, Ukraine [2]V. N. Karazin Kharkiv National University, Kharkiv, Ukraine [3]Warsaw University of Technology, Warsaw, Poland [4]Ivan Franko National University of Lviv, Lviv, Ukraine

The increasing use of high-frequency electromagnetic technologies, including advanced radar systems, millimetre-wave communications, and emerging sub-terahertz applications, creates a growing demand for lightweight, flexible, and efficient electromagnetic shielding materials. Conventional conductive shields predominantly reflect incident radiation, whereas practical applications increasingly require absorption-dominant shielding that minimizes secondary electromagnetic interference. This work presents two complementary strategies for developing thin, scalable polymer–inorganic composites with enhanced microwave and sub-terahertz absorption: engineering magnetic core–satellite pigment fillers and integrating functionally graded multilayer coatings with woven carbon fabric metastructures. The first strategy involves modifying an industrial copper chromite-based pigment with metallic nanoparticles to enhance its electromagnetic response. The original multiphase pigment, comprising predominantly $CuCr_2O_4$ spinel together with chromium oxide and hematite, exhibits interfacial polarization but relatively weak magnetic properties. Surface functionalization with an aminosilane followed by the chemical reduction of nickel or silver precursors produces core–satellite architectures. Nickel decoration increases the saturation magnetization approximately fourteen-fold, from 3.5 to 48 emu/g, and raises the composite permittivity from 6.8 to 8.8. In metal-backed X-band measurements, an epoxy composite containing nickel-decorated pigment achieves a reflection-loss minimum of -24.7 dB at 10.2 GHz with a thickness of only 2.6 mm, corresponding to more than 99% absorption at the resonance minimum. In contrast, silver decoration produces comparatively modest improvements, highlighting the importance of magnetic losses in conjunction with dielectric dissipation. The second strategy exploits the intrinsic quasi-periodic architecture of twill-woven carbon fabric as a scalable electromagnetic metastructure. The fabric is coated with a functionally graded sequence of plasticized epoxy layers containing graphite nanoplatelets and magnetic fillers, including nickel or γ-Fe2O3. The layer arrangement is designed to provide a gradual impedance transition from air towards the conductive substrate while combining ohmic, dielectric, magnetic, and geometric resonance effects. The resulting flexible composites are approximately 1.3-1.8 mm thick. Free-space quasi-optical measurements demonstrate absorption-related shielding contributions reaching 75-80 dB across the 90-330 GHz range, accompanied by reflection-related shielding contributions below approximately 5 dB over most of the measured band and near-zero reflection above 250 GHz. The response also exhibits pronounced polarization dependence associated with the fabric weave. A transfer-matrix model incorporating magnetic dispersion and anisotropic effective permittivity reproduces the measured behaviour using a consistent parameter set, supporting the interpretation that the observed performance arises from

coupled resonances rather than a simple additive effect of individual layers. Auxiliary samples further demonstrate the critical role of the first graphite-containing layer in establishing impedance matching and coupling the multilayer stack to the fabric metastructure.

Together, these results establish complementary materials-design approaches for lightweight, absorption-dominant electromagnetic shielding. Combining engineered magnetic fillers with naturally structured carbon fabrics offers a promising, scalable route towards broadband absorbers for high-frequency electronics, radar-related applications, and electromagnetic protection.

Cite as: Oleksandr Zaichenko et al., "Functionally Graded Polymer-Inorganic Composites as Advanced Wideband Microwave Absorbers", in *Book of Abstracts of the 27th Symposium on Photonics and Optics (SPO 2026)*, Kyiv, 2–6 November 2026, p. 93.

Fr3.1 ORAL · FRIDAY 13:00 CET · 14:00 KYIV #255

Structural and optical properties of undoped and Sn-doped β-Ga2O3 thin films deposited by ultrasonic spray pyrolysis

Polina Shamrovska, D. R. T. Zahn

Chemnitz University of Technology, Chemnitz, Germany

β-Ga2O3 thin films have gained significant research interest due to their wide bandgap, high thermal stability, and high breakdown voltage, making them suitable for e.g. UV photodetectors. In this work, undoped and Sn-doped β-Ga2O3 thin films were deposited on c-plane sapphire substrates via ultrasonic spray pyrolysis extending our previous studies based on conventional spray coating. The use of a different deposition system, together with the introduction of Sn doping, provides a basis for investigating the influence of deposition conditions and dopant incorporation on film properties. The deposition was performed with Ga(NO3)3 dissolved a 1 : 1 water-ethanol mixture at a substrate temperature of 190 °C and post-deposition annealing was performed at 1000 °C. The films were characterized by Raman spectroscopy, atomic force microscopy, X-ray diffraction, and optical transmittance.

The stoichiometric β-phase Ga2O3 films revealed a preferred (-201) orientation in agreement with previous results [1]. The samples show transparency of up to 85% in the visible range with absorption edge at ~250 nm. The results obtained reveal that ultrasonic spray pyrolysis allows the fabrication of polycrystalline and transparent β-Ga2O3 films suitable for further studies of ohmic contact formation and for applications in solar-blind UV photodetectors.

[1] Housei Akazawa, Vacuum, 2016, 123: 8-16.

Cite as: Polina Shamrovska et al., "Structural and optical properties of undoped and Sn-doped β-Ga2O3 thin films deposited by ultrasonic spray pyrolysis", in *Book of Abstracts of the 27th Symposium on Photonics and Optics (SPO 2026)*, Kyiv, 2–6 November 2026, p. 95.

Fr3.2 ORAL · FRIDAY 13:15 CET · 14:15 KYIV #303

Exhibition of spatial dispersion in optical properties of lattices of plasmonic nanoparticles

Eugene Bortchagovsky[1,2], D. Fang[3], M. Fleischer[3], D. R. T. Zahn[2,4]

[1] V. Lashkaryov Institute of Semiconductor Physics of the National Academy of Sciences of Ukraine, Kyiv, Ukraine [2] Semiconductor Physics, Chemnitz University of Technology, Chemnitz, Germany [3] University of Tübingen, Tübingen, Germany [4] Center for Materials, Architectures and Integration of Nanomembranes (MAIN), Chemnitz University of Technology, Chemnitz, Germany

We demonstrate that spatial dispersion plays an important role in optical properties of layers of plasmonic (interacting) nanoparticles. It results particularly in the dependence of the effective optical properties of such structures on the angle of incidence of the exciting light as well as on the orientation of the lattice in relation to the plane of incidence even though formally such lattices are isotropic. Both effects cannot be described by any standard dielectric tensor and demand the inclusion of spatial dispersion.

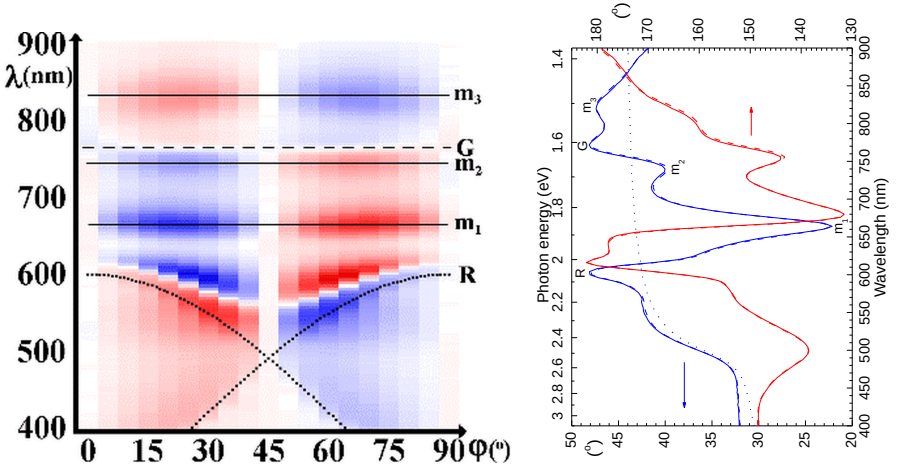


Figure. Color coded value of m_{13} element of the Müller matrix for the square lattice with a period of 350 nm of gold discs with a diameter of 260 nm versus the orientational angle and ellipsometric spectra measured at the orientation along the sides of squares. Dotted line is the spectrum of the clean substrate. m_1-m_3 mark lattice modes, while G – gap mode and R – Rayleigh anomaly.

Illumination of a square lattice of circular symmetrical particles along any of four planes of symmetry (rows or diagonals) produces no cross-polarization with an effective birefringence at inclined incidence due to the elliptical shape of the Fresnel zones. Such a birefringence is fixed by the plane of incidence, so effective optical constants along two orthogonal axes replace each other at a rotation of the lattice by 90°. At other non-symmetrical orientations cross-polarization arises well seen in the non-diagonal elements of measured Müller matrix. Such a behavior is shown in Figure 1 with color coded values of the m_{13} element of the Müller matrix

FRI

for a lattice of disc-like particles with a diameter of 260 nm and a period of 350 nm versus the orientation angle of the lattice in relation to the plane of incidence and the wavelength. Spectra of ellipsometric angles measured along rows (0°) and along columns (rotated by 90°) also shown in the Figure coincide completely and demonstrate total coincidence of the resonance positions with the non-zero values of cross-polarization. Only the gap mode, which field is almost totally concentrated between particles and their image in the substrate and no crosstalk of particles exists is not exhibited in the m_{13} map. It is an additional argument supporting the creation of effective birefringence and spatial dispersion as a collective effect of interacting particles.

Cite as: Eugene Bortchagovsky et al., "Exhibition of spatial dispersion in optical properties of lattices of plasmonic nanoparticles", in *Book of Abstracts of the 27th Symposium on Photonics and Optics (SPO 2026)*, Kyiv, 2–6 November 2026, p. 96.

Fr3.3 ORAL · FRIDAY 13:30 CET · 14:30 KYIV #239

Effect of Nanoconfinement on Thermal Transport in Porous Silicon / Phase Change Material Composites

Vladyslav Tsehelnyi[1], Lesia Chepela[2], Pavlo Lishchuk[2], Mykola Borovyi[2], David Lacroix[1], Mykola Isaiev[1]

[1] LEMTA, CNRS – University of Lorraine, Nancy, France [2] Taras Shevchenko National University of Kyiv, Kyiv, Ukraine

Thermal management plays a crucial role in improving the efficiency of next-generation electronic devices, renewable energy systems, and building thermal regulation. Among thermal management technologies, phase-change materials (PCMs) have attracted considerable attention due to their ability to store and release large amounts of latent heat during nearly isothermal phase transitions [1]. While most research focuses on bulk material optimization through molecular engineering [2,3], material synthesis, and device-level design, the influence of nanoscale confinement on the phase behavior and thermal transport properties of PCMs remains an important research challenge.

In this work, we investigate the effects of nanoconfinement on the thermal transport properties of widely used organic PCMs, including hexadecane, eicosane, docosane, and tricosane [4]. To this end, porous silicon (porSi) matrices with porosities of 45%, 55%, and 65% and a porous layer thickness of approximately 50 μm were fabricated by electrochemical etching of p-type (100) silicon wafers. The thermal conductivity of the resulting porSi/PCM composites was characterized using the gas-microphone photoacoustic technique [5], which also enables non-destructive, in situ investigation of phase transitions and thermophysical properties.

To interpret the experimental results, molecular dynamics simulation data [6] were incorporated into an effective-medium model, providing a link between molecular-scale phenomena and the macroscopic thermal response. This combined approach suggests that the observed increase in thermal conductivity upon PCM crystallization is associated with reduced geometrical frustration of alkane chains and a decrease in interfacial thermal resistance within the confined nanopores.

The results highlight the important role of nanoscale confinement in governing the phase-dependent thermal transport properties of PCMs. Furthermore, porSi/PCM composites provide a versatile model system for combining experimental characterization with molecular-scale simulations, offering valuable insights into heat transfer in confined geometries and supporting the development of advanced materials for thermal management applications.

Acknowledgement. This publication presents results obtained within the research projects “Development of Advanced Phase Change Composite Systems for Efficient Use of Thermal Energy” (Ministry of Education and Science of Ukraine, No. 0124U001084) and the ANR project “PROMENADE,” No. ANR-23-CE50-0008.

[1] S. Wang et al., “Phase-change materials for thermal management,” 2026, Nature Research. doi: 10.1038/s41578-026-00959-7.

[2] J. Chen et al., “Phase-locked constructing dynamic supramolecular ionic conductive elastomers with superior toughness, autonomous self-healing and recyclability,” Nature Communications, vol. 13, no. 1, Dec. 2022, doi: 10.1038/s41467-022-32517-4.

[3] J. H. Lee and S. H. Kim, "Synthesis and characterization of biopolyurethane crosslinked with castor oil-based hyperbranched polyols as polymeric solid–solid phase change materials," Sci. Rep., vol. 12, no. 1, Dec. 2022, doi: 10.1038/s41598-022-17390-x.

[4] S. Kahwaji and M. A. White, "Organic phase change materials for thermal energy storage: Influence of molecular structure on properties," Nov. 01, 2021, MDPI. doi: 10.3390/molecules26216635.

[5] P. Lishchuk et al., "Thermal transport properties of porous silicon filled by ionic liquid nanocomposite system," Sci. Rep., vol. 13, no. 1, Dec. 2023, doi: 10.1038/s41598-023-32834-8.

[6] V. Mandrolko and M. Isaiev, "Tailored thermal transport in phase change materials-based nanocomposites through interfacial structuring," International Communications in Heat and Mass Transfer, vol. 172, Mar. 2026, doi: 10.1016/j.icheatmasstransfer.2026.110544.

Cite as: Vladyslav Tsehelnyi et al., "Effect of Nanoconfinement on Thermal Transport in Porous Silicon / Phase Change Material Composites", in *Book of Abstracts of the 27th Symposium on Photonics and Optics (SPO 2026)*, Kyiv, 2–6 November 2026, p. 98.

Fr4.1 POSTER · FRIDAY 13:45 CET · 14:45 KYIV #200

Hydrostatic Piezopotential in Unpoled Polycrystalline Particles: Finite Element Analysis of Grain Disorder, Cavitation Loading and Electrolyte Screening in Lead-Free Piezocatalysts

Saicharen Lakshmanan

Sri Sathya Sai Institute of Higher Learning, Puttaparthi, India

Piezocatalysis with ultrasonically driven ferroelectric powders is usually rationalised with the longitudinal coefficient d_{33}, even though the particles are unpoled and cavitation loading is close to hydrostatic. We build an open-source finite element framework (FEniCSx) for the coupled electromechanical problem and use it to ask which material property actually controls the surface potential available for redox reactions.

We first verify the solver against closed-form results: static capacitance (0.00% error), the Bessel radial resonance of a free disc, and the exact solution for a homogeneous particle under uniform pressure, $\Delta\phi = g_h p L_3$ with $g_h = d_h/\varepsilon_{33}^T$ and $d_h = d_{33} + 2d_{31}$, reproduced to five significant figures. Mesh convergence reaches 0.005% in the steepest loading case.

Three results follow. (i) Random grain orientation in an unpoled polycrystalline particle lowers the root-mean-square surface potential by only about 29% relative to a single crystal and then plateaus, because cancellation is a volume-average effect that surface chemistry does not sample. (ii) A cavitation bubble close to the particle raises the potential difference by up to 91% compared with uniform loading at identical surface-averaged pressure, an increase driven entirely by the pressure gradient. (iii) Coupling the particle to a linearised Poisson-Boltzmann electrolyte gives an analytic crossover parameter $\Pi = \varepsilon_w G(\kappa a)/\varepsilon_{33}^T$ that separates a g_h-controlled regime from a d_h-controlled regime. Low-permittivity materials such as PVDF and $LiNbO_3$ remain in the d_h regime in water regardless of ionic strength.

Applied to a 25-material panel, the screened figure of merit shows essentially no rank correlation with d_{33} (Spearman $\rho = -0.10$ for 1 µm particles in dye solution), while the unscreened g_h ranking survives only for small particles in deionised water. Applied to lead-free BNT-based ceramics, the analysis shows that acceptor hardening, which raises the mechanical quality factor, can reduce g_h several-fold, so piezocatalysis and resonant sensing applications may favour opposite compositions.

Cite as: Saicharen Lakshmanan, "Hydrostatic Piezopotential in Unpoled Polycrystalline Particles: Finite Element Analysis of Grain Disorder, Cavitation Loading and Electrolyte Screening in Lead-Free Piezocatalysts", in *Book of Abstracts of the 27th Symposium on Photonics and Optics (SPO 2026)*, Kyiv, 2–6 November 2026, p. 100.

Fr4.2 POSTER · FRIDAY 13:49 CET · 14:49 KYIV #238

Alkali Volatilization as a Hidden Compositional Variable in Ta-Modified KNN: Electrical Characterisation and Preliminary Pencil-Lead-Break Response

Ayush K. Samal, Saicharen Lakshmanan, Swarup Kundu
Sri Sathya Sai Institute of Higher Learning, Puttaparthi, India

Ta-modified potassium sodium niobate (KNN) ceramics are promising lead-free piezoelectric materials for sensing applications. In this study, the nominal composition $(K_{0.47}Na_{0.545})(Nb_{0.55}Ta_{0.45})O$ reported in the literature to exhibit enhanced piezoelectric performance through polymorphic phase-transition (PPT) tuning, was investigated [1]. The ceramics were prepared by solid-state reaction and sintered at 1100–1250 °C in a loosely covered crucible. X-ray diffraction revealed pseudo-cubic symmetry without discernible orthorhombic–tetragonal peak splitting. The dielectric permittivity decreased from 548 to 362 over 30–400 °C at 10 kHz, with frequency dispersion and no distinct PPT anomaly. The measured piezoelectric coefficient was $d_{33} = 72$ pC/N, compared with the literature-reported value of 333 pC/N. Polarisation–electric-field hysteresis loops exhibited a slim response, with $P_r/P_{max} \approx 0.22$ and an estimated internal bias field magnitude of approximately 2.91 kV/cm.

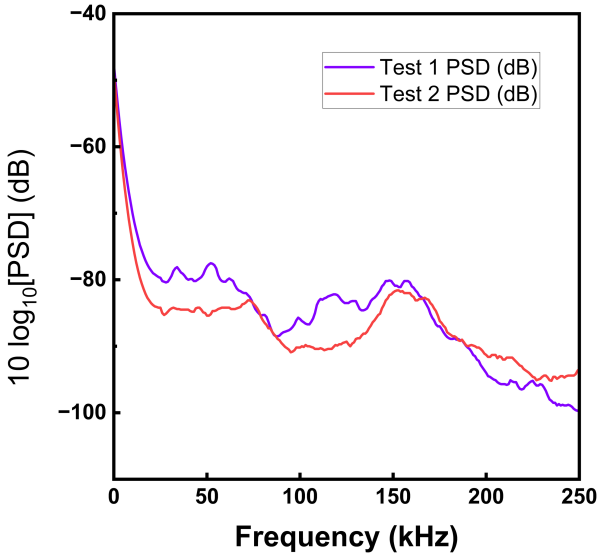


Figure. PSD comparison of two successive PLB tests on Ta-modified KNN, showing a common broad spectral maximum at 150–160 kHz and preliminary repeatability of the response.

Taken together, these observations suggest a response consistent with an effective Nb/Ta phase-diagram composition near $x \approx 0.60$, despite the nominal Ta fraction of $x = 0.45$. This

apparent discrepancy is hypothesised to arise from alkali volatilisation during sintering, which may alter A-site stoichiometry and thereby influence the dielectric and piezoelectric response [2]. As an additional assessment of acoustic response, the ceramic pellet was bonded to an aluminium beam using epoxy and evaluated using the Hsu–Nielsen pencil-lead-break (PLB) method. Two successive lead breaks were recorded using an oscilloscope, and the resulting power spectral density (PSD) profiles were analysed over 0–250 kHz. The smoothed spectra exhibited a Pearson correlation of 0.920 and a mean absolute difference of 3.34 dB, indicating preliminary repeatability for the tested pellet–beam assembly. A common spectral feature appeared near 40–50 kHz, while local maxima occurred near 148–153 kHz in the 100–200 kHz region. These findings demonstrate initial acoustic coupling and detection of transient stress-wave responses. Further compositional verification, repeated measurements across multiple specimens, and electromechanical-impedance measurements under baseline and controlled-damage conditions are required to establish the proposed volatilisation mechanism and assess the material's suitability for structural-health-monitoring applications.

[1] Sung, Y. S.; Baik, S.; Lee, J. H.; Ryu, G. H.; Do, D.; Song, T. K.; Kim, M. H.; Kim, W. J. Appl. Phys. Lett. 2012, 101, 012902.

[2] Wang, Y.; Damjanovic, D.; Klein, N.; Hollenstein, E.; Setter, N. J. Am. Ceram. Soc. 2007, 90, 3485–3489.

[3] de Almeida, V. A. D.; Baptista, F. G.; de Aguiar, P. R. Piezoelectric Transducers Assessed by the Pencil Lead Break for Impedance-Based Structural Health Monitoring. IEEE Sensors Journal 2015, 15(2), 693–702. https://doi.org/10.1109/JSEN.2014.2352171.

Cite as: Ayush K. Samal et al., "Alkali Volatilization as a Hidden Compositional Variable in Ta-Modified KNN: Electrical Characterisation and Preliminary Pencil-Lead-Break Response", in *Book of Abstracts of the 27th Symposium on Photonics and Optics (SPO 2026)*, Kyiv, 2–6 November 2026, p. 101.

Fr4.3 POSTER · FRIDAY 13:53 CET · 14:53 KYIV #208

Sintering temperature influence on phase stability of scandium-stabilized ZrO_2 ceramics

Vita Prosolenko[1], Nadiia Korsunska[2], Oleksandr Melnichuk[1], Liudmyla Melnichuk[1], Oksana Vrublevska[1], Volodymyr Alekseyenko[1], Ivan Blokha[1], Larysa Khomenkova[2]

[1]Nizhyn Mykola Gogol State University, Nizhyn, Ukraine [2]V. Lashkaryov Institute of Semiconductor Physics of the National Academy of Sciences of Ukraine, Kyiv, Ukraine

In this work the structural evolution of scandium-stabilized zirconia ceramics co-doped with cerium and gadolinium as a function of sintering temperature in the range of 1100–1500 °C was investigated. Two compositions were studied: 1Ce10ScSZ (1 mol.% CeO_2 – 10 mol.% Sc_2O_3 – 89 mol.% ZrO_2) and 0.5Ce0.5Gd10ScSZ (0.5 mol.% CeO_2 – 0.5 mol.% Gd_2O_3 – 10 mol.% Sc_2O_3 – 89 mol.% ZrO_2). X-ray diffraction shows that the initial powders demonstrate a single-phase cubic fluorite structure. Sintering of the Ce–ScSZ ceramics results in partial transformation into a rhombohedral phase at 1100 °C, whereas the Gd–Ce–ScSZ samples retain the cubic phase across all investigated temperatures, demonstrating enhanced structural stability.

The rhombohedral phase formation in Ce–ScSZ ceramics is attributed to residual porosity, which is confirmed by stabilization the cubic phase under reduced heating rate resulting in suppression of porosity. Raman scattering measurements confirm the transformation of phase composition.

The study emphasizes that phase stability in scandium-stabilized zirconia depends not only on dopant type and concentration but also on porosity and powder characteristics. While the rhombohedral phase observed at 1100 °C has limited relevance for dense solid electrolyte membranes in SOFCs, it becomes significant for NiO–ZrO_2(Sc,Ce) anodes, where both ionic conductivity and porosity are required. The findings provide insights into optimizing of powder composition and sintering conditions to achieve stable cubic phases in zirconia-based ceramics, thereby improving their applicability in energy and radiation-hard technologies.

Keywords: scandium-stabilized zirconia, co-doping, cubic–rhombohedral transformation, sintering temperature, XRD, Raman scattering.

Cite as: Vita Prosolenko et al., "Sintering temperature influence on phase stability of scandium-stabilized ZrO_2 ceramics", in *Book of Abstracts of the 27th Symposium on Photonics and Optics (SPO 2026)*, Kyiv, 2–6 November 2026, p. 103.

Fr4.4 POSTER · FRIDAY 13:57 CET · 14:57 KYIV #219

Dispersion analysis of IR spectra of $Mg_xZn_{1-x}O$ ceramics: phonon behaviour and phase composition

Viktor Bardakov, Liudmyla Melnichuk
Nizhyn Mykola Gogol State University, Nizhyn, Ukraine

$Mg_xZn_{1-x}O$ solid solutions make it possible to tune the band gap of ZnO smoothly into the ultraviolet region. However, in ceramic materials the hexagonal wurtzite and cubic phases coexist over a wide composition range, so the nominal composition does not reflect the actual phase state that determines the optical and electrical properties. Infrared (IR) reflectance spectroscopy is sensitive both to lattice vibrations and to the phase state, which makes it an effective contactless diagnostic method. While the phonon modes of epitaxial MgZnO films have been well studied, an adequate dispersion model for ceramics over the entire composition range has not yet been proposed.

A series of $Mg_xZn_{1-x}O$ ceramic samples sintered at 1100 °C with a nominal MgO content of $0 \le x \le 1$ was studied. Specular IR reflectance spectra were recorded at room temperature with a Shimadzu IRTracer-100 FTIR spectrometer in the range 240–4000 cm^{-1}. The analysis was performed using a dispersion model for a polycrystalline two-phase material. The dielectric function of each phase is represented in factorized form with separate damping coefficients for the TO and LO phonons and includes two E_1 oscillators (ZnO-like and MgO-like) for the hexagonal phase and one F_{1u} oscillator for the cubic phase. The two-phase mixture is described within the Bruggeman effective-medium approximation with the cubic-phase volume fraction fc, and the surface roughness is taken into account by the factor $\exp[-(4\pi\sigma\nu)^2]$. The model parameters were determined by the least-squares method.

For hexagonal ceramics ($x \le 0.30$) the model reproduces the experimental spectra with a root-mean-square deviation of 0.008–0.014. The reststrahlen band splits into ZnO-like ($\nu_{TO1} \approx$ 405–413 cm^{-1}, $\nu_{LO1} \approx$ 497–505 cm^{-1}) and MgO-like ($\nu_{TO2} \approx$ 508–514 cm^{-1}, $\nu_{LO2} \approx$ 618–630 cm^{-1}) modes, which shows that the two-mode behaviour of E_1 phonons known for films appears in ceramics already at $x = 0.03$. For pure ZnO ceramics the model gives $\nu_{TO} = 405$ cm^{-1}, $\nu_{LO} = 590$ cm^{-1} and $\varepsilon_\infty = 3.71$, in good agreement with single-crystal data. The mode frequencies and $\varepsilon_\infty \approx$ 3.4–3.9 saturate at $x \ge$ 0.05–0.10 (corresponding to $x \approx$ 0.10–0.15 in films), which indicates limited solubility of Mg in the wurtzite lattice. At $x \ge 0.40$ the LO edge of the cubic phase appears near 700 cm^{-1}, and the cubic-phase fraction increases from fc ≈ 0.5 at $x = 0.40$ to ≈ 1 at $x \ge 0.9$. For Mg-rich samples, qualitative agreement is achieved. The roughness parameter $\sigma \approx$ 0.25–0.33 μm hardly depends on composition, which reflects the quality of surface preparation rather than the properties of the material.

The proposed approach enables contactless estimation of the phonon parameters, the effective composition of wurtzite grains and the phase composition of oxide-based ceramic solid solutions.

Keywords: MgZnO ceramics, IR reflectance, two-mode phonon behaviour, dispersion analysis, phase composition.

FRI

Cite as: Viktor Bardakov et al., "Dispersion analysis of IR spectra of $Mg_xZn_{1-x}O$ ceramics: phonon behaviour and phase composition", in *Book of Abstracts of the 27th Symposium on Photonics and Optics (SPO 2026)*, Kyiv, 2–6 November 2026, p. 104.

Fr4.5 POSTER · FRIDAY 14:01 CET · 15:01 KYIV #222

Effect of ZnO electrical conductivity on the composition of hexagonal and cubic phases in MgxZn1-xO ceramics

Oleksandr Melnichuk[1], Nadiia Korsunska[2], Liudmyla Melnichuk[1], Maksym Strilets[1], Larysa Khomenkova[2]

[1]Nizhyn Mykola Gogol State University, Nizhyn, Ukraine [2]V. Lashkaryov Institute of Semiconductor Physics of the National Academy of Sciences of Ukraine, Kyiv, Ukraine

The influence of the electrical conductivity of the initial ZnO powder on the structural, optical properties and chemical composition of MgxZn1-xO ceramics was investigated. Ceramic samples containing 10-30 mol.% Mg were prepared from ZnO and MgO powders and sintered in air at 1050 °C for 3 h. Two series of samples were prepared using ZnO powders with different electrical conductivities. Photoluminescence (PL), photoluminescence excitation (PLE) spectroscopy, scanning electron microscopy (SEM), and energy-dispersive X-ray spectroscopy (EDX) were used to investigate the formation and composition of the solid-solution phases.

The optical spectra revealed a more pronounced blue shift of the excitonic peak in samples prepared from low-resistive ZnO powder, indicating a higher Mg content in the hexagonal phase. EDX analysis confirmed that increasing the electrical conductivity of the initial ZnO powder resulted in higher Mg content in the hexagonal-phase grains and higher Zn content in the cubic-phase grains. In Mg0.2Zn0.8O ceramics prepared from high-resistive ZnO powder, the Mg content in the hexagonal phase was approximately 5-6 %, whereas the Zn content in the cubic phase was 10-11 %. In samples prepared from low-resistive powder, these values increased to 9-12 % Mg and approximately 17 % Zn, respectively. The results indicate that the formation and chemical composition of both phases depend on the electrical conductivity of the initial ZnO powder that is determined by concentration of interstitial zinc. A possible mechanism is proposed in which interstitial Zn migrates to grain boundaries and incorporates into MgO, promoting Mg enrichment of the grain boundaries due to self-compensation process. This facilitates the incorporation of Mg into ZnO and may promote the simultaneous formation of the hexagonal and cubic solid-solution phases during sintering. The findings demonstrate that the defect structure of the starting powder is an important factor governing the phase composition of MgxZn1-xO ceramics.

Keywords: MgxZn1-xO ceramics, ZnO electrical conductivity, interstitial zinc, hexagonal phase, cubic phase, photoluminescence, EDX.

Cite as: Oleksandr Melnichuk et al., "Effect of ZnO electrical conductivity on the composition of hexagonal and cubic phases in MgxZn1-xO ceramics", in *Book of Abstracts of the 27th Symposium on Photonics and Optics (SPO 2026)*, Kyiv, 2–6 November 2026, p. 106.

Fr4.6 POSTER · FRIDAY 14:05 CET · 15:05 KYIV #228

Frustrated total internal reflection (Otto geometry) in a ZnO/6H-SiC structure: coupling through an air gap, a simulation study

Oleksii Sakhniuk

Nizhyn Mykola Gogol State University, Nizhyn, Ukraine

Attenuated total reflection (ATR) is a convenient way to probe thin films of wide-bandgap semiconductors in the far infrared. For the ZnO/6H-SiC system, whose reststrahlen bands lie at about 378–590 and 788–970 cm^{-1}, the prism, incidence angle and air gap determine which bands can be excited. We simulate the Otto configuration (prism / air gap / ZnO film / 6H-SiC substrate), where the evanescent wave couples to the film-substrate structure.

Both crystals are treated as uniaxial media with the optic axis normal to the surface. The ordinary ($\varepsilon_\perp$) and extraordinary ($\varepsilon_\parallel$) permittivities are described separately by a Lorentz phonon oscillator plus a Drude free-carrier term. Reflectance for s and p polarization is computed using one multilayer characteristic-matrix (Abelès) algorithm covering external reflection and ATR; for a single film it reproduces the Airy formula to about 10^{-15}. Calculations use a 0.8 μm film (carrier density 10^{18} cm^{-3}, mobility 50 $\mathrm{cm}^2/(\mathrm{V\,s})$) on a substrate ($10^{17}$ cm^{-3}, 100 $\mathrm{cm}^2/(\mathrm{V\,s})$), a uniform plane-parallel gap and a frequency-independent prism index. Unless stated otherwise, the prism is KRS-5 ($n = 2.37$) and the internal incidence angle is $\theta = 35^\circ$.

The critical angle $\theta_c = \arcsin(1/n)$ is 25.0° for KRS-5, 17.1° for Si and 14.5° for Ge. Ge transmits only above about 780 cm^{-1}, making the ZnO band inaccessible, whereas KRS-5 (cutoff about 250 cm^{-1}) covers both bands. For p polarization, clear reflectance minima appear at about 510–555 cm^{-1} (ZnO) and 830–880 cm^{-1} (6H-SiC). For s polarization, ZnO-band reflectance stays above 43% for all gaps considered, so p polarization is required.

The ZnO-band minimum depth depends non-monotonically on gap thickness d_{gap}: R_{min} is about 19% at 0.5 μm, 5.7% at 1 μm, 0.1% at 1.5 μm, 3.5% at 2 μm, 74% at 5 μm and 99% at 10 μm. The minimum shifts from 511 to 554 cm^{-1} as the gap grows from 0.5 to 5 μm. For a 2 μm gap, R_{min} is about 8.9% at 28°, 2.8% at 30°, 3.5% at 35°, 23% at 40° and 74% at 55°. Useful angles thus extend from a few degrees to about 10° above θ_c.

The minima are associated with surface and guided phonon-polariton modes. Practical starting conditions are a KRS-5 prism, p polarization, a 1.5–2 μm gap and a 30–35° angle. Calculated spectra will be compared with measured ATR spectra, and the inverse problem for film thickness, carrier density and mobility will be solved using the same model.

Cite as: Oleksii Sakhniuk, "Frustrated total internal reflection (Otto geometry) in a ZnO/6H-SiC structure: coupling through an air gap, a simulation study", in *Book of Abstracts of the 27th Symposium on Photonics and Optics (SPO 2026)*, Kyiv, 2–6 November 2026, p. 107.

Fr4.7 POSTER · FRIDAY 14:09 CET · 15:09 KYIV #249

Effect of Fluoride Modification on the Structure and Luminescence of Europium-Doped Phosphomolybdate Glasses

Kateryna Terebilenko, Yelyzaveta Karpenko
Taras Shevchenko National University of Kyiv, Kyiv, Ukraine

Amorphous oxide materials are of considerable interest for optical applications because of their isotropic nature, which ensures uniform optical properties regardless of the direction of light propagation. In contrast to crystalline materials, glasses do not exhibit long-range structural order or intrinsic optical anisotropy, making them promising candidates for functional optical components and luminescent materials. In particular, phosphate-molybdate glasses offer a versatile matrix for incorporating rare-earth ions, whose spectroscopic properties are highly sensitive to the local structural environment.

In this study, Eu-doped sodium phosphate–molybdate materials with the nominal composition 40Na2O–40P2O5–20MoO3 were modified with varying amounts of NaF. The samples were prepared by the melt-quenching technique. The starting components were thoroughly mixed, melted in a platinum crucible at 1000 °C for 1h. The melt was then poured onto a carbon substrate to promote rapid cooling and facilitate glass formation. The resulting materials were investigated using powder X-ray diffraction (XRD), diffuse reflectance spectroscopy, and photoluminescence spectroscopy to evaluate their structural and optical properties as a function of NaF content.

The results reveal a nonlinear dependence of Eu(III) luminescence characteristics on the NaF content, indicating that fluoride incorporation induces complex changes in the local structural environment of europium ions. Rather than producing a simple, gradual modification of the glass network, NaF addition appears to affect the coordination environment and local symmetry of Eu(III) centres in a composition-dependent manner. These findings highlight the complex interplay between glass composition, local structure, and luminescence response, providing insights into the design of fluoride-modified phosphate-molybdate glasses with tailored optical properties.

Cite as: Kateryna Terebilenko et al., "Effect of Fluoride Modification on the Structure and Luminescence of Europium-Doped Phosphomolybdate Glasses", in *Book of Abstracts of the 27th Symposium on Photonics and Optics (SPO 2026)*, Kyiv, 2–6 November 2026, p. 108.

Fr4.8 POSTER · FRIDAY 14:13 CET · 15:13 KYIV #271

Optical and electrophysical properties of some porous phosphate-molybdate glasses

Vasyl Cherevyshnyi[1], Volodymyr Boyko[2], Vitalii Chornii[2], Maksym Kremenskoy[1,3], Oleg Olikh[1], Serhii Nedilko[1]

[1]Taras Shevchenko National University of Kyiv, Kyiv, Ukraine [2]National University of Life and Environmental Sciences of Ukraine, Kyiv, Ukraine [3]Novations LLC, Kyiv, Ukraine

Porous materials with a large specific surface area are used in batteries, supercapacitors, sensors, nanogenerators, and drug delivery systems. Porous (foamed) glass and glass-ceramics also attract attention because they can be produced from industrial waste. The mechanical and thermal properties of such systems are well studied. Their optical and electrophysical properties remain largely overlooked, although it is these properties that determine the suitability of a material for optoelectronic and sensing devices. Glass of the P_2O_5–MoO_3–K_2O–Bi_2O_3 system has a low melting temperature and intrinsic photoluminescence (380–850 nm), but porous glass of this composition has not been studied yet.

The base glass $27.18P_2O_5$–$36.24MoO_3$–$31.71K_2O$–$4.86Bi_2O_3$ was synthesized by melt quenching. The glass was ground into a powder, mixed with polyvinyl acetate (10:1 by weight), and pressed into pellets under a pressure of 200 bar. The pellets were annealed at 550 °C for 2 h. The samples were studied by optical and scanning electron microscopy, energy-dispersive X-ray spectroscopy (EDX), diffuse reflectance, photoluminescence (λ_{ex} = 473 nm), and current–voltage characteristics measurements.

Porous glass with open pores ranging from approximately 1 to 100 μm in size (macropores, according to the IUPAC classification) was obtained through simple thermal annealing. No crystalline phases were observed in the SEM images, indicating that the samples are glass rather than glass-ceramics. EDX analysis revealed the presence of a carbon component resulting from the decomposition and combustion of polyvinyl acetate. The following effects are associated with this component:

- a sharp decrease in the diffuse reflectance over the entire spectral range, caused by multiple scattering and by light absorption by carbon micro- and nanoparticles;
- a decrease in the optical band gap: direct band gap from 3.72 to 2.49 eV and indirect band gap from 2.94 to 1.44 eV;
- an approximately tenfold increase in photoluminescence intensity and a larger contribution of the long-wavelength band associated with Bi^{2+} ions and molybdate groups with oxygen vacancies;
- the appearance of electrical conductivity (the resistance of the base glass exceeds 2×10^{11} Ω, so its current–voltage characteristics could not be measured).

The current–voltage curves of the porous glass depend on the probe position, are asymmetric with respect to the polarity of the bias voltage, and exhibit ohmic behavior only over limited voltage ranges. These findings indicate a nonuniform distribution of carbon inclusions, an incompletely formed percolation network, and the presence of distinct charge-transport channels.

Porous phosphate-molybdate glass has been produced using a simple thermal annealing method involving a mixture of glass powder and polyvinyl acetate. The carbon component formed during this process substantially alters the optical properties of the glass by reducing reflectance and the band gap while enhancing luminescence. It also imparts electrical conductivity. These properties can be controlled by varying the polyvinyl acetate content, annealing temperature, and pressing pressure. Further studies will focus on filling the pores with micro- and nanosized phosphors, in particular the mechanoluminescent material $SrAl_2O_4$:Eu,Dy.

Cite as: Vasyl Cherevyshnyi et al., "Optical and electrophysical properties of some porous phosphate-molybdate glasses", in *Book of Abstracts of the 27th Symposium on Photonics and Optics (SPO 2026)*, Kyiv, 2–6 November 2026, p. 109.

Fr4.9 POSTER · FRIDAY 14:17 CET · 15:17 KYIV #261

Optical and dielectric properties of gelatin incorporated with K2Eu(PO4)(WO4) microcrystals

Vitalii Chornii[1,2], Serhii Nedilko[1], Viktor Borysiuk[1], Maksym Lazarenko[1]

[1]*Taras Shevchenko National University of Kyiv, Kyiv, Ukraine* [2]*National University of Life and Environmental Sciences of Ukraine, Kyiv, Ukraine*

Gelatin is a natural polymer widely used in the food, cosmetics, and biomedical industries. In particular, gelatin hydrogels are used as dressings for wound management and tissue regeneration. Macroporous gelatin-based hybrid hydrogels also have potential applications in regenerative medicine, particularly in bone and cartilage repair. However, gelatin has several limitations that restrict its use as a high-technology material. Some of these limitations, including low mechanical strength and poor thermal stability, can be addressed by developing functional composite materials. It is also worth noting that interactions between the gelatin matrix and incorporated inorganic particles may enhance the properties of the latter. For example, the photoluminescence intensity of gelatin@ZnO particles was reported to be 50% higher than that of the pristine oxide [1].

In this work, the effects of K2Eu(PO4)(WO4) red phosphor on the optical and dielectric properties of the gelatin matrix were investigated. K2Eu(PO4)(WO4)@gelatin composites prepared by gelatin and oxide phosphor simultaneously grinding, were characterized using optical microscopy, ATR-FTIR, diffuse reflectance, photoluminescence, and dielectric spectroscopies.

The results demonstrated that grinding reduced the gelatin particle size from approximately 400–900 μm to 40–300 μm. Changes in the amide-related bands in the ATR-FTIR spectra of gelatin suggest that some moisture was released from the samples during grinding. The light absorption of raw and ground gelatin in the 220–400 nm spectral range was attributed to the absorption of peptide bonds in proteins and aromatic residues. The estimated band gap value was identical for the gelatin and K2Eu(PO4)(WO4)@gelatin composite samples, indicating that the fundamental electronic properties of the polymer were unchanged. The composite sample exhibited an additional absorption band with a peak near 260 nm, which was attributed to O→Eu charge-transfer transitions. The photoluminescence intensity of the three gelatin components, with band maxima at 512 nm, 596 nm, and 674 nm, decreased by a factor of two in the composite compared with the gelatin sample. The temperature-dependent photoluminescence and dielectric properties of gelatin indicated an interaction between gelatin and the phosphor. Thus, K2Eu(PO4)(WO4)@gelatin can be considered a luminescent composite that exhibits additional functional properties compared to those of individual components.

Acknowledgement. The study was financed by the National Research Foundation of Ukraine (project № 2025.07/0341)

[1] N. Babayevska, Ł. Przysiecka, G. Nowaczyk, et al. *Materials* **14** (2020) 103.

Cite as: Vitalii Chornii et al., "Optical and dielectric properties of gelatin incorporated with K2Eu(PO4)(WO4) microcrystals", in *Book of Abstracts of the 27th Symposium on Photonics and Optics (SPO 2026)*, Kyiv, 2–6 November 2026, p. 111.

Fr4.10 POSTER · FRIDAY 14:21 CET · 15:21 KYIV #204

Mechanical properties of a Ti–Cu nanocomposite prepared by mechanical alloying

Mykola Melnichenko, Sergiy Revo, Yaroslav Zhuk
Taras Shevchenko National University of Kyiv, Kyiv, Ukraine

The use of mechanochemical activation of metal powders, as well as their mixtures, in planetary mills opens up broad prospects for the creation of new nanocomposite materials. A characteristic feature of this type of activation is that, after it is used to process mixtures, the particle morphology, size, and phase composition change. Ti–Cu nanocrystalline materials, synthesized by mechanical alloying of elemental Ti and Cu powders, have long attracted the attention of researchers due to their numerous applications in the military, industrial, automotive manufacturing, and aerospace sectors. In addition, in modern medicine, titanium is widely used to manufacture implants that replace hard tissues. The hardness of pure titanium ranges from approximately 0.7 GPa to 1.2 GPa, while that of the Ti-6Al-4V titanium alloy ranges from 3.0 to 3.7 GPa. It should be noted that in industrial casting, the hardness of pure titanium doubles when alloyed with copper or silver.

In this study, Ti–10%Cu nanocomposites were synthesized in a planetary high-energy ball mill from elemental Ti and Cu powders. Elemental titanium (Ti) and copper (Cu) powders with a purity of 99.6% and an average particle size of 100 μm were used. Mixtures of the initial Ti and Cu powders were processed cyclically (cycle time: 5 minutes) in a planetary high-energy ball mill for 120 minutes. The temperature of the working area inside the mill jars did not exceed 100°C during processing. The rotational speed of the jars is 1480 rpm, the acceleration is 50 g, and the pressure on the particles of material in the cups is on the order of 5 GPa. The mechanically activated powder mixtures were compacted in a mold under a pressure of 30 GPa, after which they were sintered in an argon atmosphere at a temperature of 950°C for 30 minutes. Meyer hardness was determined, which is the average pressure on the contact surface between the indenter and the specimen. The load varies from 0 to 100 grams according to a simple "load–unload" cycle. The mechanical properties of the Ti–Cu nanocomposites obtained were analysed. It should be emphasized that the hardness of the Ti–Cu materials obtained in this study is higher than that of traditional bulk alloys. For example, when a 100-gram load was applied to the indenter, the hardness of the Ti-10%Cu nanocomposite was 4.7 GPa. This impressive result is primarily due to the nanostructured state formed during the mechanical grinding process. However, the Young's modulus of the resulting Ti–Cu nanocomposite is lower than that of the bulk alloy and is equal to 50 GPa. The resulting Ti-Cu nanocomposite, with a hardness of 4.7 GPa, can be used not only in industry, automotive manufacturing, and the aerospace sector, but also in the military for use in armor plates. While the Ti-Cu nanocomposite corresponds to mid-grade armor steel, it offers significant advantages due to the lighter weight of the armor plates.

Cite as: Mykola Melnichenko et al., "Mechanical properties of a Ti–Cu nanocomposite prepared by mechanical alloying", in *Book of Abstracts of the 27th Symposium on Photonics and Optics (SPO 2026)*, Kyiv, 2–6 November 2026, p. 112.

Fr4.11 POSTER · FRIDAY 14:25 CET · 15:25 KYIV #202

Order in nanoparticles-doped liquid crystals

R Karapinar

Burdur Mehmet Akif Ersoy University, Burdur, Türkiye

Applying nanotechnology to liquid crystalline materials is a promising research area. The nanoparticles can produce interesting optical properties in the liquid crystals. This effect results in lower operating voltages for liquid crystal devices. In this study, we discuss the presence of nanoparticles in a nematic liquid crystal mixture and the determination of the order parameter in pure and nanoparticle-doped liquid crystal materials. Nanoparticles with a concentration of 3% by weight create nanocolloids. At such low concentrations, the nanocolloid appears similar to a pure liquid crystal with no apparent evidence of nanoparticles because the low nanoparticle concentration does not perturb the director field in the liquid crystal medium. It has been observed that nanocolloids exhibit a higher order parameter than that of a pure liquid crystal.

Cite as: R Karapinar, "Order in nanoparticles-doped liquid crystals", in *Book of Abstracts of the 27th Symposium on Photonics and Optics (SPO 2026)*, Kyiv, 2–6 November 2026, p. 113.

Fr4.12 POSTER · FRIDAY 14:29 CET · 15:29 KYIV #218

Optical Absorption as a Probe of Fluorination and Crystalline Phase in P(VDF-TrFE): A Density Functional Theory Study

Oleksii Makarenko, Yuriy Hizhnyi, Zakhar Baranchykov
Taras Shevchenko National University of Kyiv, Kyiv, Ukraine

Poly(vinylidene fluoride-co-trifluoroethylene), P(VDF-TrFE), is a ferroelectric polymer of interest for flexible electronics, sensors, and energy-harvesting devices. Its optical response depends on both crystalline structure and chemical composition, making spectroscopy a potentially useful tool for identifying phase composition and fluorination-related structural changes. However, the sensitivity of different optical parameters to these changes is not uniform. This study uses density functional theory (DFT) to compare the optical properties of α- and β-phase P(VDF-TrFE) crystals and assess their suitability for spectroscopic characterization.

The calculations were performed using the CASTEP package within the generalized gradient approximation and the PBE exchange-correlation functional. Three α-phase structural models containing 2.1%, 4.2%, and 6.25% fluorine substitutions were investigated, alongside a β-phase model with 4.2% fluorine content. Optical absorption, reflectance, refractive indices, and Raman spectra were analyzed to evaluate the sensitivity of these observables to fluorination and crystalline phase.

The calculated absorption spectra reveal a systematic increase in absorption in the 7–9 eV region as fluorination increases in the α-phase models. The absorption onsets also differ by more than 1 eV between these models, suggesting that absorption spectroscopy may help distinguish structures with different fluorination levels. For α- and β-phase models with the same fluorine content, the absorption edges exhibit an approximately 2 eV displacement, providing a potential spectral indicator of crystalline phase. In contrast, reflectance spectra show relatively similar profiles: the α-phase reaches a maximum of approximately 0.40 near 23 eV, while the β-phase reaches approximately 0.31 near 25 eV. Such similarities may complicate reliable phase identification based on reflectance alone. Differences in refractive indices are likewise limited over parts of the spectrum, reducing the expected discriminative power of ellipsometric measurements.

Raman spectra provide complementary structural information, particularly through phase-dependent peak positions and intensity redistribution in the 500–1500 cm^{-1} and 3000–3200 cm^{-1} regions. The combined results indicate that optical absorption and Raman spectroscopy offer complementary means of distinguishing fluorination levels and crystalline structures, whereas reflectance and refractive-index measurements may be less diagnostic when used independently.

This computational comparison establishes a basis for selecting spectroscopic observables for the characterization of P(VDF-TrFE) and highlights the importance of combining complementary techniques when analyzing structurally complex polymeric materials.

Cite as: Oleksii Makarenko et al., "Optical Absorption as a Probe of Fluorination and Crystalline Phase in P(VDF-TrFE): A Density Functional Theory Study", in *Book of Abstracts of the 27th Symposium on Photonics and Optics (SPO 2026)*, Kyiv, 2–6 November 2026, p. 114.

Fr5.1 POSTER · FRIDAY 14:33 CET · 15:33 KYIV #279

Comparison of Theoretical and Experimental Raman and Infrared Spectra of P(VDF-TrFE): Phase and Composition Sensitivity

Dmytro Zaporoshchenko, Oleksii Makarenko, Yurii Hizhnyi, Zakhar Baranchykov
Taras Shevchenko National University of Kyiv, Kyiv, Ukraine

Poly(vinylidene fluoride-co-trifluoroethylene), P(VDF-TrFE), is a ferroelectric polymer whose vibrational spectra depend on crystalline structure and chemical composition. Interpreting these spectra requires distinguishing phase-dependent features from changes associated with TrFE content. This study compares density functional theory (DFT) predictions with published infrared and Raman measurements to evaluate the experimental relevance of calculated phase and composition sensitivity.

Calculations were performed using CASTEP within the generalized gradient approximation and the PBE exchange-correlation functional. Three α-phase structural models with fluorine substitution levels of 2.1%, 4.2%, and 6.25% were investigated alongside a β-phase model with a 4.2% substitution level. With one H-to-F substitution per converted repeat unit, the adopted model compositions correspond to nominal TrFE contents of 12.5, 25, and 37.5 mol.% for the α phase and 25 mol.% for the β phase. Published infrared [1] and Raman [2,3] spectra were digitized and compared using reference-band normalization, without empirical frequency shifts or rescaling.

The infrared comparison reveals local correspondence in band positions and phase-dependent intensity distributions. The experimental profile is dominated by absorption near $1183\,\mathrm{cm}^{-1}$, corresponding closely to the β-model band near $1181\,\mathrm{cm}^{-1}$. The α model predicts a neighboring band near $1171\,\mathrm{cm}^{-1}$. These features provide reference points for comparing the calculated structures with experiment.

The Raman comparison at matched nominal composition distinguishes the two calculated phases more directly. The models exhibit different dominant-band positions and intensity distributions in the 780–$900\,\mathrm{cm}^{-1}$ region, with the β-phase maximum closer in frequency to experiment. Peak positions and relative intensities thus provide complementary criteria for assessing phase-dependent spectral patterns.

Analysis of the wider concentration series shows that these signatures also depend on TrFE content. Across the α models, the dominant Raman band moves towards higher wavenumbers with increasing substitution, following the direction observed experimentally [2]. The experimental contribution in the 1340–$1380\,\mathrm{cm}^{-1}$ region strengthens, whereas bands near 1280 and $1430\,\mathrm{cm}^{-1}$ generally weaken across the copolymer series [3]. The α models exhibit composition-dependent intensity redistribution near 1280–1300 and $1430\,\mathrm{cm}^{-1}$, providing additional spectral regions for comparison.

Combined infrared and Raman analysis therefore provides complementary information on phase and composition sensitivity. The comparison establishes band-dependent agreement between theory and experiment and supports the combined use of Raman and infrared spectroscopy for evaluating composition and local structure. Reliable interpretation requires multiple spectral markers, consideration of composition and measurement conditions, and independent structural information.

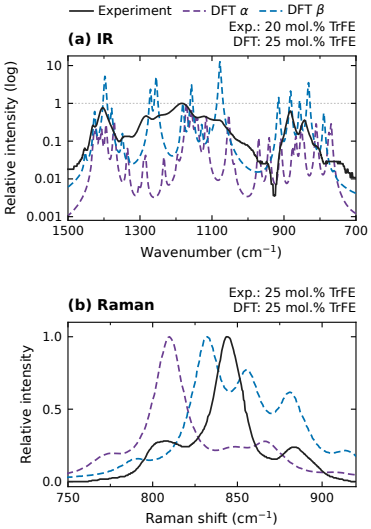


Figure. Digitized P(VDF-TrFE) IR (a: 20 mol.% TrFE [1]) and Raman (b: 25 mol.% [2]) spectra are compared with nominal 25 mol.% α/β DFT spectra. Solid/dashed: experiment/theory; each is normalized to its IR band near $1183\,\mathrm{cm}^{-1}$ or Raman maximum within 780–$900\,\mathrm{cm}^{-1}$.

[1] Arrigoni, A.; Brambilla, L.; Bertarelli, C.; Serra, G.; Tommasini, M.; Castiglioni, C. P(VDF-TrFE) nanofibers: structure of the ferroelectric and paraelectric phases through IR and Raman spectroscopies. RSC Advances 2020, 10(62), 37779–37796. https://doi.org/10.1039/D0RA05478J

[2] Resende, P. M.; Isasa, J.-D.; Hadziioannou, G.; Fleury, G. Deciphering TrFE Fingerprints in P(VDF-TrFE) by Raman Spectroscopy: Defect Quantification and Morphotropic Phase Boundary. Macromolecules 2023, 56(23), 9673–9684. https://doi.org/10.1021/acs.macromol.3c01700

[3] Tashiro, K.; Kobayashi, M. Vibrational spectroscopic study of the ferroelectric phase transition in vinylidene fluoride-trifluoroethylene copolymers: 1. Temperature dependence of the Raman spectra. Polymer 1988, 29(3), 426–436. https://doi.org/10.1016/0032-3861(88)90359-X

Cite as: Dmytro Zaporoshchenko et al., "Comparison of Theoretical and Experimental Raman and Infrared Spectra of P(VDF-TrFE): Phase and Composition Sensitivity", in *Book of Abstracts of the 27th Symposium on Photonics and Optics (SPO 2026)*, Kyiv, 2–6 November 2026, p. 115.

Fr5.2 POSTER · FRIDAY 14:37 CET · 15:37 KYIV #229

Aziridinium Cation based Cadmium Halide Hybrids

Danylo Kreiman[1], Sergiu Shova[2], Olesia Kucheriv[1], Illia Guralskyi[1]

[1] *Taras Shevchenko National University of Kyiv, Kyiv, Ukraine* [2] *"Petru Poni" Institute of Macromolecular Chemistry, Iași, Romania*

Hybrid metal halides have attracted considerable attention as functional materials owing to their structural diversity and tunable optical and electronic properties. In particular, hybrid perovskites are promising candidates for applications in optoelectronics, photodetection, and light-emitting devices. However, the widespread use of lead-based perovskites raises concerns regarding the toxicity of lead and its potential environmental impact. The development of lead-free alternatives is therefore an important direction in the search for more environmentally compatible functional materials. Cadmium-based hybrid halides represent an alternative compositional family with potentially useful optical properties[1,2].

The properties of hybrid metal halides depend on both the inorganic framework and the organic cation[3]. While methylammonium-based cadmium halides, such as $CH_3NH_3CdBr_3$, have previously been investigated in terms of their crystal structures and optical band gaps, the effects of introducing alternative organic cations remain less explored. In particular, aziridinium, a cyclic organic cation, offers an opportunity to investigate how changes in cation identity influence the structural and optical characteristics of cadmium halides. Extending this family may help establish broader structure–property relationships in hybrid metal-halide materials.

Herein, we report the synthesis and characterization of two aziridinium cadmium halides, $(AzrH)CdCl_3$ and $(AzrH)CdBr_3$ (AzrH = aziridinium), expanding the range of organic cations investigated in cadmium-based hybrid halides. The compounds were prepared by reacting the corresponding starting materials in the respective acids, followed by isolation of the crystalline products by filtration and drying. Their crystal structures were determined by single-crystal X-ray diffraction. The phase consistency of the bulk crystalline samples was examined by powder X-ray diffraction, with the experimental patterns showing agreement with those simulated from the single-crystal structural data.

Optical measurements revealed band gaps of 5.36 eV for $(AzrH)CdCl_3$ and 3.62 eV for $(AzrH)CdBr_3$. The substantial decrease in band gap upon replacing chloride with bromide demonstrates the pronounced influence of halide composition on the optical properties of these materials. These findings establish aziridinium cadmium halides as an additional family of hybrid metal-halide compounds and provide a starting point for further investigations of their structural diversity and composition-dependent optical behaviour.

[1] Kalthoum, R.; Ben Bechir, M.; Ben Rhaiem, A. $CH_3NH_3CdCl_3$: A Promising New Lead-Free Hybrid Organic–Inorganic Perovskite for Photovoltaic Applications. Physica E: Low-dimensional Systems and Nanostructures 2020, 124, 114235.

[2] Alonso, J. A.; Kayser, P.; Hong, B. K.; Álvarez-Galván, M. C.; Fauth, F.; López, C. A. Mechano-Chemical Synthesis, Structural Features and Optical Gap of Hybrid CH3NH3CdBr3 Perovskite. Materials 2021, 14 (20), 6039.

[3] Hautzinger, M. P.; Mihalyi-Koch, W.; Jin, S. A-Site Cation Chemistry in Halide Perovskites. Chem. Mater. 2024, 36 (21), 10408–10420.

Cite as: Danylo Kreiman et al., "Aziridinium Cation based Cadmium Halide Hybrids", in *Book of Abstracts of the 27th Symposium on Photonics and Optics (SPO 2026)*, Kyiv, 2–6 November 2026, p. 117.

Fr5.3 POSTER · FRIDAY 14:41 CET · 15:41 KYIV #246

Band-structure evolution in Cs2AgxNa1-xInCl6 double perovskites and its manifestation in VUV-excited photoluminescence

Denys Orlov[1], Oleksii Makarenko[1], Yaroslav Zhydachevskyy[2], Yuriy Hizhnyi[1]

[1]Taras Shevchenko National University of Kyiv, Kyiv, Ukraine [2]Institute of Physics, Polish Academy of Sciences, Warsaw, Poland

Lead-free double perovskites $Cs_2NaInCl_6$ (CNIC) and its Ag-alloyed derivatives $Cs_2Ag_xNa_{1-x}InCl_6$ (CANIC) are promising down-converting phosphors for solar-blind UV detection, where emission must be excited near the fundamental absorption edge. Tuning them requires an atomic-level picture of how Ag and dopants reshape the electronic structure and the photoluminescence excitation (PLE) spectra.

We report first-principles calculations for the series $x = 0, 0.1, \ldots, 1$ and for CNIC:Ag, CNIC:Sb and CANIC:Bi. The alloys were modelled in 320-atom supercells with Na and Ag sharing a 32-site cation sublattice. As x does not fix which sites are replaced, candidate Na/Ag arrangements, part of them pre-selected by machine learning, were optimized within DFT and the lowest-energy one kept. We then computed band structures, densities of states and absorption spectra (CASTEP, GGA-PBE+U), with U reproducing the experimental gaps of CNIC (5.6 eV) and $Cs_2AgInCl_6$ (3.2 eV). The results are compared with photoluminescence measured under synchrotron excitation (100-330 nm, 10-300 K).

From the calculated densities of states we constructed a scheme that illustrates the evolution of the CANIC bands with increasing Ag content and the positions of the Sb and Bi defect levels within the gap.

In the host, Cl p states form the valence-band top and In s states the conduction-band bottom; Ag reshapes both. A single Ag_{Na} substitution creates an Ag d level 0.8 eV above the valence-band top. From $x = 0.1$ they broaden into an Ag d subband, $\sim$1.2 eV wide at $x = 0.8$, merging with the valence band at $x = 1$. Ag s subbands move the conduction-band bottom down by about 1.0 eV. Together these reduce the gap by 2.17 eV across the series. Sb_{In} creates a deep level at 1.8 eV, and Bi_{In} two levels, the shallower one at 0.15 eV.

This scheme explains the measured PLE spectra. For CNIC, the 190 and 215 nm bands are assigned to transitions into the lower conduction subband, and the 150 nm band into its upper part. All Ag-alloyed samples show an extra peak at 185 nm, independent of x, from charge-transfer excitation of the $[InCl_6]^{3-}$ host. The broad bands above 220 nm instead shift from 255 to 275 nm and beyond 330 nm with Ag content. They arise within the Ag subsystem and follow the calculated gap narrowing, as does the linear decrease of the Stokes shift.

The calculated absorption edge positions follow the measured trend across the series, showing that the U corrections compensate the DFT underestimation and that the calculated spectra can be used to interpret the experiment. For CNIC:Sb the measured bands at 3.5-4.2 and 4.5-5.2 eV are reproduced and assigned to Sb $s \rightarrow$ In s and Sb $s \rightarrow$ Sb p transitions. For CANIC:Bi an extra measured band has no calculated counterpart, as the calculations predict only a 0.15 eV edge shift.

FRI

The calculated scheme allows the origin of the electronic transitions involved in PL excitation in the UV/VUV region to be discussed. The nature of the additional Bi-related band remains open.

Cite as: Denys Orlov et al., "Band-structure evolution in Cs2AgxNa1-xInCl6 double perovskites and its manifestation in VUV-excited photoluminescence", in *Book of Abstracts of the 27th Symposium on Photonics and Optics (SPO 2026)*, Kyiv, 2–6 November 2026, p. 119.

Fr5.4 POSTER · FRIDAY 14:45 CET · 15:45 KYIV #278

Singlet Oxygen Generation by Different Types of MXenes ($Ti_3C_2T_x$) and Ti_3AlC_2 and Ti_3SiC_2 MAX Phases under Near-IR Excitation

Nazarii Tkach, Antonina Naumenko, Vladyslav Kudrya
Taras Shevchenko National University of Kyiv, Kyiv, Ukraine

MXenes-two-dimensional transition metal carbides-and their precursor MAX phases are considered promising agents for photothermal and photodynamic therapy owing to their absorption in the near-IR region, where biological tissues are most transparent. However, the factors governing the balance between photothermal and photodynamic excitation relaxation channels in MXenes remain poorly understood. The aim of this work is to compare the optical properties and, especially, the optical manifestations of singlet oxygen ($^1O_2$) generation for three $Ti_3C_2T_x$ samples (one single-layer and two multilayer samples of different origin) and the Ti_3AlC_2 and Ti_3SiC_2 MAX phases.

The studied compounds (at a concentration of $2 \cdot 10^{-3}$ M) were prepared in DMSO and ethanol. Absorption spectra were recorded using a Cary 60 spectrophotometer (Agilent), and luminescence spectra were measured on a Horiba FluoroMax spectrofluorometer; especially, $^1O_2$ luminescence (1100-1350 nm) was registered using a liquid-nitrogen-cooled DSS detector.

The absorption spectrum of one of the multilayer $Ti_3C_2T_x$ samples contains an intense broad absorption band with maximum at ~775 nm. For the single-layer sample, this band is weakly pronounced, whereas for the second multilayer sample only a monotonic increase in absorption in the IR region is observed. The MAX phases absorb in the UV region (270, 303-305 nm) and exhibit strong emission at ~365 nm (with the additional band at ~470 nm for Ti_3SiC_2). Under 780 nm excitation, the band at ~1270 nm characteristic of $^1O_2$ luminescence was recorded for most samples. It is most intense for the multilayer $Ti_3C_2T_x$ without a pronounced absorption band at 775 nm, distinct for single-layer $Ti_3C_2T_x$ and Ti_3SiC_2, and weak for Ti_3AlC_2. Conversely, the sample with the most intense absorption at 775 nm generates almost no $^1O_2$. For single-layer $Ti_3C_2T_x$, the $^1O_2$ luminescence intensity is higher in ethanol than in DMSO.

Thus, the efficiency of $^1O_2$ generation by MXenes under IR excitation is determined neither by structural features nor by the intensity of IR absorption, but depends on the synthesis route of the material. Surface chemistry and defect structure likely play a decisive role, which should be taken into account when selecting MXenes for photodynamic therapy.

Acknowledgement. The work was performed with financial support by the grant 2025.07/0400 from the National Research Foundation of Ukraine.

Cite as: Nazarii Tkach et al., "Singlet Oxygen Generation by Different Types of MXenes ($Ti_3C_2T_x$) and Ti_3AlC_2 and Ti_3SiC_2 MAX Phases under Near-IR Excitation", in *Book of Abstracts of the 27th Symposium on Photonics and Optics (SPO 2026)*, Kyiv, 2–6 November 2026, p. 121.

Fr5.5 POSTER · FRIDAY 14:49 CET · 15:49 KYIV #281

Optical Properties and Singlet Oxygen Generation in Tryptanthrin/MoS_2 Nanosystems

Nazarii Tkach, Antonina Naumenko, Vladyslav Kudrya
Taras Shevchenko National University of Kyiv, Kyiv, Ukraine

Tryptanthrin (Try) is a natural indoloquinazoline alkaloid with a broad spectrum of biological activity that is considered a potential photosensitizer for photodynamic therapy. However, the generation of singlet oxygen $^1O_2$ by Try in ethanol is inefficient. One way to enhance the photosensitizing ability of organic dyes is to combine them with two-dimensional transition metal dichalcogenides. The aim of this work was to investigate the effect of MoS_2 nanolayers on the optical properties of Try and $^1O_2$ generation by Try.

Tryptanthrin (Try), MoS_2 samples, and their mixtures in ethanol were investigated. Absorption spectra were recorded on a Cary 60 spectrophotometer (Agilent), while luminescence and luminescence excitation spectra were measured on a Horiba FluoroMax spectrofluorometer. The efficiency of $^1O_2$ generation was evaluated from its luminescence intensity in the near-IR region (1100-1350 nm) using a liquid-nitrogen-cooled DSS detector.

The absorption spectrum of Try contains bands at 252, ~315, ~335, and ~392 nm, while its luminescence spectrum exhibits a broad band peaking near 525 nm as well as a short-wavelength indole UV band at ~345-360 nm (under UV excitation). In the absorption spectra of Try/MoS_2 mixtures, the dye bands are preserved and characteristic long-wavelength absorption bands of MoS_2 (~630 and ~690 nm) appear. Adding MoS_2 causes strong quenching of the visible luminescence of Try: the intensity of the 525 nm band decreases sharply (including relative to the short-wavelength indole band at ~360 nm) even when the dye concentration is doubled. Under 395 nm excitation, the Try solution shows no noticeable $^1O_2$ signal. In contrast, for the Try/MoS_2 mixtures, a distinct band at 1265-1270 nm characteristic of $^1O_2$ luminescence is recorded, which is significantly more intense than that for MoS_2 samples without tryptanthrin.

The obtained results indicate effective interaction of Try with the MoS_2 surface and possible energy/charge transfer between the components promoting $^1O_2$ formation. Try/MoS_2 nanosystems can be considered as promising materials for singlet oxygen photosensitization.

Cite as: Nazarii Tkach et al., "Optical Properties and Singlet Oxygen Generation in Tryptanthrin/MoS_2 Nanosystems", in *Book of Abstracts of the 27th Symposium on Photonics and Optics (SPO 2026)*, Kyiv, 2–6 November 2026, p. 122.

Fr5.6 POSTER · FRIDAY 14:53 CET · 15:53 KYIV #205

Silicon incorporation and dislocation-related traps in GeSn and GeSiSn layers on Si: an impedance and photocurrent study

Andrii Pocherpailo[1], Serhiy Kondratenko[1], Oleksandr Datsenko[1], Stanislav Krakovskyi[1], Petro Kovanzhi[1], Petro Lytvyn[2], Yuriy Mazur[3], Gregory J. Salamo[3]

[1]Taras Shevchenko National University of Kyiv, Kyiv, Ukraine [2]V. Lashkaryov Institute of Semiconductor Physics of the National Academy of Sciences of Ukraine, Kyiv, Ukraine [3]Institute of Nano Science and Engineering, University of Arkansas, Fayetteville, AR, USA

GeSn and GeSiSn are promising group-IV materials for Si-integrated infrared optoelectronics. Incorporating Sn shrinks the bandgap and, at sufficient content, makes it direct [1]. Because Sn is poorly soluble in Ge, these alloys must be grown far from equilibrium. This generates misfit and threading dislocations whose cores create band-like gap states that control carrier recombination [2]. Si is added to compensate the Sn-induced lattice expansion, but its effect on electrically active defects cannot be deduced from structural data alone.

We combine impedance spectroscopy, lateral photocurrent (PC) spectroscopy and surface imaging to compare two layers with identical Sn content grown on Si(001) via a Ge buffer: a 44 nm binary $Ge_{0.934}Sn_{0.066}$ layer and a 65 nm ternary $Ge_{0.817}Si_{0.117}Sn_{0.066}$ layer.

SEM and AFM show that both films are continuous and grew two-dimensionally. Their RMS roughness over 2×2 μm^2 is 0.40 nm for GeSn and 0.31 nm for GeSiSn. Neither film shows Sn segregation, so metallic shunting paths can be ruled out. Both surfaces share a buffer-inherited undulation (period 2–3 μm, amplitude $\sim$10 nm) and 10–15 nm pits at densities of $\sim 10^{10}$ cm^{-2}. GeSiSn additionally shows isolated 150–200 nm islands at $(7 \pm 2) \times 10^7$ cm^{-2} ($\sim$2% coverage), which are too sparse to affect lateral transport. The electrical responses are therefore directly comparable.

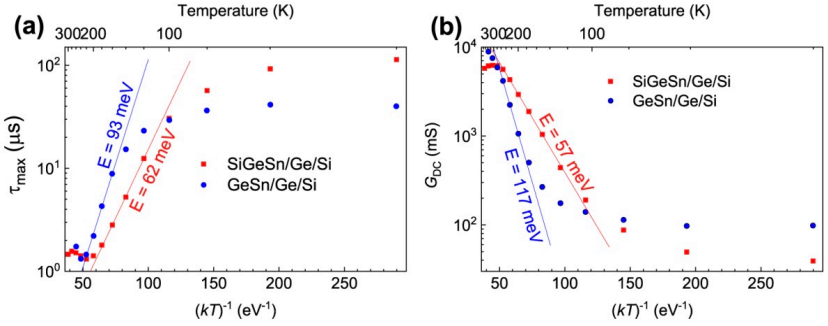


Figure. Temperature-dependent conductivity relaxation time (a) and dc conductance (b) of the studied structures. The lines are functions $\propto \exp[\pm E/(kT)]$

In the lateral geometry, the conductivity relaxation time τ_{max} and the dc conductance G_{DC} are thermally activated at high temperatures. They follow $\exp[\pm E/(kT)]$ with E = 90–120 meV for GeSn and $\sim$60 meV for GeSiSn. Weaker low-temperature dependences are tentatively

FRI

attributed to mobility variation. The binary-layer energies agree with dislocation-related levels near $E_V + (85\text{–}90)$ meV, the dominant Shockley–Read–Hall centres in Ge-rich GeSn [3].

The PC spectra show an onset above 0.7 eV from the Ge(Si)Sn absorption edge, a Ge-buffer contribution above 0.8 eV, and a strong Si-substrate band above 1.1 eV. The PC at 0.95 eV drops sharply above $\sim$220 K. The quenching energies, 280 meV for GeSiSn and $\sim$140 meV for GeSn, exceed the impedance energies, as expected, since PC quenching reflects competition between collection and trap-assisted recombination, whereas impedance probes thermal emission from the same states.

The lower activation energy of the ternary alloy indicates that Si does not eliminate dislocation-related traps but broadens their energy distribution.

Acknowledgement. This work was supported by the National Research Foundation of Ukraine (project 2023.03/0060).

[1] D. Grützmacher *et al.*, Appl. Phys. A **129**, 1 (2023).

[2] A. Giunto, A. Fontcuberta i Morral, Appl. Phys. Rev. **11**, 041333 (2024).

[3] S. Gupta *et al.*, Appl. Phys. Lett. **113**, 022102 (2018).

Cite as: Andrii Pocherpailo et al., "Silicon incorporation and dislocation-related traps in GeSn and GeSiSn layers on Si: an impedance and photocurrent study", in *Book of Abstracts of the 27th Symposium on Photonics and Optics (SPO 2026)*, Kyiv, 2–6 November 2026, p. 123.

Fr5.7 POSTER · FRIDAY 14:57 CET · 15:57 KYIV #244

Investigation of the influence of natural scenes conditions on thermal contrast and detection range of phase-change materials

Yevhen Melezhyk, Zinoviia Tsybrii

V. Lashkaryov Institute of Semiconductor Physics of the National Academy of Sciences of Ukraine, Kyiv, Ukraine

Phase-change materials (PCMs) and PCM-based metamaterials represent an emerging field of research. These materials can change their infrared emissivity under external stimuli such as applied electric current, mechanical strain, or optical laser pulses. Owing to this ability, they find applications in various industries, from novel building materials and fabrics to drug delivery, solar panel design, and special applications. Research in the literature usually focuses on material fabrication, growth, and laboratory characterization. Such studies make it possible to optimize material design to achieve the largest possible IR emissivity switching range, which is not always the most cost-effective solution.

However, these studies do not address what emissivity ranges are actually needed to manage the thermal contrast of typical PCM-covered ground objects in various real-world scenarios. In such scenarios, the apparent temperature of PCM-covered surfaces and their thermal contrast with the background are significantly affected by weather conditions (insolation, cloud cover, ambient air temperature, humidity, time of day, season, etc.).

Thus, the goals of this work were twofold: to investigate the influence of weather and scene factors on the apparent thermal contrast of PCM-covered surfaces with varying infrared emissivity, and to estimate the effect of this contrast variation on the detection range of ground objects.

We simulated the relative change in the maximum detection range (MDR) of such objects caused by changes in their apparent thermal contrast, using the Johnson criteria [1]. Our results showed that a tenfold decrease in the contrast value reduces the MDR by approximately one third. Since these calculations assume a uniform background temperature, they can serve as an upper-bound estimate, while real background clutter would further degrade the MDR.

We also systematized field measurement data available in the literature on the thermal dynamics of typical European landscapes in winter and summer. This allowed us to estimate the temperature swings of typical background objects (such as soil, asphalt, tree canopy, grass, rocks, snow, and ice) over the diurnal cycle in different seasons. On this basis, we estimated which IR emissivity switching ranges would be sufficient for thermal contrast management of PCM-covered ground objects with different intrinsic temperatures.

By combining the obtained data, we systematized the requirements for the design of novel PCMs for various thermal contrast management applications.

Acknowledgement. This work was partially supported by the National Academy of Sciences of Ukraine (projects #0125U000799 and III-10-24).

[1] Ye.O. Melezhyk, Z.F. Tsybrii, V.V. Zabudsky et al., Numerical estimations of the maximal distance of target detection in the IR spectrum with decreasing the target–background temperature contrast // Semiconductor Physics, Quantum Electronics & Optoelectronics, 2024, V. 27, No. 4, P. 397–403.

Cite as: Yevhen Melezhyk et al., "Investigation of the influence of natural scenes conditions on thermal contrast and detection range of phase-change materials", in *Book of Abstracts of the 27th Symposium on Photonics and Optics (SPO 2026)*, Kyiv, 2–6 November 2026, p. 125.

Fr5.8 POSTER · FRIDAY 15:01 CET · 16:01 KYIV #214

Low-Cost Real-Time Frame-to-Event Converter for Prototyping Event-Based Obstacle Detection

Vitalii Bortnik, Volodymyr Borovytsky

National Technical University of Ukraine "Igor Sikorsky Kyiv Polytechnic Institute", Kyiv, Ukraine

Frame-based cameras read out all pixels at a fixed rate, whether or not the scene changes. In dynamic scenes, fast objects blur, dynamic range is limited, latency is bounded by the frame period, and static regions are transmitted redundantly. In event-based cameras, each pixel responds independently to log-brightness changes and asynchronously emits an event carrying its coordinates, polarity and timestamp, with latency down to 15 μs and 120 dB dynamic range, which suits fast obstacle detection and collision avoidance. However, event-based cameras and their development tools are expensive and scarce, which slows the development of event-based algorithms

We propose a low-cost converter, a board with a camera module and an STM32 microcontroller, that makes a commodity frame-based camera emulate an event-based camera, producing events (nx, ny, t, p) in real time. The microcontroller compares each new frame with a per-pixel reference log-brightness level. When the change exceeds the contrast threshold C, an ON (p = 1) or OFF (p = 0) event is emitted; a change of n thresholds yields n events and shifts the reference by nC. The timestamp t is interpolated between consecutive frames, as in ESIM and v2e, and corrected for the readout time of row ny.

An OV7670 (QVGA, 30 fps) or another DCMI-compatible sensor connects to an STM32H743. DCMI byte-select mode keeps only the luminance Y, and DMA writes it into ping-pong buffers, so frame k is processed while frame k+1 arrives. A 256-entry lookup table maps Y to log intensity, a 16-bit map holds the reference levels, and a 1 MHz timer timestamps VSYNC and HSYNC. Auto exposure, gain and white balance are disabled to avoid spurious events. Each 40-bit event holds polarity (1 bit), nx and ny (12 bits each) and time from frame start (15 bits). Events are sent via USB CDC in per-frame packets whose header carries the frame timestamp.

The key limitation is frame-based readout: a change is reported only after the next frame is captured, processed and sent. At 30 fps, waiting and readout alone take up to 67 ms, over 4,000 times longer than in an event-based camera; higher frame rates and row-wise processing shorten but cannot remove this delay. Further limitations: temporal resolution equals the frame period, with aliasing above 15 Hz; dynamic range is about 48 dB (8-bit output, fixed exposure), causing noise in dark regions; motion blur and rolling-shutter skew; and USB Full Speed cannot carry the 2.3 million events/s of full-frame changes. Thus, the converter is unsuitable for microsecond-response applications. But it has important advantages: low-cost hardware, real-time operation and output reproducing the format and sparsity of event streams. Since static regions are not transmitted, it reduces the data sent to and analyzed by the host while events per frame stay below 20% of the pixel count (a 40-bit event data packet equals five 8-bit pixels). It suits algorithm development and testing, spiking neural network training, event-based vision research and education in computer vision, robotics and automation.

Cite as: Vitalii Bortnik et al., “Low-Cost Real-Time Frame-to-Event Converter for Prototyping Event-Based Obstacle Detection”, in *Book of Abstracts of the 27th Symposium on Photonics and Optics (SPO 2026)*, Kyiv, 2–6 November 2026, p. 127.

Fr5.9 POSTER · FRIDAY 15:05 CET · 16:05 KYIV #254

Water in Structures and Vibrations of Cellulose and Methylcellulose

Danylo Morozov[1], Viktor Borysiuk[1], Vitalii Chornii[2], Serhii Nedilko[1]

[1]Taras Shevchenko National University of Kyiv, Kyiv, Ukraine [2]National University of Life and Environmental Sciences of Ukraine, Kyiv, Ukraine

Cellulose is an abundant renewable polymer with potential applications in sustainable packaging, coatings and functional composites. Its hydroxyl groups enable hydrogen bonding and chemical modification, providing opportunities to tailor its interactions with other components. Methylcellulose, a cellulose derivative obtained by partial methyl substitution, is also used as a film-forming material and polymer matrix. Comparing these materials offers an opportunity to examine how changes in chemical structure affect interactions with water. This is relevant because moisture can influence the structure and properties of cellulose-based materials. The present study aims to clarify the roles of methyl substitution and hydration in the vibrational response of cellulose and methylcellulose by combining Fourier-transform infrared (FTIR) spectroscopy with density functional theory (DFT) calculations. Experimental spectra of specimens with and without preliminary drying were recorded over 450–4000 cm^{-1} using a Shimadzu IRTracer-100 spectrometer with an attenuated total reflection accessory. Complementary DFT calculations were performed at the B3LYP/6-31G level for cellulose and methylcellulose trimers, designated CL3 and MC3, with and without explicit water molecules. In MC3, methyl substitution at O2 and O6 provides a defined model for examining the effect of replacing hydroxyl hydrogens with methyl groups. The analysis considers O–H and C–H stretching vibrations, C–O and C–O–C vibrations, and the contribution of water. Particular attention is given to changes in band positions, relative intensities and profiles, as well as to the dependence of calculated vibrations on local hydrogen-bond arrangements. Atomic displacement vectors are examined alongside unscaled harmonic frequencies to distinguish polymer and water motions and identify their coupling. This combined approach is intended to help separate the spectral effects of chemical substitution from those associated with hydration and sample preparation. The study can provide a molecular basis for interpreting overlapping infrared bands and assessing the sensitivity of spectral features to water interactions. Such understanding could support the selection of drying and storage conditions for reproducible measurements and inform the development of cellulose-based films, coatings and functional composites whose performance depends on moisture. The calculations complement the experimental analysis by linking spectral features to local interactions between the polymer and water molecules.

Cite as: Danylo Morozov et al., "Water in Structures and Vibrations of Cellulose and Methylcellulose", in *Book of Abstracts of the 27th Symposium on Photonics and Optics (SPO 2026)*, Kyiv, 2–6 November 2026, p. 129.

Fr6.1 POSTER · FRIDAY 15:30 CET · 16:30 KYIV #272

Formation and properties of barrier structures based on p-CdTe:Cl fabricated by laser-induced indium doping

Serhii Levytskyi

V. Lashkaryov Institute of Semiconductor Physics of the National Academy of Sciences of Ukraine, Kyiv, Ukraine

Single-crystal semi-insulating CdTe and $Cd_{1-x}Zn_xTe$ (x=0.1) materials are highly promising for high-efficiency X- and γ-ray detectors operating at room temperature. Utilizing diode-type potential barriers (p-n junctions or Schottky barriers) significantly reduces dark current and noise levels compared to homogeneous detectors, which is critical for photon-counting and spectrometry modes. However, classical diffusion p-n junctions in p-CdTe:Cl are strictly limited by thermal constraints and self-compensation. Laser-induced doping with indium (In) as a donor impurity offers an efficient alternative for barrier formation.

Experimental samples (6x6x0.5 mm) were prepared from semi-insulating p-CdTe:Cl wafers ($\rho \approx 2 \cdot 10^9$ Ω·cm). After abrasive wire sawing, the damaged surface layers were removed via chemical-mechanical polishing with bromine-containing etching compositions. A thin Au film (0.8 μm, 5x5 mm^2) was deposited onto one side. Thermal annealing of the Au/p-CdTe:Cl structure in a pure hydrogen atmosphere (T ≈ 280°C, 8–10 min) ensured an ohmic contact and surface stoichiometrization. A thin In film (0.5 μm, 5x5 mm^2) was deposited onto the opposite surface. Modification was performed by irradiating the In film with a single nanosecond pulse from a Nd:YAG laser at an energy density of ≈0.11 J/cm^2. Subsequently, the remaining In was dissolved in hydrochloric acid, and contact pads (Ø 0.8 mm) with lead wires were deposited at the center. Electrical and photoelectric properties were studied at T ≈ 293 K. During spectral photoconductivity measurements in the photovoltaic mode, the In contact pads were shaded.

The current-voltage (I-V) characteristics of the fabricated structures exhibit a distinct diode-like behavior, with forward bias corresponding to a negative voltage polarity at the In contact. The reverse I-V branch lacks a dark current saturation region and shows smooth pre-breakdown behavior, indicating a negligible diffusion component and a predominant role of generation and surface current components. Under forward bias voltages U ≥ 6 V, the I-V curve linearizes in semi-logarithmic coordinates, confirming an exponential current behavior under high carrier injection into the i-region, consistent with n-i-p junction theory. The spectral photosensitivity under illumination from the shaded In contact side (0.40–0.86 μm) maintains a constant photoresponse sign (negative polarity at the In contact), verifying the presence of a single potential barrier. The maximum saturation open-circuit photovoltage under a 250 W quartz-halogen lamp was 90±5 mV at T ≈ 293 K. Etching the near-surface CdTe:Cl region on the In contact side to a depth of ≈0.12 μm resulted in the complete disappearance of the photovoltaic effect and a fundamental alteration of the I-V characteristics.

The experimental results are explained by a laser-pulse-induced conduction-type inversion in the thin near-surface region of p-CdTe:Cl due to In donor implantation, forming a sharp n-p junction. Based on the data, the parameters of the equilibrium energy band diagram for these CdTe:Cl n-p junctions are discussed.

Cite as: Serhii Levytskyi, “Formation and properties of barrier structures based on p-CdTe:Cl fabricated by laser-induced indium doping”, in *Book of Abstracts of the 27th Symposium on Photonics and Optics (SPO 2026)*, Kyiv, 2–6 November 2026, p. 130.

Fr6.2 POSTER · FRIDAY 15:34 CET · 16:34 KYIV #220

Deep Level Admittance Spectroscopy of PEDOT:PSS/Si Heterostructure

Oleh Bozhko, Oleksandr Datsenko, Serhiy Kondratenko
Taras Shevchenko National University of Kyiv, Kyiv, Ukraine

PEDOT:PSS/Si heterostructures are promising for silicon-based photovoltaics. The transparent polymer behaves as a p-type semiconductor and forms a p–n heterojunction with n-Si, which separates electron–hole pairs photogenerated in silicon. In this work, a vertical PEDOT:PSS/n-Si structure was studied by temperature-dependent admittance spectroscopy.

The PEDOT:PSS layer was deposited onto an n-Si substrate ($4.5\ \Omega \cdot$ cm) by drop-casting followed by spin-coating. A semitransparent Au film and InGa eutectic served as the top and bottom electrodes, respectively.

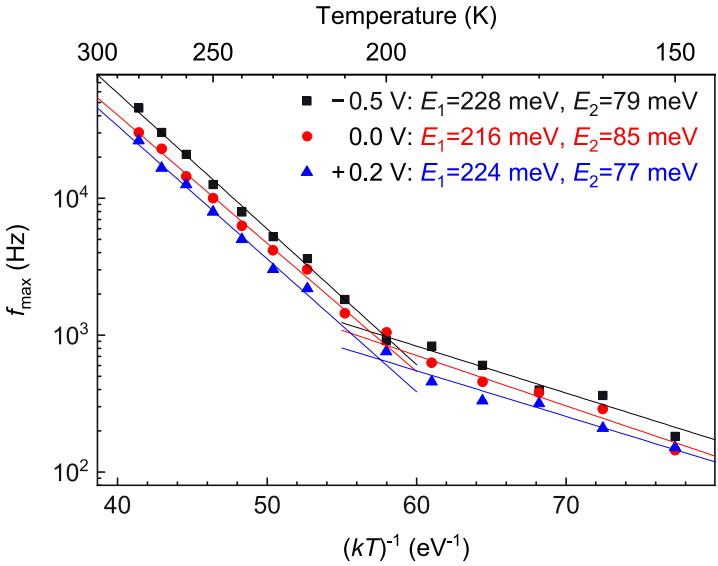


Figure. Arrhenius plot of the resonant frequencies under different biases with estimated activation energies.

The structure was found to be rectifying, and the Mott-Schottky plot ($1/C^2$ versus V) showed a barrier height of 0.65 eV at the PEDOT:PSS/Si interface. A photovoltage signal appeared at photon energies above the Si band gap (1.1 eV). Frequency (f) spectra of the admittance $Y = G + j \cdot B$ (G is conductance, B is susceptance) were measured from 0.1 to 1000 kHz under dc biases of –0.5, 0 and +0.2 V and ac amplitude of 100 mV at temperatures from 10 to 300 K. From 150 to 300K, the frequency dependence of G/f revealed a peak. The peak position $f_{\max}$ was found to shift towards higher temperatures T when heating.

The Arrhenius plots of $f_{\max}$ versus $1/(kT)$ (k is Boltzmann constant) in Fig. 1 showed two linear sections where the dependence followed function $\propto \exp[-E/(kT)]$. The dependence

FRI

slope below 200 K allowed to extract the conductivity activation energy $E = 81 \pm 4$ meV, while the value of 222 ± 6 meV was obtained from the section from 200 to 280 K. The sign and magnification of the bias affected the results negligibly. The activation energies are attributed to the depths of acceptor-like states at the PEDOT:PSS/Si interface, which contribute to the conductivity via thermal activation.

Acknowledgement. This work was supported by the National Research Foundation of Ukraine (project 2023.03/0060).

Cite as: Oleh Bozhko et al., "Deep Level Admittance Spectroscopy of PEDOT:PSS/Si Heterostructure", in *Book of Abstracts of the 27th Symposium on Photonics and Optics (SPO 2026)*, Kyiv, 2–6 November 2026, p. 132.

Fr6.3 POSTER · FRIDAY 15:38 CET · 16:38 KYIV #274

Heterogeneity and oxidation of layered porous silicon studied by spectroscopic ellipsometry

Taras Veremeichyk, Kateryna Yablochkova, Oleksii Makarenko, Viktoriya Shevchenko

Taras Shevchenko National University of Kyiv, Kyiv, Ukraine

Single-layer (porosity 64 % and 48 %) and double-layer porous silicon (PS) samples about 5 μm thick, formed by electrochemical etching of p^+-Si(100) at 200 and 50 mA/cm^2, were studied before and after thermal annealing in air. Spectroscopic ellipsometry $\Psi(\lambda)$, $\Delta(\lambda)$ spectra were analysed in the transparent near-infrared region using a sequence of models: a homogeneous Cauchy layer, two- and three-component (Si + SiO2 + voids) Bruggeman effective-medium approximations, and a layer with a depth gradient of the refractive index. The obtained thicknesses agree with scanning electron microscopy, and the porosities agree with gravimetry. In the double-layer sample, the porosities of the two layers (71 % and 52 %) match those of the single-layer samples etched at the same current densities. The layer etched at 200 mA/cm^2 is nearly homogeneous in depth, whereas the layer etched at 50 mA/cm^2 shows a pronounced inhomogeneity that persists after annealing. Before annealing, the oxide is confined to a thin near-surface layer, as confirmed by EDS oxygen profiles. After annealing, the oxygen content increases markedly throughout the layers, the layer thickness increases and the refractive index decreases. The highly porous layer oxidizes completely and contains ≈ 56 % SiO2 while retaining a large fraction of pores, whereas in the less porous layer the oxide fills nearly the entire pore volume. A volume-balance analysis that accounts for the volume expansion upon Si → SiO2 conversion ($\kappa \approx 2.27$) shows that the amount of silicon is conserved and that the degree of oxidation is governed by the initial porosity and layer expansion. The approach enables non-destructive evaluation of porosity, oxide fraction, oxidation degree and inhomogeneity of individual layers in PS multilayers.

Cite as: Taras Veremeichyk et al., "Heterogeneity and oxidation of layered porous silicon studied by spectroscopic ellipsometry", in *Book of Abstracts of the 27th Symposium on Photonics and Optics (SPO 2026)*, Kyiv, 2–6 November 2026, p. 134.

Fr6.4 POSTER · FRIDAY 15:42 CET · 16:42 KYIV #206

Electrical Tuning of the Graphene Mode in a One-Dimensional Terahertz Photonic Microcavity with a Multilayer Graphene Stack: Effects of Gate Voltage and Number of Layers

Solmaz Salary[1], Behrooz Rezaei[2], Samad Roshan Entezar[3]

[1] *University of Tabriz, Tabriz, Iran* [2] *Department of Condensed Matter, Faculty of Physics, University of Tabriz, Tabriz, Iran* [3] *Department of Optics and Laser, Faculty of Physics, University of Tabriz, Tabriz, Iran*

Graphene-based photonic structures make it possible to control terahertz waves with an electric voltage. In this work, we study a symmetric one-dimensional photonic microcavity made of two mirror-image Bragg reflectors, $\mathrm{PC}_1 = (AB)^5$ and $\mathrm{PC}_2 = (BA)^5$, with a stack of s graphene layers at their junction. Layer A has a refractive index $n_A = 2.35 + 0.0014i$ and a thickness of $4\,\mu$m, and layer B has $n_B = 3.61$ and a thickness of $2\,\mu$m. We do not use an ordinary dielectric defect layer. Instead, we use the mirror symmetry of the structure itself, which supports a localized mode at the central interface even without graphene.

We calculate the optical response at normal incidence in the terahertz range using the transfer matrix method. The conductivity of graphene is described by the Kubo model and converted into an effective permittivity of a thin homogeneous layer. The chemical potential is controlled by the gate voltage through $\mu_c = \hbar v_F \sqrt{\pi a_0 V_g}$.

The two mirrors share a common band gap from about 7.8 to 10.2 THz, and their reflectances differ by less than 0.02. Inside this gap we find two interface modes. The first is a geometric mode at 9.33 THz with a transmittance of about 0.93. It comes from the mirror symmetry and shifts by only about 0.01 THz when graphene is added, so it is almost independent of graphene. The second is a graphene mode, which appears only when enough graphene layers are present. For $s = 10$ and $V_g = 10$ V, it is located at 8.19 THz with a transmittance of 0.96.

The graphene mode can be tuned in two ways. First, it appears for $s = 7$ at 7.90 THz and moves to 8.70 THz at $s = 20$, a total shift of about 0.8 THz. The shift caused by each added layer becomes smaller as s grows. Second, for $s = 10$, raising V_g from 5 V to 120 V moves the mode from 7.91 THz to 8.98 THz, a shift of about 1.07 THz. This shift is strong at low voltages and saturates at high voltages, which is expected because μ_c grows as $\sqrt{V_g}$. In both cases the peak transmittance stays above 0.94.

These results show that the number of graphene layers is a necessary condition for effective electrical tunability, while the geometric mode stays almost fixed. The structure may be useful for electrically tunable terahertz filters.

Keywords: photonic crystal, interface mode, graphene, electrical tunability, transfer matrix method

Cite as: Solmaz Salary et al., "Electrical Tuning of the Graphene Mode in a One-Dimensional Terahertz Photonic Microcavity with a Multilayer Graphene Stack: Effects of Gate Voltage and Number of Layers", in *Book of Abstracts of the 27th Symposium on Photonics and Optics (SPO 2026)*, Kyiv, 2–6 November 2026, p. 135.

FRI

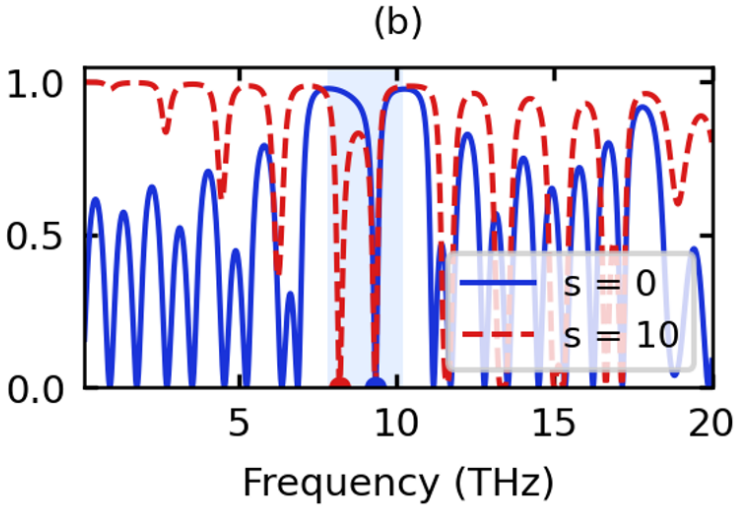


Figure. Reflectance of the whole structure for $s = 0$ (blue) and $s = 10$ (red, dashed) with $V_g = 10$ V. The shaded area marks the common gap of PC_1 and PC_2.

Fr6.5 POSTER · FRIDAY 15:46 CET · 16:46 KYIV #265

Sub-Terahertz Penetration Loss Measurements at 131.6 GHz for Indoor Environments

Andrii Shekera

V. Lashkaryov Institute of Semiconductor Physics of the National Academy of Sciences of Ukraine, Kyiv, Ukraine

Sub-Terahertz (sub-THz) radiation is one of the candidate bandwidths for 6G and future wireless networks due to its ability to deliver much higher data rates and greater capacity than lower-frequency bands. However, its shorter wavelength leads to significant free-space path loss (FSPL) in line-of-sight (LOS) conditions for a given link distance and fixed antenna gains. In non-line-of-sight (NLOS) scenarios, signal penetration loss is also substantially higher compared to lower frequencies, which can severely limit network coverage. Consequently, analyzing NLOS penetration loss across various building materials at THz frequencies is essential for accurate indoor link budget design and performance evaluation. To address this, our study measures the penetration loss and attenuation of some basic construction materials within the sub-THz band at 131.6 GHz. The blocks of the transmitting and the receiving units are based on a heterodyne architecture and facilitate the transmission and reception of signals in the terahertz frequency range, specifically between 130 and 134 GHz. The intermediate frequency range is 2–4 GHz.

Results show that the penetration loss changes on this range extensively based on the material properties and material thickness, ranging from 3.2 dB to 10.8 dB for Medium-Density Fibreboard at (0.3-0.6) cm, and 5.8 dB to 15.1 dB for Plywood at (0.4-1.2) cm at 131.6 GHz. The highest attenuation of 14.5 dB/cm was observed for Plywood at 131.6 GHz. Overall, the penetration loss and attenuation increase with greater material thickness for all the materials.

These results could be helpful for developing accurate penetration models of common building materials for ray-tracing simulations and further building THz wireless channel models that accurately predict the penetration loss.

Acknowledgement. This work was supported by the DAAD project "Sustainable Optical Materials and Methods: Education and Research Infrastructure (SOMMER!)".

Cite as: Andrii Shekera, "Sub-Terahertz Penetration Loss Measurements at 131.6 GHz for Indoor Environments", in *Book of Abstracts of the 27th Symposium on Photonics and Optics (SPO 2026)*, Kyiv, 2–6 November 2026, p. 137.

Fr6.6 POSTER · FRIDAY 15:50 CET · 16:50 KYIV #213

Concepts for propagation-invariant spatiotemporal optical vortex formation

Claudia Zenkova, Dmytro Ivanskyi, Andrii Karabchyivskyi
Yuriy Fedkovych Chernivtsi National University, Chernivtsi, Ukraine

In recent decades, considerable attention has been paid to the study of structured light with transverse angular momentum. For example, transverse spin angular momentum arises in tightly focused circularly polarized Gaussian beams and evanescent fields. The concept of the formation of transverse orbital angular momentum (OAM) is gaining relevance, which consist in development of spatiotemporal optical vortices with vortex phase in spatiotemporal plane [1]. The question arises of the theoretical development of methods for generating such wave packets with transverse OAM, robust to dispersion and diffraction during propagation both in free space and in optically inhomogeneous media.

Spatiotemporal wave packets (STWP) is a special class of propagation invariant impulse fields [1-2], in which the spatial and temporal degrees of freedom are related through a specially formed spectral correlation. Unlike a conventional pulsed beam, where spatial and spectral coordinates can be considered as independent variables, in STWP each spectral frequency (ω) corresponds to a certain transverse spatial frequency (k_x or k_y). This non-separability of spatial and spectral degrees of freedom that determines a number of unusual properties of STWP, in particular the possibility of controlling the group velocity and forming diffraction-free, propagation invariant modes [2].

A variety of STWP are spatiotemporal optical vortices (STOV), for which the fundamental spatial-spectral correlation is supplemented by a phase singularity. The phase vortex in the x-t coordinates is due to the modulation of the spectral phase in k_x-ω space. However, conventional Gaussian STOVs are not propagation invariant with respect to their vortex structure and the wave packet envelope [1]. Recent investigations show, that Bessel-Gaussian STOVs [3] are more robust, allowing the conservation of the wave packet structure during propagation in free space and an anomalously dispersive medium over a much longer distances. However, Bessel-Gaussian STOVs formed by modulating the spectral phase in the frequency domain are not inherently invariant, as they have separate temporal and spatial degrees of freedom.

The most successful way to modulate the propagation-invariant STWP is the spatiotemporal Fourier synthesis [2], which provides phase modulation in the spatial-spectral (x-ω) plane. Combination of the conditions for the propagation-invariant STWP formation and the vortex phase in the spatial-temporal coordinates by means of phase (and possibly amplitude) modulation in the x-ω domain (Fig. 1) allows to form propagation-invariant STOVs. It is expected to find conditions for the preserving of such wavepackets characteristics (amplitude envelope, phase vortex in x-t, topological charge, transverse OAM, etc.) during propagation both in free space and dispersive medium, with the elimination of spectral uncertainty [2]. The next expected step is to find ways to increase the robustness of such pulses when propagating in a turbid (multiple scattering) and/or turbulent medium.

[1] Tripathi N, Hancock SW, Milchberg HM. Transverse orbital angular momentum of spatiotemporal optical vortices: setting the record straight. Opt Express 2025;33:41766-41776. doi: 10.1364/OE.568833

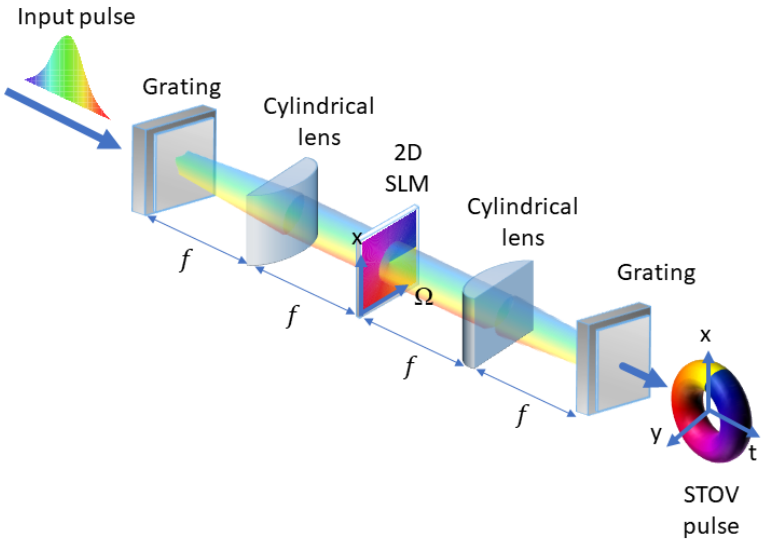


Figure. Scheme of the spatiotemporal Fourier synthesis for propagation invariant optical wave packets formation [2]

[2] Yessenov M, Hall LA, Schepler KL, Abouraddy AF. Space-time wave packets. Adv Opt Photon. 2022;14(3):455-570. doi: 10.1364/AOP.450016

[3] Chen W, et al. Time diffraction-free transverse orbital angular momentum beams. Nat Commun. 2022;13:4021. doi: 10.1038/s41467-022-31623-7

Cite as: Claudia Zenkova et al., "Concepts for propagation-invariant spatiotemporal optical vortex formation", in *Book of Abstracts of the 27th Symposium on Photonics and Optics (SPO 2026)*, Kyiv, 2–6 November 2026, p. 138.

Fr6.7 POSTER · FRIDAY 15:54 CET · 16:54 KYIV #198

High-resolution fabrication of diffractive optical elements by direct laser writing

Dmytro Manko, Ievgen Beliak

Institute for Information Recording of the National Academy of Sciences of Ukraine, Kyiv, Ukraine

The development of micro- and nanooptics requires improved methods for forming diffractive optical elements with linear dimensions comparable to or significantly smaller than the wavelength. The resolution of traditional optical lithography systems is limited by the diffraction limit.

It is shown that the diffraction limitation can be overcome by using a nonlinear exposure characteristic of the recording medium, optimizing the spatial distribution of the laser beam intensity, and using materials with a threshold mechanism for photostructural transformations.

It was proved that the improvement in resolution is possible with picosecond and femtosecond pulses. For pulse durations ranging from 10 fs to 100 ps, excitation and relaxation processes of charge carriers predominate, whereas for pulse durations exceeding 100 ps, the influence of structural changes and thermal diffusion increases. Reducing the pulse duration allows localization of the energy impact and reduces the thermal influence on adjacent areas of the structure. In the literature reviewed, the formation of quantum dots in a polymer nanocomposite matrix ensured the recording of lines 65 nm wide, which is approximately 1/8 of the laser wavelength. The use of AgInSbTe thermal resist allowed the production of features approximately 130 nm in size, corresponding to approximately 1/3 of the wavelength of the recording laser.

The experimental part of the study was aimed at the formation of code sequences for a modulation disk using direct laser recording. Recording was performed with a 405 nm laser on a glass substrate coated with a photoresist layer. The substrate rotated at a frequency of 7 rps. The linear velocity in the recording zone was approximately 0.8 m/s. The focused laser beam moved stepwise along the radius of the substrate. An automatic focusing system with a piezoelectric lens drive was used to compensate for axial deviations. The runout of the substrates used did not exceed 10 μm.

The quality of the formed elements was assessed based on the surface profile, microrelief, and width of the transition region between the chromium-coated area and the open surface of the glass substrate. The studies were conducted using scanning tunneling microscopy. For samples produced by contact lithography, the width of the transition region was 4.5 μm. Using direct laser writing, this value was reduced to 2.0 μm. Thus, the transition width was reduced by 2.5 μm, or approximately 55.6%, and the resolution of the modulation disk pattern increased by 2.25 times. Structural components of DOEs with a characteristic relief depth of 0.3–0.4 μm were formed on chalcogenide semiconductor films.

Keywords: direct laser writing, diffractive optical element, modulation disk, submicron structure, chalcogenide photoresist, spatial resolution, Bessel beam.

Cite as: Dmytro Manko et al., "High-resolution fabrication of diffractive optical elements by direct laser writing", in *Book of Abstracts of the 27th Symposium on Photonics and Optics (SPO 2026)*, Kyiv, 2–6 November 2026, p. 140.

FRI

Fr6.8 POSTER · FRIDAY 15:58 CET · 16:58 KYIV #301

Tracking the thermostimulated diffusion in the structures 'Ag–$As_{40}S_{60}$ superthin film' with surface plasmon-polaritons

Sergii Mamykin, V. I. Mynko, I. Z. Indutnyi, M. V. Sopinskyy, V. A. Dan'ko

V. Lashkaryov Institute of Semiconductor Physics of the National Academy of Sciences of Ukraine, Kyiv, Ukraine

Thin structures Ag–thin film of chalcogenide glasses (ChG) have attracted the attention of researchers for 60 years, ever since the effect of light stimulated diffusion of silver into ChG was discovered by M. T. Kostyshyn, K. V. Michailovska and P. F. Romanenko [1]. This is due to the rich physicochemical nature of the phenomena occurring within these structures, resulting in a wide variety of practical applications (information recording, inorganic resists, the fabrication of optical elements and holograms, photovoltaic absorbers, among others). Recently, researchers have become increasingly interested in photo- and thermostimulated diffusion of Ag into superthin (tens of nanometers thick) chalcogenide layers [2, 3] to form the elements of radiation-hard non-volatile memory, which is in high demand, particularly in the space industry.

The porosity of superthin ChG layers affects both the photo- and thermally stimulated diffusion of Ag, as well as structural transformations within them. Due to the small thickness of these layers and the sensitivity of Ag–ChG structures to irradiation, studying photo- and thermally stimulated processes in such structures using traditional methods presents challenges. We have applied a method based on surface plasmon-polariton (SPP) resonance, commonly used in optical sensors, to study Ag–ChG structures with chalcogenide layer thicknesses of 10–20 nm [4,5]. In this approach, a substrate with a profiled surface in the form of a diffraction grating was used to excite SPPs at the interface between silver and ChG layer.

This study examines the thermally stimulated diffusion of Ag into superthin porous $As_{40}S_{60}$ films thermally deposited onto the silver grating. Annealing of the samples was conducted in the temperature range of 100–130 °C. Changes in the film due to silver diffusion were registered by tracking the position and shape changes of the SPP resonance in the angular dependence of specular reflection of p-polarized He-Ne laser radiation (λ = 632.8 nm).

The detection of SPP resonance shifts enabled the determination of changes in the refractive index of the $As_{20}S_{30}$ layer due to silver doping, and subsequently, the calculation of the kinetics of thermally stimulated Ag concentration growth in the $As_{40}S_{60}$ film, as well as the corresponding decrease in silver layer thickness (δd_{Ag}). At all annealing temperatures, the δd_{Ag} kinetics exhibited linear segments with respect to $t^{1/2}$ (t – annealing time), allowing estimation of the Ag diffusion coefficients. It was found that the temperature dependence of the diffusion coefficient follows the Arrhenius equation with activation energy E_a = 1.5 eV. The obtained value of E_a coincides with the activation energy for thermal diffusion of silver in thick, nonporous $As_{40}S_{60}$ films. This means that the key stage in the process of thermally stimulated diffusion of silver into ultrathin porous $As_{40}S_{60}$ films is also interatomic diffusion into the chalcogenide matrix.

Acknowledgement. The authors express their gratitude to the National Academy of Sciences of Ukraine for support within the framework of the project 0125U000799 "New physical principles and technologies for the development of the element base of modern infrared photoelectronics".

FRI

[1] M. T. Kostyshin, E. V. Mikhailovskaya, P. F. Romanenko. Sov. Phys. Solid State 8: 451 (1966).

[2] H. Park et al. SN Applied Sciences 2: 2111 (2020).

[3] P. Priyadarshini et al. RSC Adv. 12: 9599–9620 (2022).

[4] I. Indutnyi, S. Mamykin, V. Mynko et al. J. Non-Cryst. Solids 649: 123333 (2025).

[5] I. Z. Indutnyi, V. I. Mynko, M. V. Sopinskyy, S. V. Mamykin. Thin Solid Films 824: 140705 (2025).

Cite as: Sergii Mamykin et al., "Tracking the thermostimulated diffusion in the structures 'Ag–$As_{40}S_{60}$ superthin film' with surface plasmon-polaritons", in *Book of Abstracts of the 27th Symposium on Photonics and Optics (SPO 2026)*, Kyiv, 2–6 November 2026, p. 141.

Fr6.9 POSTER · FRIDAY 16:02 CET · 17:02 KYIV #252

Automatic Control System for a Precision Diffuse Optical Emitter

Viktor Shyshkin, Volodymyr Borovytsky
National Technical University of Ukraine "Igor Sikorsky Kyiv Polytechnic Institute", Kyiv, Ukraine

Precision diffuse optical emitters (PDOEs) based on integrating spheres are used for radiometric calibration of digital cameras, optical sensors, and optoelectronic systems, in particular for measuring response linearity and spatial nonuniformity and for determining correction parameters of focal plane arrays. In modern PDOEs, the integrating sphere mixes radiation spatially, while high-power light-emitting diodes (LEDs) provide compactness, high luminous efficacy, and electronic flux control. Long-term stability of the emitter is critical to measurement reproducibility.

LEDs differ in luminous flux, spectral power distribution, forward voltage, and flux-current dependence. These characteristics, which can be nonlinear, vary with supply conditions, junction temperature, and operating time. Changes in the contributions of individual LEDs alter the luminance of the exit aperture and degrade the uniformity of its luminance distribution.

To ensure long-term stable operation, a modular automatic control system with individual LED current control, optical feedback, and temperature compensation is being developed. The PDOE contains three high-power Cree XM-L2 LEDs with active cooling inside an integrating sphere (internal diameter 266 mm, exit aperture diameter 50 mm). Illuminance was measured with a TENMARS TM-208A meter. After preliminary channel balancing, the illuminance with all LEDs on, 40 mm from the exit aperture, was 1773, 7530, and 7820 lx in the three investigated modes (highest-to-lowest ratio 4.41:1). In the highest-illuminance mode, currents of 1840, 2100, and 1790 mA produced 2643, 2639, and 2640 lx for the individual LEDs. These results support independent control and individual calibration of each LED channel.

The system comprises a control computer, an independent constant-current driver for each LED, and digital modules communicating with the computer via a serial interface. Optical feedback will use a photodiode channel with operational amplifiers, analog-to-digital conversion, and spectrum-dependent calibration; a multichannel spectral sensor will monitor visible spectral bands, and thermocouples will measure circuit board temperatures. Proportional-integral illuminance control will be combined with temperature calibration models and a slower spectral correction loop. LED currents are derived from a current-temperature-luminous flux characteristic matrix obtained by individual LED calibration within electrical and thermal limits.

The software lets users set the exit-aperture illuminance or luminance, a reference spectral response, current and temperature limits, per-LED characteristic matrices, and measurement parameters. It displays illuminance, responses in eight spectral bands, temperatures, current setpoints and deviations, time plots, and alarms in text and graphical form, keeps operating conditions, including supply voltage and LED temperature, within limits, and logs all measurements and applied corrections.

The proposed system is expected to provide long-term stable PDOE operation with an adjustable exit-aperture brightness held constant during radiometric calibrations. This would

enable serial production in Ukraine of PDOEs with precision comparable to leading international manufacturers at a considerably lower price.

Cite as: Viktor Shyshkin et al., "Automatic Control System for a Precision Diffuse Optical Emitter", in *Book of Abstracts of the 27th Symposium on Photonics and Optics (SPO 2026)*, Kyiv, 2–6 November 2026, p. 143.

Fr6.10 POSTER · FRIDAY 16:06 CET · 17:06 KYIV #256

The influence of spectral composition and intensity of LED phytolighting on the growth of higher and lower plants

Borys Snopok[1], Demyd Pekur[1], Praskoviya Boltovets[1], Vasyl Kornaga[1], Viktoriya Petlovana[2], Yuriy Kolovzarov[1]

[1] V. Lashkaryov Institute of Semiconductor Physics of the National Academy of Sciences of Ukraine, Kyiv, Ukraine [2] Taras Shevchenko National University of Kyiv, Kyiv, Ukraine

The provision of fresh foodstuffs in extreme conditions is almost entirely dependent on the state of artificial lighting technology for indoor farming. The primary technological challenges associated with this approach are twofold: the substantial energy consumption and the paucity of information regarding optimal lighting procedures to maximize crop yields. This underscores the clear advantage of light-emitting diode (LED) technology in this domain, enabling the requisite degree of control over the indoor farming environment.

It is evident that utilizing unoptimised LED arrays instead of solar light constitutes a stress factor for plants. This is due to the fact that they do not encompass the complete spectrum of sunlight and are thus unable to adequately substitute for it. It is evident that plants are capable of perceiving numerous parameters of ambient light signals, including quantity, quality, direction, and duration. However, the influence of the spectral quality of light remains to be fully elucidated. Consequently, the study of the influence of the spectral composition of artificial light on plant growth has become a highly relevant issue. Microgreens, in addition to green algae, are considered to be valuable and highly convenient experimental models for such research due to their compact size and rapid growth rate.

The objective of this study was to compare the effects of light spectral composition and intensity on the growth of sunflower (Helianthus annuus) microgreens and green algae Haematococcus pluvialis, a promising source of astaxanthin. Six combinations of LED light sources were utilised: red light, blue light, white light, blue-red light (50%-50%), white-red light (50%-50%), and white-red-blue light (60%-30%-10%).

It was demonstrated that the spectral composition of the LED arrays exerted a significant influence on plant growth. Specifically, it was found that for sunflower microgreens, maximum wet mass was achieved under pure blue light and a combination of white and red, while the combination of blue and red demonstrated the lowest growth. It is noteworthy that a twofold reduction in light intensity resulted in an increase in plant wet mass for all six spectral combinations. It can be explained by a response to a stress factor, as evidenced by the observation that while leaf size remained constant, stem length increased, leading to an overall increase in wet mass.

In the case of Haematococcus pluvialis, it has been demonstrated that the implementation of white light fosters substantial culture growth, characterised by augmented cell density. However, it does not stimulate an increase in astaxanthin production. Concurrently, the utilization of high-intensity blue light induced the accumulation of secondary carotenoids, notably astaxanthin. However, this stimulation was accompanied by a detrimental effect on culture growth. It is evident that further research is required for ascertain the optimal conditions.

In conclusion, it can be deduced that the composition of artificial lighting generated by LED arrays exerts a substantial influence on the growth of both higher and lower plants. This clearly demonstrates that ensuring safety in extreme conditions requires further development of both specialised LED modules and lighting methods that are optimised for specific agricultural crops.

Cite as: Borys Snopok et al., "The influence of spectral composition and intensity of LED phytolighting on the growth of higher and lower plants", in *Book of Abstracts of the 27th Symposium on Photonics and Optics (SPO 2026)*, Kyiv, 2–6 November 2026, p. 145.

Fr6.11 POSTER · FRIDAY 16:10 CET · 17:10 KYIV #269

Optical–Digital Analysis of Leaf Venation: Integrating Light and Scanning Electron Microscopy with Digital Morphometry

Andriy Yakunov[3], Iryna Kosakivska[2], Maksym Kremenskoy[3,4], Oksana Futorna[1,2], Vladislava Badanina[5]

[1] Educational and Scientific Institute of High Technologies, Taras Shevchenko National University of Kyiv, Kyiv, Ukraine [2] M. G. Kholodny Institute of Botany of the National Academy of Sciences of Ukraine, Kyiv, Ukraine [3] Faculty of Physics, Taras Shevchenko National University of Kyiv, Kyiv, Ukraine [4] Novations LLC, Kyiv, Ukraine [5] Educational and Scientific Centre "Institute of Biology and Medicine", Taras Shevchenko National University of Kyiv, Kyiv, Ukraine

The digitisation of botanical collections and modern optical image analysis expand the opportunities for quantitative assessment of plant morphological traits. Standardising optical measurements and processing parameters reduces observer subjectivity and improves data comparability. Open access to high-resolution images, metadata and algorithms supports reproducible analysis and reuse of bio-optical data.

Leaf venation architecture is relevant to systematics, comparative anatomy, evolutionary biology and plant physiology. The vascular system provides diagnostic traits and forms an optically heterogeneous network associated with mesophyll water supply and with leaf hydraulic and light-scattering properties. Studying it requires high-resolution imaging, reproducible measurements and physical and anatomical interpretation.

This study aims to substantiate quantitative venation analysis in ImageJ/Fiji and to assess its integration with light and scanning electron microscopy for investigating grass leaf structure.

Light micrographs and macro-images of leaves with reticulate venation of Acer L., Quercus L., Betula L., Tilia L. and Populus L. were used to develop image processing algorithms. Computational analysis employed ImageJ/Fiji plugins and custom Java modules. The workflow combines textural, fractal and geometric–topological analyses of optical contrast. Processing comprises region-of-interest segmentation, greyscale conversion, adaptive thresholding and skeletonisation, which reduces vein images to single-pixel-wide centrelines. Networks are represented as graphs, with edges corresponding to vein segments and nodes to branching points, junctions and endpoints. Parameters include vein segment length, tortuosity and orientation, network connectivity and the area of enclosed meshes (areoles). Texture, fractal dimension and lacunarity are also assessed. Application to other network-like structures, such as microcrack networks in materials science, requires separate validation.

Adaptation of the workflow to Poaceae Barnhart accounts for the anisotropy of parallel venation by analysing longitudinal and transverse veins separately. The algorithms are configured to quantify the number of longitudinal veins of each type, intervein spacing, the number of transverse veins per unit area and the total vein length per unit area for each vein group, taking leaf blade geometry into account.

For anatomical validation, cleared-leaf images were compared with transverse sections and epidermal micrographs from adjacent regions. Light microscopy reveals the structure of vascular bundles and surrounding tissues. Scanning electron microscopy complements this analysis by characterising epidermal surface topography, stomatal arrangement and the organisation of costal (over-vein) and intercostal (interveinal) zones.

The proposed integration of digital morphometry and microscopy offers prospects for comprehensive analysis of grass leaf structure, comparison of species and genotypes, and assessment of the diagnostic value of venation traits. Comparing morphoanatomical parameters with statistical analyses of optical measurements, including light transmission and scattering, may clarify the information content and functional significance of these parameters, provided that it is supported by physiological and biophysical data. Implementing this approach requires standardised optical image acquisition, anatomical validation and experimental verification.

Cite as: Andriy Yakunov et al., "Optical–Digital Analysis of Leaf Venation: Integrating Light and Scanning Electron Microscopy with Digital Morphometry", in *Book of Abstracts of the 27th Symposium on Photonics and Optics (SPO 2026)*, Kyiv, 2–6 November 2026, p. 147.

Fr6.12 POSTER · FRIDAY 16:14 CET · 17:14 KYIV #266

Structural properties of chitosan and chitosan-based composites

Diana Hurova[1], Serhii Cherednychenko[1], Nikolay Galtsov[1], Tamara Bednarchuk[2], Yuliia Horbatenko[1]

[1] B. Verkin Institute for Low Temperature Physics and Engineering of the National Academy of Sciences of Ukraine, Kharkiv, Ukraine [2] W. Trzebiatowski Institute of Low Temperature and Structure Research, Polish Academy of Sciences, Wrocław, Poland

Chitosan is a semicrystalline natural polymer whose structural organization is strongly influenced by intermolecular hydrogen bonding, hydration, and preparation conditions [1, 2]. Incorporation of carbon-based nanomaterials, particularly thermally reduced graphene oxide (trGO), can substantially modify the molecular packing and crystalline ordering of the polymer matrix. In this work, the structural features of pure chitosan and chitosan-based composites with different trGO concentrations are investigated using X-ray diffraction (XRD), with infrared (IR) and Raman spectroscopy considered as complementary methods for characterizing molecular interactions and local structural changes.

XRD analysis reveals that pure chitosan exhibits a semicrystalline structure characterized by broad diffraction maxima at $2\theta \approx 9.4°$ and 21.2°, together with several relatively sharp crystalline reflections. The diffraction pattern is consistent with the coexistence of ordered crystalline domains and disordered regions, with possible contributions from hydrated and anhydrous structural forms [1, 2].

The incorporation of trGO leads to significant changes in the diffraction patterns. At low filler concentrations (1–4 wt.%), additional reflections appear near $2\theta \approx 14°$ and 17°, accompanied by broadening of the main diffuse maximum at 20–21°. These changes suggest a rearrangement of the polymer chains and a reduction in crystalline ordering, potentially associated with intermolecular interactions between chitosan and trGO. At a trGO concentration of approximately 10 wt.%, the emergence of a diffraction contribution near $2\theta \approx 25.4°$ indicates the development of graphene-rich domains and increased structural heterogeneity. Further increases in filler concentration promote the formation of a more complex multiphase structure.

IR and Raman spectroscopy provide complementary means of investigating the vibrational characteristics of chitosan, particularly the functional groups involved in hydrogen bonding and their possible interactions with graphene-based components. Their correlation with XRD results can help distinguish changes in molecular interactions from modifications of crystalline packing.

The obtained XRD results demonstrate that the incorporation of trGO substantially affects the structural organization of chitosan, leading to a concentration-dependent transformation from a predominantly polymer-ordered system toward a heterogeneous composite structure. Combined diffraction and vibrational spectroscopy studies can provide a more comprehensive understanding of the relationship between molecular interactions and structural ordering in chitosan-based materials.

Acknowledgement. This work was partly supported by NASU (RSW of young scientist №12/04-2025) and the National Research Foundation of Ukraine (Project № 2023.03/0012).

[1] K. Ogawa, T. Yui, M. Miya, Biosci. Biotechnol. Biochem. 56, 858–862 (1992). https://doi.org/10.1271/bbb.56.858.

[2] K. Okuyama, K. Noguchi, M. Kanenari et al., Carbohydr. Polym. 41, 237–247 (2000). https://doi.org/10.1016/S0144-8617(99)00142-3.

[3] K. Kosowska, P. Domalik-Pyzik, M. Nocuń, J. Chłopek, Mater. Chem. Phys. (2018). https://doi.org/10.1016/j.matchemphys.2018.05.076.

Cite as: Diana Hurova et al., "Structural properties of chitosan and chitosan-based composites", in *Book of Abstracts of the 27th Symposium on Photonics and Optics (SPO 2026)*, Kyiv, 2–6 November 2026, p. 149.

Fr6.13 POSTER · FRIDAY 16:18 CET · 17:18 KYIV #304

Quantitative Assessment of Tryptophan Content in the Blood Plasma of Oropharyngeal Cancer Patients

Tymur Isokov[1], Ivan Gnatyuk[1], Daryna Doni[2], Serhij Verevka[2], Volodymyr Kizim[2], Alla Tarasenko[3], Olesia Volovenko[4], Oleksii Klymenko-Ulianov[5], Olena Gnatyuk[1], Galyna Dovbeshko[1]

[1]Institute of Physics of the National Academy of Sciences of Ukraine, Kyiv, Ukraine [2]State Institution "O. S. Kolomiychenko Institute of Otolaryngology of the National Academy of Medical Sciences of Ukraine", Kyiv, Ukraine [3]O. V. Palladin Institute of Biochemistry of the National Academy of Sciences of Ukraine, Kyiv, Ukraine [4]Taras Shevchenko National University of Kyiv, Kyiv, Ukraine [5]V. P. Kukhar Institute of Bioorganic Chemistry and Petrochemistry of the National Academy of Sciences of Ukraine, Kyiv, Ukraine

Quantitative analysis of blood plasma metabolites is an important tool for assessing metabolic alterations associated with various pathological conditions [1]. In particular, the analysis of free amino acids can provide valuable information for the diagnosis and monitoring of cancer [2]. However, comprehensive amino acid profiling typically requires sophisticated analytical instrumentation and costly reagents, limiting its application in routine clinical practice. Owing to its intrinsic fluorescence, tryptophan can be quantified using relatively simple spectrofluorimetric methods, making it a promising analyte for the spectroscopic assessment of biological fluids.

In this study, blood plasma samples were analyzed from 17 patients with oropharyngeal cancer who had previously had COVID-19. Plasma was separated by centrifugation at 4000 rpm for 20 min. A pooled plasma sample obtained from three healthy individuals served as the control.

High-molecular-weight proteins and peptides were precipitated by adding an equal volume of 10% perchloric acid, followed by centrifugation. The resulting supernatant was diluted with phosphate buffer to a final pH of 7.5. Fluorescence spectra were recorded using an Edinburgh Instruments FS5 spectrofluorometer over the wavelength range of 280–550 nm. Upon excitation at 280 nm, a characteristic fluorescence emission maximum was observed at approximately 347 nm. Tryptophan concentrations in the plasma samples were determined using a calibration curve constructed from fluorescence intensity measurements of tryptophan solutions of known concentrations prepared in a matrix similar to that used for sample preparation.

The results revealed a noticeable difference in the content in free tryptophan levels among patients with oropharyngeal cancer compared with the pooled control sample. The measured concentrations were both higher and lower than the control value, with no consistent trend across the patient group. This variability may reflect the combined effects of multiple pathological processes. On the one hand, enhanced tissue catabolism associated with oncological disease alters the composition of circulating amino acids. On the other hand, previous studies indicate that both COVID-19 and oncological pathology may lead to decreased tryptophan levels in the bloodstream.

These findings support the potential use of spectrofluorimetric analysis for monitoring free tryptophan levels in the blood plasma of patients with oropharyngeal cancer, particularly those with a history of COVID-19 or other viral infections. Further studies involving larger patient

cohorts and appropriate control groups are needed to clarify the relationship between tryptophan levels, cancer-associated metabolic alterations, and previous viral infections.

[1] C. A. Kraft et al., Quantitative Analysis of Protein-Lipid Interactions Using Tryptophan Fluorescence. Sci. Signal. 2, pl4-pl4 (2009). https://doi.org/10.1126/scisignal.299pl4

[2] Liu M, Wang X, Wang L, Ma X, Gong Z, Zhang S, Li Y. Targeting the IDO1 pathway in cancer: from bench to bedside. J Hematol Oncol. 11(1), 100 (2018). https://doi.org/10.1186/s13045-018-0644-y

Cite as: Tymur Isokov et al., "Quantitative Assessment of Tryptophan Content in the Blood Plasma of Oropharyngeal Cancer Patients", in *Book of Abstracts of the 27th Symposium on Photonics and Optics (SPO 2026)*, Kyiv, 2–6 November 2026, p. 151.

Fr6.14 POSTER · FRIDAY 16:22 CET · 17:22 KYIV #305

Effect of Si doping and annealing on optical properties of MOCVD-grown β-Ga_2O_3 thin films

Andrii Kozak[1], Volodymyr Romanyuk[2], Miriam Krettová[1], Ondrej Pohorelec[1], Michal Sobota[1], Lenka Pribusová Slušná[1], Iryna Kozak[1], Igor Píš[1], Peter Nádaždy[1], Marek Pribus[3], Milan Ťapajna[1], Mariia Voitovych[2], Roman Redko[2], Mykola Semenenko[2], Olga Kondratenko[2], Sergii Mamykin[2], Andrey Sarikov[2], Filip Gucmann[1]

[1]Institute of Electrical Engineering, Slovak Academy of Sciences, Bratislava, Slovakia [2]V. Lashkaryov Institute of Semiconductor Physics of the National Academy of Sciences of Ukraine, Kyiv, Ukraine [3]Institute of Inorganic Chemistry, Slovak Academy of Sciences, Bratislava, Slovakia

Gallium oxide (Ga_2O_3) has emerged as a promising ultra-wide bandgap semiconductor with potential applications in power electronics, solar-blind deep-ultraviolet optoelectronics, gas sensors, and X-ray detectors. Depending on the polymorph (α, β, γ, and κ), it features a bandgap of 4.4 - 5.6 eV, a high breakdown electric field of ~8 MV/cm, and a figure of merit that overcomes that of SiC and GaN. Among these polymorphs, the monoclinic β-Ga_2O_3 phase is thermodynamically the most stable and extensively investigated, and the methods for large-size single-crystal wafer fabrication are well-established. Nevertheless, high bulk production costs motivate intensive development of heteroepitaxial and non-epitaxial thin films.

Understanding optical transition characteristics, surface electronic structure, and local bond configurations of Ga_2O_3 thin films is crucial for controlling their electronic properties and evaluating overall film quality. The local bond configurations can be investigated by theoretical modeling (e.g., DFT calculations) and experimental techniques such as XPS, FTIR, Raman spectroscopy, and TEM analysis. In this work, Raman and FTIR spectroscopy were employed to investigate the evolution of these local configurations and their effect on optical transmittance, refractive index dispersion, and optical bandgap of Ga_2O_3 thin films. For this purpose, the films with different Si-doping levels (0.01 and 0.1 mol.%) were grown by MOCVD to a thickness of 135-250 nm on sapphire, Si, and SiO_2 substrates using Ga(acac)3 as the gallium source and TEOS as the silicon dopant precursor, followed by thermal annealing at 550°C in a forming gas atmosphere. XRD and XPS analyses confirmed successful growth of the β-Ga_2O_3 phase with a near-stoichiometric Ga/O atomic ratio of 0.69. Raman and FTIR spectra clearly demonstrated coexistence of octahedral (GaO_6) and tetrahedral (GaO_4) Ga coordination environments. While these local configurations remained unaffected by Si doping, thermal annealing induced noticeable structural rearrangement, marked by an increase in tetrahedral GaO_4 bonds. Conversely, optical properties, including high transparency exceeding 95% and an optical bandgap of 4.9-5.3 eV, were primarily defined by the Si-doping level, showing no sensitivity to annealing. Multi-angle spectroscopic ellipsometry (250–2100 nm) was utilized to extract complex refractive index dispersion and film thickness, implementing a two-layer model accounting for a 14–22 nm surface roughness layer. The refractive index at 633 nm was found to range within 1.91–1.99, showing negligible sensitivity to thermal annealing. The most pronounced variation of the refractive index arose from the choice of substrate, where low doped films on SiO_2 demonstrated a sufficient decrease to ~1.91.

Overall, the findings of the work demonstrate the ability to independently control local bond configurations and optical properties of Ga_2O_3 thin films through annealing and doping. In particular, annealing in forming gas goes beyond simple hydrogen passivation of oxygen vacancies by actively promoting formation of new Ga-O bonds.

Acknowledgement. This work was supported by the Slovak Research and Development Agency (project No. SK-UA-25-0079) and by the Ministry of Education and Science of Ukraine (project No. M/61-2026).

Cite as: Andrii Kozak et al., "Effect of Si doping and annealing on optical properties of MOCVD-grown β-Ga_2O_3 thin films", in *Book of Abstracts of the 27th Symposium on Photonics and Optics (SPO 2026)*, Kyiv, 2–6 November 2026, p. 153.

Author index

Bold code: presenting author.

A

Adhiri, R. Fr2.2
Alekseyenko, V. Fr4.3
Althammer, M. Mo3.1
Antonin, S. Th2.2, Th4.4
Arbouet, A. Mo2.2

B

Babich, D. **We1.3**
Badanina, V. Fr6.11
Banhart, F. Mo2.2
Baranchykov, Z. **Fr4.12**, Fr5.1
Bardakov, V. **Fr4.4**
Bauer, G. We3.2
Bednarchuk, T. Fr6.12
Beinik, I. **We2.5**
Beliak, I. **Th2.3**, Th2.4, Fr6.7
Bell, H. G. Mo1.1
Ben Achour, E. We3.2
Bergman, A. Mo4.3
Bermejo-Ortiz, J. We3.2
Besana, I. We1.3
Bezguba, V. We1.3, **We3.1**
Bhardwaj, A. We4.8
Blazevicius, D. Th3.6
Blokha, I. Fr4.3
Boltovets, P. **Fr6.10**
Borchert, M. Mo3.3
Borkovska, L. We3.3
Borovyi, M. Fr3.3
Borovytsky, V. Fr5.8, Fr6.9
Bortchagovsky, E. **Fr3.2**
Bortnik, V. **Fr5.8**
Borysiuk, V. Fr4.9, Fr5.9
Botu, S. Mo1.1
Boyko, V. Fr4.8
Bozhko, O. **Fr6.2**
Brouwer, P. W. Mo3.1, Mo3.3
Brüstle, M. We1.3
Bulira, P. We1.3
Burri, C. Mo1.1
Bušina, M. Mo3.1, Mo3.3

C

Caha, O. We3.2
Cailleau, H. **Mo2.1**
Calvi, M. We1.3
Chang, C.-H. Th3.6
Chegel, V. Fr1.3
Chehil, Y. Th2.3
Chepela, L. Fr3.3
Cherednychenko, S. Fr6.12
Cherevyshnyi, V. **Fr4.8**
Chornii, V. Fr2.1, Fr4.8, **Fr4.9**, Fr5.9
Chukova, O. We1.3, We3.3
Cibiraite-Lukenskiene, D. **Th4.5**
Clémence, M. Mo1.1
Colțuneac, D. Mo2.2, **Mo2.3**

D

Dan'ko, V. A. Fr6.8
Danylenko, I. Th4.4
Datsenko, O. Fr5.6, Fr6.2
de Vaulchier, L.-A. We3.2
Delin, A. Mo4.3
Demydov, I. Fr2.6
Demydov, P. Fr1.3
Derzhypolska, L. **Fr1.1**
Di Russo, E. **Th2.1**
Dimitriev, O. **Th3.6**
Dizdarević, F. Mo1.1
Dmytruk, A. Th2.2
Doni, D. Fr6.13
Dovbeshko, G. Fr6.13
Drozdenko, M. We4.7
Drube, W. We1.3
Dubikovskyi, O. Th4.4
Dzhagan, V. Th1.3, Th1.4, Th1.5, Th2.2, Th4.3, Th4.4
Dzhahan, V. **Th1.3**

E

Efremov, O. Th4.4
Elalaoui, Y. **Fr2.2**
Eriksson, O. Mo4.3
Esposito, V. Mo1.1

F

Fan, F.-C. Th3.6
Fang, D. Fr3.2
Farkaš, A. Mo3.3
Farkas, G. We4.7
Fedoryak, A. Th3.6
Fleischer, M. Fr3.2
Follath, R. We1.3
Franke, O. Mo3.1, Mo3.3
Frazer, T. Mo1.1
Fritsky, I. O. Th3.5
Fu, L. We3.2
Fullerton, E. Mo1.1
Futorna, O. **Fr6.11**

G

Galtsov, N. Fr6.12
García-Fernández, P. Fr2.3
Gedvilas, M. **Th1.1**
Georgiev, R. We2.4
Gerber, S. Mo1.1
Ghosez, P. Fr2.3
Gladkikh, P. We4.9
Gloskovskii, A. We1.3
Gnatyuk, I. Fr6.13
Gnatyuk, O. Fr6.13
Godziszewski, K. Fr2.6
Goennenwein, S. T. B. Mo3.3
Gomez-Ortiz, F. Fr2.3
Grigalevicius, S. Th3.6
Grolimund, D. We1.3
Gucmann, F. Fr6.14
Gudymenko, O. Th2.2
Gueckstock, O. Mo3.3
Guk, I. **We4.9**
Guldner, Y. We3.2
Guralskyi, I. . . **Th3.1**, Th3.2, Th3.3, Th3.4, Th3.5, Fr5.2
Gurieva, G. **Th4.1**

H

Hada, M. Mo2.2
Hajlaoui, M. We3.2
Haleliuk, D. Th3.1, **Th3.4**
Harhay, K. Fr2.6
Havryliuk, D. **Th1.4**, Th1.5
He, X. Fr2.3
Heinrich, M. We3.2
Hertling, L. Th4.3
Hizhnyi, Y. Fr4.12, Fr5.1, Fr5.3
Hoffmann, M. Mo1.1
Horbatenko, Y. Fr6.12
Htun, S. Mo1.1
Hu, W. Mo1.1
Hua, N. N. **Mo1.1**
Huang, S.-W. Mo1.1, Th3.6
Hurova, D. **Fr6.12**
Huzan, M. **We2.3**

I

Indutnyi, I. Z. Fr6.8
Isaiev, M. Fr3.3
Isaieva, O. Th2.2
Isokov, T. **Fr6.13**
Ivakhno-Tsehelnyk, O. **Th4.3**
Ivanauskaite, P. Th4.5
Ivanskyi, D. **Fr6.6**
Izhyk, O. Fr2.6

J

Jakob, G. Mo3.3
Janod, E. Mo1.3
Jechumtál, J. Mo3.1, Mo3.3
Jeppson, S. Mo1.1
Jeromin, A. We3.3
Jia, X. Mo1.1
Jungwirth, T. Mo3.1
Junquera, J. Fr2.3
Just, D. M. We1.3

K

Kai, H. We4.8
Kampfrath, T. Mo3.1, Mo3.3
Kapush, O. Th2.2
Karabchyivskyi, A. Fr6.6

Karapinar, R. **Fr4.11**
Karbivskyy, V. We1.3
Karpenko, Y. Fr4.7
Kašpar, Z. Mo3.1, Mo3.3
Khomenkov, D. We3.3
Khomenkov, V. We3.3
Khomenkova, L. **We3.3**, Fr4.3, Fr4.5
Khutko, M. Fr1.3
Kizim, V. Fr6.13
Kläui, M. Mo3.3
Klymenko-Ulianov, O. Fr6.13
Kołodziej, J. J. We1.2
Kolovzarov, Y. Fr6.10
Kominko, Y. We4.8
Kondratenko, O. Fr6.14
Kondratenko, S. Th1.3, Th4.3, Fr5.6, Fr6.2
Korchovyi, A. Th1.3, Th1.4, Th1.5
Kordyuk, A. We1.3, We3.1
Kornaga, V. Fr6.10
Korsunska, N. We3.3, Fr4.3, Fr4.5
Kosakivska, I. Fr6.11
Kosiachkin, Y. **We4.5**
Kotlov, A. We3.3
Kovalenko, G. We4.9
Kovalenko, M. V. We4.8
Kovanzhi, P. Fr5.6
Kozak, A. **Fr6.14**
Kozak, I. Fr6.14
Kozoriz, K. We3.3
Krakovskyi, S. Fr5.6
Kramer, P. Mo1.1
Kreiman, D. Th3.1, **Fr5.2**
Kremenskoy, M. Fr4.8, Fr6.11
Krettová, M. Fr6.14
Krizman, G. We3.2
Krucaite, G. Th3.6
Kubaščík, P. Mo3.1, **Mo3.3**
Kucheriv, O. Th3.1, Th3.2, Th3.3, **Th3.5**, Fr5.2
Kudrya, V. Fr5.4, Fr5.5
Kukreja, R. Mo1.1
Kulbachynskyi, O. Th1.4
Kundu, S. Fr2.4, Fr4.2
Kurleto, R. We1.2, We3.2
Kužel, P. Mo3.1

L

Lachhab, T. Fr2.2
Lacroix, D. Fr3.3
Lakshmanan, S. **Fr2.4**, **Fr4.1**, Fr4.2
Lamb, E. Mo1.1
Lazarenko, M. Fr4.9
Léa, D. **Mo2.2**, Mo2.3
Leiviskä, M. Mo3.1
Lemke, H. T. Mo1.1
Lemut, G. Mo3.1
Leonenko, E. V. Fr1.2
Levchuk, A. **Mo3.2**
Levytskyi, S. Th1.5, **Fr6.1**
Liamets, O. Fr1.2
Lisauskas, A. Th4.5
Lishchuk, P. Fr3.3
Lopatynskyi, A. **Fr1.3**
Lorenc, M. Mo1.3, Mo2.2, Mo2.3
Lytvyn, P. Th1.3, Th1.4, Th1.5, Th2.2, Fr5.6
Lytvyn, V. Fr1.3

M

Madhavi, M. Mo1.1
Majou, A. We3.2
Mak, J. Mo3.1
Makarenko, O. Fr4.12, Fr5.1, Fr5.3, Fr6.3
Mamykin, S. **Fr6.8**, Fr6.14
Mandal, R. **Mo1.3**
Manko, D. **Fr6.7**
Manko, O. **Th2.4**
Mankowsky, R. Mo1.1
Marendziak, A. We1.3
Mariette, C. Mo1.3
Matuška, R. Mo3.1
Maziar, D. Th4.4
Mazur, M. V. Th2.2
Mazur, N. Th1.4, Th1.5
Mazur, Y. Fr5.6
Mba, H. Mo2.2
McConnell, A. Mo1.1
McGuinness, C. **We2.4**
Melezhyk, Y. **Fr5.7**
Melnichenko, M. **Fr4.10**
Melnichuk, L. We3.3, Fr4.3, Fr4.4, Fr4.5

Melnichuk, O. We3.3, Fr4.3, **Fr4.5**
Mihailović, D. Mo1.1
Miranda, I. Mo4.3
Mitina, N. Fr2.6
Młynarczyk, M. We1.3
Morozov, D. **Fr5.9**
Mukherjee, B. **Fr2.3**
Müller, K. Mo3.1
Mynko, V. I. Fr6.8

N

Nádaždy, P. Fr6.14
Nádvorník, L. **Mo3.1**, Mo3.3
Naumenko, A. Fr5.4, Fr5.5
Nebesnyi, R. Fr2.6
Nedilko, S. Fr2.1, Fr4.8, Fr4.9, Fr5.9
Němec, P. Mo3.1, Mo3.3
Nowak, P. We1.3

O

Olejník, K. Mo3.3
Olikh, O. Fr4.8
Olszowska, N. **We1.2**, We3.2
Onishi, Y. We3.2
Opel, M. Mo3.1
Orlov, D. **Fr5.3**
Orlov, V. We4.8

P

Padhi, K. K. Fr2.4
Padniuk, Y. We4.8
Pankratova, M. **Mo4.3**
Paris, E. **We2.2**
Pashchenko, M. **Fr1.4**
Patthey, L. We1.3, **We2.1**
Pekur, D. Fr6.10
Petkus, R. Th4.5
Petlovana, V. Fr6.10
Petrenko, O. **We4.6**
Petrosova, H. Th3.1, **Th3.3**
Pezeril, T. **Mo1.2**
Picher, M. Mo2.2
Píš, I. Fr6.14
Piwowarczyk, P. We2.4
Pocherpailo, A. **Fr5.6**
Podshebiakin, A. **Fr1.2**
Pohorelec, O. Fr6.14
Popov, O. Fr2.5
Pribus, M. Fr6.14
Pribusová Slušná, L. Fr6.14
Privault, G. Mo2.2
Prokhnenko, O. **We4.3**
Prokhorets, S. We4.9
Prosolenko, V. **Fr4.3**
Pshenychna, H. Fr2.5

R

Rabiller, P. Mo2.2
Rao, P. Mo1.1
Ravnik, J. Mo1.1
Redko, R. Fr6.14
Reichlova, H. Mo3.1
Revo, S. Fr4.10
Rezaei, B. Fr6.4
Rivkin, L. We1.3
Robinson, I. Mo1.1
Rogach, A. L. We4.8
Romanyuk, B. Th4.4
Romanyuk, V. Fr6.14
Roshan Entezar, S. Fr6.4
Roslund, L. We2.5
Rosmus, M. We3.2
Rudychev, E. We4.9
Rutschmann, A. Mo1.1
Ryukhtin, V. **We4.7**

S

Sabov, T. **Th4.4**
Sajeev, L. We3.2
Sakhatska, A. **We4.8**
Sakhatskyi, K. We4.8
Sakhniuk, O. **Fr4.6**
Salamo, G. J. Fr5.6
Salary, S. **Fr6.4**
Samal, A. K. **Fr4.2**
Sander, M. Mo1.1
Sandhop, M. We1.3
Sarikov, A. Fr6.14
Sato, T. Mo1.1
Scheufele, M. Mo3.1

Schlitz, R. Mo3.3
Schmoranzerová, E. Mo3.1, Mo3.3
Schneidewind, A. We2.4, **We4.1**
Schorr, S. Th4.1
Schwenke, J. We2.5
Seiki, R. Mo2.2
Semenenko, M. Fr6.14
Senyshyn, A. **We4.2**, We4.7
Serhiichuk, S. Th1.4, **Th1.5**
Shamrovska, P. **Fr3.1**
Shekera, A. **Fr6.5**
Shevchenko, V. Fr6.3
Shova, S. Th3.2, Th3.4, Th3.5, Fr5.2
Shpyrko, O. Mo1.1
Shvernyk, V. Fr2.5
Shyshkin, V. **Fr6.9**
Sikora, M. **We1.1**, We1.3
Sirenko, V. Y. **Th3.2**, Th3.5
Skoropata, E. M. **Mo2.4**
Smertenko, P. Th3.6
Smortsova, Y. We3.3
Snopok, B. Fr6.10
Snuverink, J. We1.3
Sobota, M. Fr6.14
Solano, J. Mo3.1
Song, S. Mo1.1
Sopinskyy, M. V. Fr6.8
Spitz, L. C. **Mo4.2**
Springholz, G. We3.2
Staub, U. **Mo4.1**
Stoleriu, L. Mo2.3
Storozh, V. Fr2.6
Stoychev, B. Mo1.1
Strilets, M. Fr4.5
Strobl, M. We4.8
Stroyuk, O. **Th4.2**
Sukhenko, I. We1.3
Sun, Y. Mo1.1
Szlachetko, J. We1.3

T

Takashiro, T. We3.2
Ťapajna, M. Fr6.14
Tarasenko, A. Fr6.13
Terebilenko, K. **Fr2.1**, **Fr4.7**
Thånell, K. We2.5
Thomas, H. Th4.3
Tikhonov, E. A. Fr1.2
Tkach, N. **Fr5.4**, **Fr5.5**
Tokoro, H. Mo2.2
Tomchuk, O. **We4.4**
Trtik, P. We4.8
Tsehelnyi, V. **Fr3.3**
Tsybrii, Z. Th1.4, Fr5.7
Tuz, V. Fr2.6

V

Vazhnenko, R. **Fr2.5**
Veremeichyk, T. **Fr6.3**
Verevka, S. Fr6.13
Verma, A. **Th1.2**
Voitovych, M. Fr6.14
Volovenko, O. Fr6.13
Vorona, I. We3.3
Vrublevska, O. Fr4.3

W

Wach, A. We1.3
Wawrzyniak, A. We1.3
Wiechecki, J. We1.3
Woltersdorf, G. Mo3.3
Wróbel, T. **We1.4**
Wu, Y. Z. Mo3.3
Wutke, D. We1.2, We3.2

X

Xia, Z. We4.8

Y

Yablochkova, K. Fr6.3
Yakovliev, A. We1.3
Yakunin, S. We4.8
Yakunov, A. Fr6.11
Yashchuk, V. P. Fr1.2
Yashchyshyn, Y. Fr2.6
Yavaş, H. Mo1.1
Ye, W. We4.8
Yevmenova, A. Th1.4
Yukhymchuk, V. Th1.4, Th1.5, **Th2.2**

Z

Zahn, D. R. T. Th4.3, Fr3.1, Fr3.2
Zaichenko, O. **Fr2.6**
Zając, M. We1.3
Zakusylo, T. **We3.2**
Zaporoshchenko, D. **Fr5.1**
Zelinsky, A. **We4.10**
Zenkova, C. Fr6.6
Zerdane, S. Mo1.1
Zhou Hagström, N. Mo1.1
Zhu, D. Mo1.1
Zhuk, Y. Fr4.10
Zhydachevskyy, Y. Fr5.3

ORGANISERS AND PARTNERS

























SPO 2026

27th Symposium on Photonics and Optics · 2–6 November 2026

www.spo.optics.org.ua · indico.psi.ch/event/19016